Beyond the Solid Core Nuclear Thermal Rocket: A Computational Investigation into Criticality and Neutronics Performance of Advanced Liquid and Gas Core Reactor Approaches for Next Generation Performance

by

Rittu S. Raju

A dissertation submitted in partial fulfillment
of the requirements for the degree of
Doctor of Philosophy
(Nuclear Engineering and Radiological Sciences)
in the University of Michigan
2022

Doctoral Committee:

Professor John E. Foster, Chair
Dr. Michael G. Houts, NASA Marshall Space Flight Center
Professor William R. Martin
Professor Kenneth G. Powell

“yes, if you call out for insight and raise your voice for understanding,
if you seek it like silver and search for it as for hidden treasures,
then you will understand the fear of the LORD and find the knowledge of God.
For the LORD gives wisdom; from his mouth come knowledge and understanding;”

Proverbs 2:3-6, ESV

Rittu S. Raju

ritzsr@umich.edu

ORCID iD: 0000-0001-7395-5324

DEDICATION

For my dad and mum, whose continuous love, support, sacrifices, and patience are present on each page of this dissertation.

ACKNOWLEDGEMENTS

First and foremost, I would like to thank my research advisor, Professor John Foster, for his guidance, support, and encouragement during my time at Michigan. I cannot ask for a better advisor than Professor Foster. I have to say that it has been a blessing to have Professor Foster as my advisor. His joy and excitement for science, space, superheroes, and research made all our conversations fun and enjoyable. I always appreciate his ability to understand student needs and his humble personality. I am thankful to Professor Foster for his willingness to take me in as his student and for helping me to secure funding for my graduate work. I do not think I would be here today without Professor Foster's patience and guidance.

Second, I would like to thank my dissertation committee, Dr. Michael Houts, Professor William Martin, and Professor Kenneth Powell. I had the pleasure of working with Dr. Houts through my NASA funding. I would like to thank Dr. Houts for always being available to talk on short notice and for always communicating back to me quickly. I appreciate your mentorship in my life during my time at Alabama. Dr. Houts' positive personality is what can change people's perspective of nuclear rockets for space application. I would like to thank Professor Martin for his time and excellent feedback on neutronics studies that enabled me to get here with my research. He went above and beyond to guide me and give me articles that helped me with my research. I would like to thank Professor Powell for his guidance with the heat transfer studies. Professor Powell's insight on heat transfer helped me to approach the heat transfer work differently than initially planned.

I would like to thank the NASA Space Technology Research Fellowship [Grant number 80NSSC18K1161] and Rackham Merit Fellowship for funding my research work at the University of Michigan. I would also like to thank previous members of the Plasma Science and Technology Lab [PSTL] – Dr. Neil Arthur, Dr. Selman Mujovic, Dr. Janis Lai, Dr. Kenneth Engeling, Dr. Adrian Lopez, and Dr. Yao Kovach. I appreciate their hard work and efforts that framed a role model for me. I would also like to thank current PSTL members Anil Bansal, Joe Groele, Roxanne Pinsky, Andria Sperry, Jenny Smith, Chelsea Tischler, Tyler Topham, Nate Wirgau, and Zimu Yang. It was a pleasure to be a part of this fun group. Things would have been lonely without you folks at PSTL.

I would also like to thank the NERS Department for its continuous support of graduate students. The department's care for us made me feel at home and made my graduate student life smoother. Many graduate students in NERS such as Aaron Tumulak have helped me with their feedback on my research. I want to thank the man behind the scenes, Garnette Roberts, our graduate student coordinator, for always being available to talk and help with things that need to be done. I would like to thank other staff members at the NERS department too who took care of the research funding paper works and helped me with various administrative work.

Now I would like to thank those people outside of the University of Michigan that made my time at Michigan a pleasant experience and gave me emotional and mental support when I needed it. This includes the large family of people in GradCRU who became my friends for life in a short time. I would like to thank my spiritual mentor, Dr. Charles Roeper, for his investment in my life during my time here at Michigan. It was also a pleasure for me to serve alongside Dr. Roeper in Cuba thrice and in the Dominican Republic once with the Filter of Hope Ministry. I

want to thank other spiritual mentors too who impacted my perspective on life – Dr. David Brzezinski, Rob Narske, Kyle Zimmerman, and Eric Johnson.

I would also like to thank my big family of Church at Michigan – Grace Bible Church (GBC) for their investment in my spiritual growth during my time at Michigan. I enjoyed my time at church and I love how GBC loved God and served the community in amazing ways. I want to thank GBC for all the opportunities that were given to me to grow as a Christian man. I want to thank my small group at GBC. Their prayers, love, and support have been a blessing in my life. I would especially like to thank Julia Slatin for her encouragement and support when I was transitioning from taking classes to doing research. Her work ethic and commitment to both work and God gave me the motivation to work better. Julia is one of the best cooks I know and I am thankful to her for cooking various foods for me and others at Church.

I want to thank my family as well. First, I would like to thank my Dad's eldest brother (Valia dad) and his family through whom we were able to immigrate to the United States. If it wasn't for Valia dad's extended hand of help, I wouldn't even be here in the U.S. I want to thank my sister, Dr. Riya Raju, for being an amazing sibling and for all the medical advice you give me. I am grateful to Riya for answering all my medical questions free of charge. I also want to thank my parents for everything they have done for me. From sacrificing many things they had in India to immigrating to the U.S for me and my sister. I have to thank my parents for giving me a good education and for pushing me to go to college and work hard. I appreciate them for always being very understanding and supportive of me.

Although I am very grateful to all the people mentioned above, I am above all thanks to my Lord Jesus Christ for always working and placing amazing people in my life. I praise God for loving the world so much that he gave his one and only begotten Son, Jesus Christ, as a

sacrificial lamb for each one of us. For those who believe, he invites us to have fellowship with him and offers us eternal life. I am thankful for God's gracious love, mercy, and patience has shown towards me. My prayer is that everyone in the world gets to experience Lord Jesus Christ and that I can bring honor and glory to His name.

> "For God so loved the world, that he gave his only Son, that whoever believes in him should not perish but have eternal life. For God did not send his Son into the world to condemn the world, but in order that the world might be saved through him." (John 3:16-17, ESV)

Rittu Sam Raju

July 2022

TABLE OF CONTENTS

LIST OF TABLES

LIST OF FIGURES

LIST OF APPENDICES

ABSTRACT

Space exploration enables humans to not only explore unknown worlds but also to satisfy the curiosity about the contents and origins of the Universe. The last and only extraterrestrial body to be explored by humans is the Moon. The next natural step is human exploration of Mars and beyond. The long trip times associated with space exploration beyond low Earth orbit pose many risks to humans such as psychological effects associated with confinement and isolation, cancer and disease associated with increased radiation dose, and deleterious effects of extended exposure to microgravity which affects a range of physiological systems such as ocular and cardiac. One approach to overcoming these challenges is limiting exposure time via high-speed transit. This requires advanced propulsion beyond conventional systems that feature high thrust and high fuel efficiency. A propulsion system that can enable such quick trip times to destinations throughout the solar system is the gas core nuclear rocket concept. The gas core nuclear rocket offers substantial advantages over chemical or electric or even solid core nuclear propulsion systems. Operating at high temperatures, the gas core nuclear rocket achieves high specific impulse and high thrust, essentially eclipsing conventional solid-core nuclear thermal rockets. Indeed the core itself is in the gaseous state and thus conventionally can operate at temperatures so high that the core itself is in the plasma state – thereby enabling the prospect of heating propellant to many times higher than the melting point of the nuclear fuel. Challenges to the realization of this technology include 1) stably confining the fissioning gas core, 2) preventing plasma erosion due to mixing, 3) optimizing the heat transfer from uranium plasma to the hydrogen propellant, 4) protecting the nozzle from the high-temperature exhaust, and 5)

obtaining a self-sustaining critical nuclear rocket engine. In this research, the criticality of an open cycle gas core nuclear rocket engine and the heat transfer from uranium to hydrogen was studied. Material properties at high temperature and high pressure were calculated or obtained from the literature. Criticality analysis was carried out in the MCNP transport code for spherical non-homogenous gas core nuclear rocket geometry. These criticality analyses proved that a self-sustaining engine can be achieved by optimizing the geometry and the heat transfer in this engine. The heat transfer analyzes were carried out from the basic heat transfer equations. The hydrogen propellant temperatures varied from 3000 K to 40,000 K depending on the uranium core temperature which varied from 10,000 K to 55,000 K. For these temperatures, a critical engine could be obtained by adjusting the amount of uranium in the system. In this modeling activity, confinement of the uranium core is assumed to be achieved hydrodynamically to reduce the loss of uranium from the system. An optimized nozzle was designed for the gas core nuclear rocket commensurate with the high chamber pressure required for this engine to operate. Using this nozzle design and energy transferred to the hydrogen propellant, the gas core nuclear rocket's performance was calculated. The calculated specific impulse ranged from 1000 s to 6200 s and the thrust ranged from 50,000 N to 300,000 N with a mass of approximately 100,000 kg. This analysis confirms that high-performance is achievable from a gas core nuclear rocket. Indeed, criticality is possible provided technical challenges of confinement and nozzle survivability are addressed.

CHAPTER 1 Introduction

Curiosity in human beings has led to exploration and discovery of wonders hidden in deep ocean vents as well as marvels far beyond Earth gleaned by robotic craft. Space itself is a vast ocean ready to be explored and experienced by humans. Space exploration address the key question– "Are we alone in this vast Universe?" Not only would human exploration of space answer such interesting questions, but it will enable humans the prospect of eventually settling worlds well beyond Earth. Current rockets have played a key role in exploration – both human and robotic. While a host of rocket propulsion systems have been explored to date, for human exploration of space beyond low Earth orbit, powerful rockets with high thrust and high impulse are needed. The ideal rocket equation or Tsiolkovsky rocket equation in Equation 1.1 gives the change in rocket velocity and its dependence on the specific impulse of the engine [1].

$$\Delta u = V_{eq} \ln \frac{m_f}{m_e} = I_{sp} g_o \ln \frac{m_f}{m_e} \tag{1.1}$$

$$I_{sp} = \frac{Thrust}{\dot{m} g_o} \tag{1.2}$$

Here u is the velocity of the rocket, V_{eq} is the equivalent velocity, m_f and m_e are the full mass (empty mass and propellant mass together) and the empty mass of the rocket respectively, I_{sp} is the specific impulse of the engine, $\dot{m}$ is the mass flow rate, and g_o is the gravitational constant. The velocity of the rocket is directly proportional to the thrust and the specific impulse as seen in Equation 1.1 and Equation 1.2. Faster velocity means a shorter trip time which makes such a rocket engine attractive for human exploration of space.

1.1 Limitation of Conventional Human Spaceflight beyond LEO

One of the major problems facing human space exploration to Mars and beyond are the physiological effects of long-term exposure to the space environment. These hazards include increased radiation dose, particularly by heavy ions associated with galactic cosmic rays, psychological impacts associated with isolation or confinement, and the deleterious effects of microgravity. Long-term human exposure to weightless conditions can cause mineral losses in bones, vision degradation, immune system suppression, and cardiovascular deconditioning [2]. Space radiation exposure increases the risk of cancer for astronauts. Sources of radiation in space can be galactic cosmic rays (GCR) originating from outside our solar system, solar event particles (SEP) and solar cosmic rays (SCR) originating from our sun, and radiation trapped in the "Van Allen Belts." [3] The annual average radiation dose per person in the U.S. is 6.2 mSv [4]. One in twenty people exposed to a 1000 mSv of radiation dose can get cancer. Table 1 shows the amount of radiation dose that astronauts will get for various space missions [5]. An estimated dose calculation for 3 years long Mars mission is 1200 mSv. Such a large amount of radiation dose can be eliminated by reducing the trip time to Mars.

Table 1.1: Missions and Radiation Dose

Space Shuttle Mission 41-C (8-day mission orbiting the Earth at 460 km)	5.59 mSv
Apollo 14 (9-day mission to the Moon)	11.4 mSv
Skylab 4 (87-day mission orbiting the Earth at 473 km)	178 mSv
ISS Mission (up to 6 months orbiting the Earth at 353 km)	160 mSv
Estimated Mars Mission (3 Yrs)	1200 mSv

Perhaps the simplest approach to reducing dose is to reduce the trip time to Mars by traveling at a faster speed. Acceleration to fast transfer orbits to Mars requires high thrust for both accelerations on the way to Mars and deceleration upon Mars approach. Because thrust is proportional to mass flow rate and exhaust velocity, to minimize fuel mass to carry out the mission it is desirable to operate at a higher exhaust velocity or specific impulse. Current and near-term envisioned propulsion systems such as chemical or advanced electric propulsion systems can ferry humans to mars over trip times of the order of a year. Such trips rely on idealized launched windows. Quick outbound trips translate into long returns. Nuclear propulsion systems are the other options for faster trips to Mars and back.

1.2 Review of Potential Solutions (options)

A variety of rocket engine systems are being developed for in-space propulsion applications. The development goal for these rocket engines is to achieve optimal high specific impulse at reasonable thrust levels so that the trip times in space can be reduced while at the same time maximizing delivered payload. NASA's technological roadmap for in-space propulsion systems categorizes different propulsion systems under four areas – chemical propulsion, non-chemical propulsion including electric propulsion, advanced propulsion technologies, and supporting technologies. Figure 1.1 is NASA's technology area breakdown structure for in-space propulsion technologies [6].

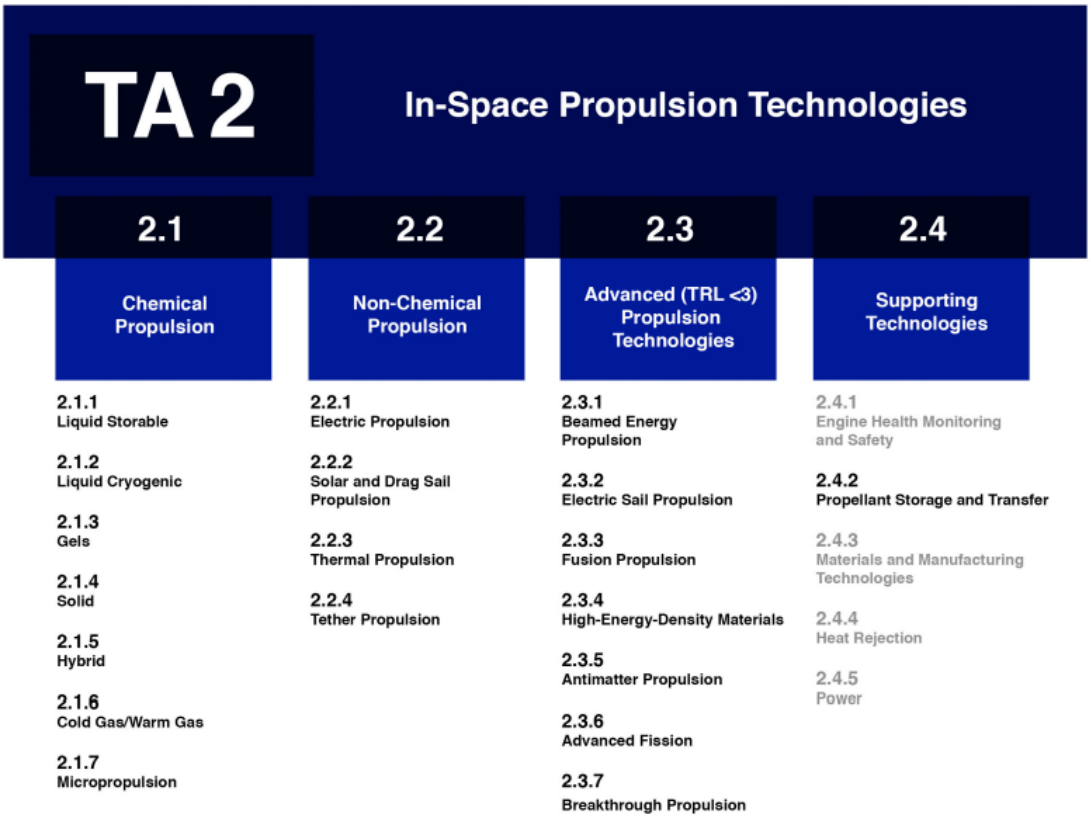

Figure 1.1: NASA's Technology Area Breakdown Structure for In-Space Propulsion Technologies.

Chemical propulsion is the most commonly used propulsion system in spaceflight. In chemical propulsion, the heat released from the reaction of chemicals in the combustion chamber is converted into a thrust-producing plume using a converging-diverging nozzle. The specific impulses of chemical rockets range from 200 s to 410 s. A round trip time to Mars using current chemical rockets will take at least 3 years [7]. Such long trip times make chemical rockets less attractive for human exploration of space. Additionally, chemical propulsion systems limit the amount of payload that can be delivered to the target.

Electric propulsion systems are the other attractive candidates for the in-space propulsion system for human exploration of space. Electric propulsion is very attractive due to its high specific impulse which enables the delivery of a significant payload to the destination. In an

electric propulsion system, electrostatic or electromagnetic fields are used to accelerate ionized propellant in plasma state to high velocities. The plasmas produced for thrust production in such systems are inherently low density and thus the thrust produced is also inherently low in comparison to chemical rockets. Ion and Hall thrusters are the most commonly used electric propulsion engines. These engines use much less propellant as compared to a chemical rocket, thus reducing the mass of the system. An attractive option that is currently being investigated utilizes nuclear power to achieve high power levels along the destination to assure sufficiently high thrust. Even an unmanned interplanetary trip time to Mars is calculated to be in the range of 200 to 600 days as illustrated in Figure 1.2 [8]. For human missions, the power levels have to be in the MW range for electric propulsion systems.

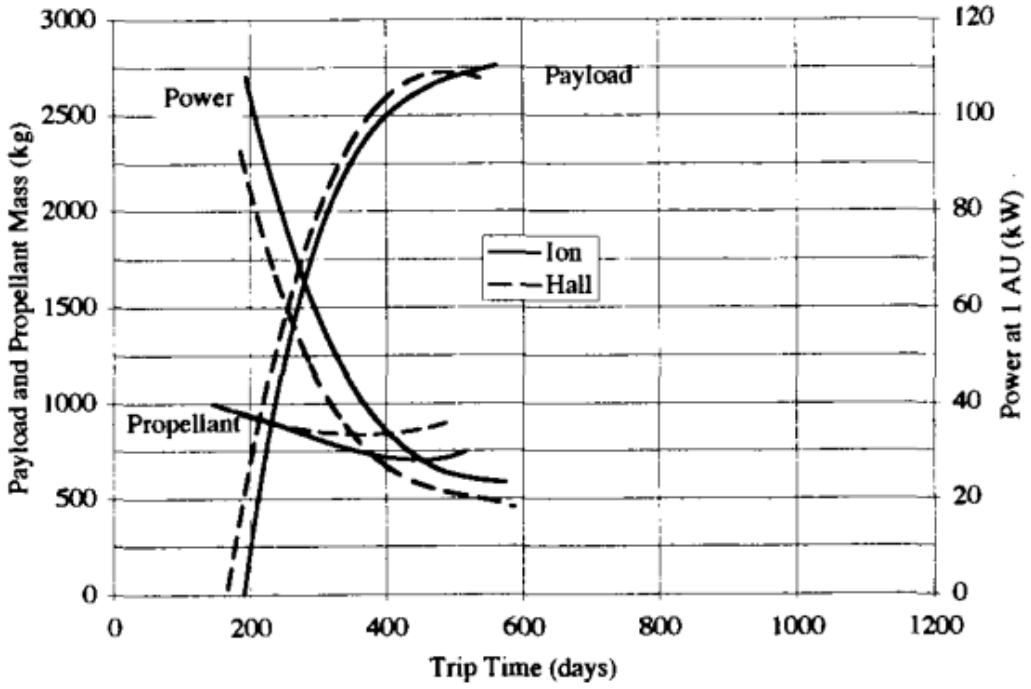

Figure 1.2: Payload, Power at 1 AU, and Propellant versus Trip Time, Interplanetary Trajectory Only.

Table 1.2 lists different propulsion systems and associated performances [9]. The table also includes solid core nuclear fission engines. The table illustrates the fact that propulsion

systems most suitable for a human mission to Mars (best combination of specific impulse and thrust to weight) remain at a low level of technological readiness.

Table 1.2: Rocket Performances Parameters for Different Propulsion Systems.

Engine Type	Specific Impulse[a] (sec)	Maximum Temperature (°C)	Thrust-to-Weight Ratio[b]	Propulsion Duration	Specific Power[c] (kW/kg)	Typical Working Fluid	Status of Technology
Chemical—solid or liquid bipropellant	200–410	2500–4100	10^{-2}–100	Seconds to a few minutes	10^{-1}–10^{3}	Liquid or solid propellants	Flight proven
Liquid monopropellant	180–223	600–800	10^{-1}–10^{-2}	Seconds to minutes	0.02–200	N_2H_4	Flight proven
Nuclear fission	500–860	2700	10^{-2}–30	Seconds to minutes	10^{-1}–10^{3}	H_2	Development was stopped
Resistojet	150–300	2900	10^{-2}–10^{-4}	Days	10^{-3}–10^{-1}	H_2, N_2H_4	Flight proven
Arc heating—electrothermal	280–1200	20,000	10^{-4}–10^{-2}	Days	10^{-3}–1	N_2H_4,H_2,NH_3	Flight proven
Electromagnetic including Pulsed Plasma (PP)	700–2500	—	10^{-6}–10^{-4}	Weeks	10^{-3}–1	H_2 Solid for PP	Flight proven
Hall effect	1000–1700	—	10^{-4}	Weeks	10^{-1}–5×10^{-1}	Xe	Flight proven
Ion—electrostatic	1200–5000	—	10^{-6}–10^{--4}	Months	10^{-3}–1	Xe	Several have flown
Solar heating	400–700	1300	10^{-3}–10^{-2}	Days	10^{-2}–1	H_2	In development

Propulsion systems with high specific impulse and high thrust are still under development and are listed under the TA2.3 area in NASA's technological roadmap. These systems are still in the research and development stages (Technology Readiness Level (TRL) < 3). The advanced fission rockets while holding much promise for human spaceflight is currently at a TRL of less than 3. This dissertation's goal is to contribute to TA2.3.6 advanced fission area of NASA's in-space propulsion technologies roadmap. TA2.4 in the roadmap is the supporting elements that are required to make in-space propulsion systems a reality.

1.3 Nuclear Fission Systems – Nuclear Thermal Rockets [Solid, Liquid, and Gas]

In nuclear thermal rockets, the propellant is heated from the heat released from controlled nuclear fission reactions. Nuclear fission is the process by which a heavier atom nucleus splits into two or more smaller nuclei – typically via absorption of a neutron and in the process releasing energy or heat. The heat comes from the release of binding energy that held the heavier atom's nucleus together. Fission reactions can be configured into a chain reaction enabling a

self-sustaining energy release process. Figure 1.3 illustrates a nuclear fission reaction of uranium-235.

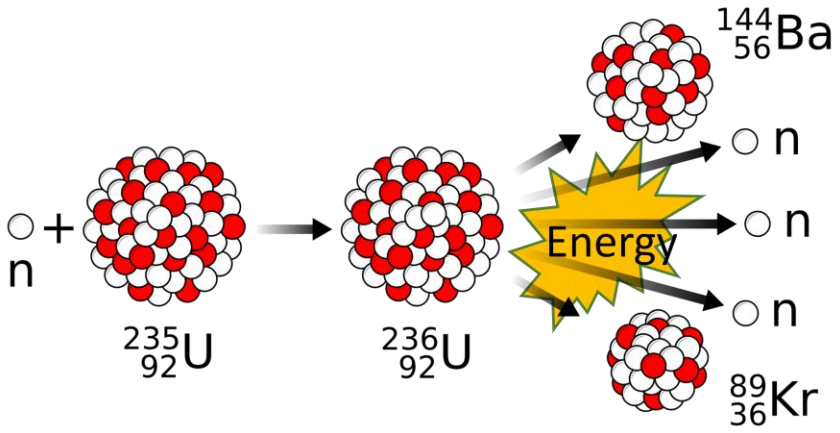

Figure 1.3: Nuclear Fission in Uranium-235 with release in energy.

A neutron collides with the uranium to cause the fission reaction. This in turn releases another three neutrons. In an uncontrolled nuclear chain reaction such as in nuclear bombs, the growth of neutrons in the system is exponential such that the energy increases suddenly and quickly. In a controlled nuclear chain reaction such as in nuclear power plants and nuclear rockets, the neutrons produced in one generation are equal to the neutrons in the previous generation. Thus, the energy release rate is constant. The ratio of neutrons produced in one generation to the neutrons in the previous generation is called the criticality of the engine (k_{eff}). This is given in Equation 1.3.

$$k_{eff} = \frac{Number\ of\ neutrons\ produced\ in\ i^{th}\ generation}{number\ of\ neutrons\ produced\ in\ the\ (i-1)^{th}\ generation} \quad (1.3)$$

In a nuclear rocket, the energy released from controlled nuclear fission is absorbed by a light propellant gas such as hydrogen and is expelled out through a converging-diverging nozzle to get thrust. Since hydrogen has the lowest atomic weight of all elements, using it generates the

highest exhaust velocity and thus specific impulse for a given reactor temperature. Indeed, it is the fact that the engine can operate on hydrogen that gives it the advantage over chemical systems, which can generate higher chamber temperature than solid core reactors but only with propellants of higher mass. Higher temperatures are possible if one relaxes the state of the fuel. For example, it is possible to configure liquid and gaseous core variants that allow for specific impulses well beyond 1200 seconds which is 3 times that of the state-of-the-art LOX-H chemical system.

1.3.1 Solid Core Nuclear Rocket

As the name suggests, in a solid core nuclear rocket the fuel core is in a solid-state typical of terrestrial nuclear power plants. This engine using advanced fuels develops a specific impulse up to 900 s. Solid core nuclear thermal propulsion is the next step for the in-space propulsion system. Previous engine work as in the Nuclear Engine for Rocket Vehicle Application (NERVA) program of the 1960s has provided a wealth of knowledge on the operation of the solid core nuclear rocket operation. Figure 1.4 illustrates the NERVA thermodynamic nuclear rocket engine [10]. Maximum chamber temperature for solid core nuclear rocket is 3500 K.

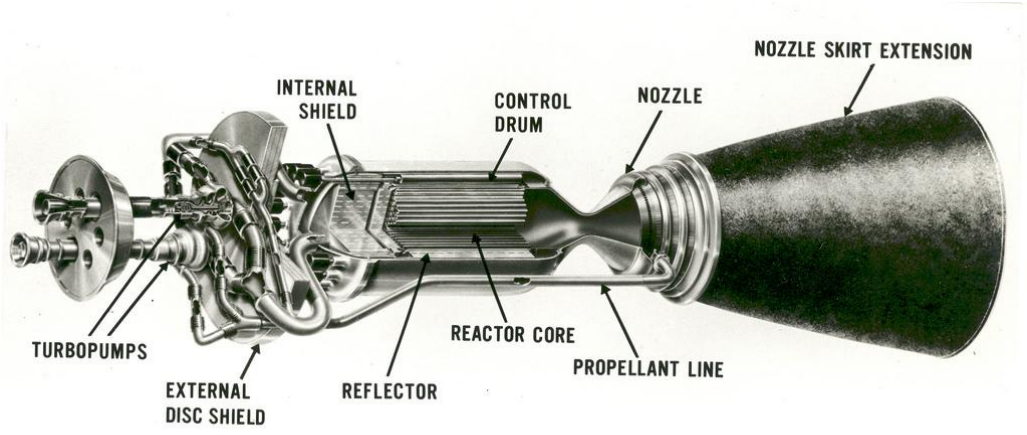

Figure 1.4: NERVA Thermodynamic Nuclear Rocket Engine Drawing.

NERVA engines were developed to utilize highly enriched uranium. Current development efforts focus on high assay low enriched uranium. In this respect, current development activities focus on fuel development and criticality under these fuel enrichments. In solid core nuclear rockets, the maximum core temperature and thus maximum specific impulse attainable is limited by the melting point of the fuel [11].

1.3.2 Liquid Core Nuclear Rocket

In a liquid core nuclear rocket, the fissioning fuel is in a molten state. The heating of the propellant happens by passing through molten fissioning fuel. Confining the fuel and achieving good heat transfer are key challenge areas for this engine. The liquid core's temperature is limited by the boiling point of the core. The projected specific impulse of this engine ranges from 900 s to 1800 s. One type of liquid core nuclear rocket currently under investigation is the centrifugal nuclear thermal rocket (CNTR). Here the molten fuel is held in place via centrifugal forces owing to the high-speed rotation of fuel elements. The maximum chamber temperature for this engine is around 5000 K. This engine and its neutronics are discussed further in chapter 6 of this dissertation. This engine is expected to enable a roundtrip time of 450 days to Mars. Roundtrip time of 420 days will make the radiation dose on astronauts considerably lower [12].

1.3.3 Gas Core Nuclear Rocket

Like the solid and liquid core nuclear rocket, the gas core nuclear rocket heats a low-Z propellant such as hydrogen and then expands it through a converging-diverging nozzle to obtain thrust. The major difference is in the gaseous phase of the fissioning fuel. This enables the gas core nuclear rocket to have higher fuel core temperature than those of solid and liquid core nuclear rockets. There is no real limit to the operating temperature of the core. Two types of gas core nuclear rockets are open-cycle gas core nuclear rockets and closed-cycle gas core nuclear

rockets. In an open-cycle gas core nuclear rocket, the fissioning core has direct interaction with the propellant as there is no wall separating the core from the propellant. The core itself is open to the nozzle and thus nuclear fuel can be entrained and lost with the passing and subsequently exiting hydrogen flow. The hydrogen gas is heated radiatively by plasma emission. In the closed-cycle gas core nuclear rocket configuration, the fissioning plasma is enclosed in a quartz envelope and thus is physically isolated from the flowing hydrogen gas thereby eliminating nuclear core fuel entrainment losses. The nuclear light bulb is an example of a closed cycle system where the hydrogen gas is heated via UV light which passes through a quartz jacket. To achieve reasonable heating, the hydrogen flow field is seeded with micron-sized particles which absorb UV and act as a heat exchange medium [6]. Figure 1.5 illustrates a closed-cycle gas core nuclear rocket [13].

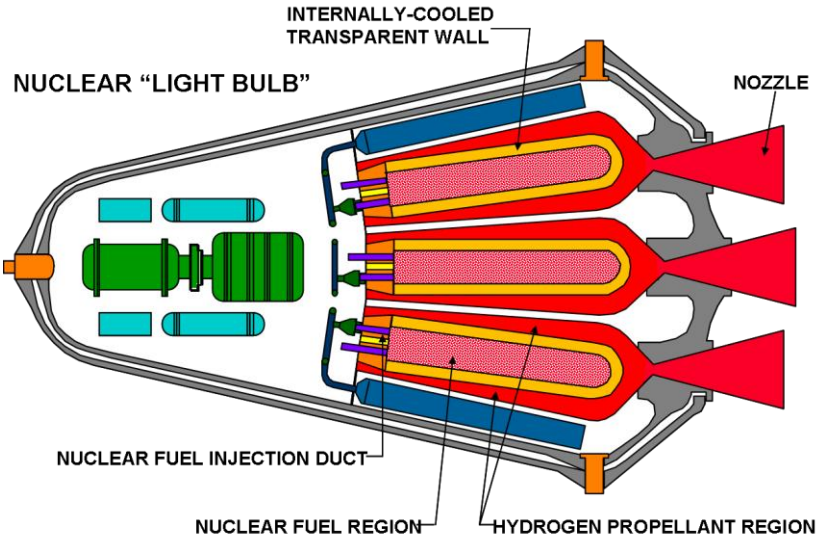

Figure 1.5: Closed-cycle gas core nuclear rocket.

1.4 Why Gas Core Nuclear Thermal Rocket?

Gas core nuclear rockets have the potential to open up the solar system to human exploration by reducing the trip time considerably. Table 1.3 lists the radiation dose calculated

for travel by chemical rocket and travel by a solid core nuclear rocket [14]. The radiation dose from a 433-day one-way chemical rocket trip to Mars is 60 rem (600 mSv) and from a 316-day nuclear rocket trip to Mars is 45 rem (450 mSv). In the case of a gas core nuclear rocket, the travel days are much lower. It can be expected that the radiation dose from travel to Mars using a gas core nuclear rocket is considerably lower than 45 rem.

Table 1.3: Comparison of Radiation exposure between chemical and nuclear rockets.

Radiation source	433-Day Mars mission using a chemical rocket	316-Day Mars mission using a nuclear rocket
Van Allen belts	2 rem[b]	2 rem
Mars surface	1	1
Galactic radiation	31	22
Solar flares	26	15
Reactor	——	5
Mission total	60 rem	45 rem

Gas core nuclear rockets are attractive because they feature high impulse ranging from 2,500 to 7,000 seconds, and high thrust ranging from 20,000 to 400,000 newtons [15]. The gas core nuclear rocket fuel is in a gaseous form allowing for arbitrarily high core temperatures (>10 times solid core operating temperature). The fuel is isolated from the material surface in the case of a gas core nuclear rocket, thus allowing the fuel to operate at super high temperatures [16]. Because specific impulse scales with the square root of the gas temperature, a significant increase in performance on conventional rockets is possible. Figure1.6 illustrates the initial mass in Earth's orbit (IMEO) versus mission time to Mars for a solid core nuclear rocket, open cycle radiative cooling gas core nuclear rocket, and regenerative cooling gas core nuclear rocket [15]. It can be seen in the figure, that gas core technologies are superior to solid core requiring less propellant to carry out fast trips to Mars.

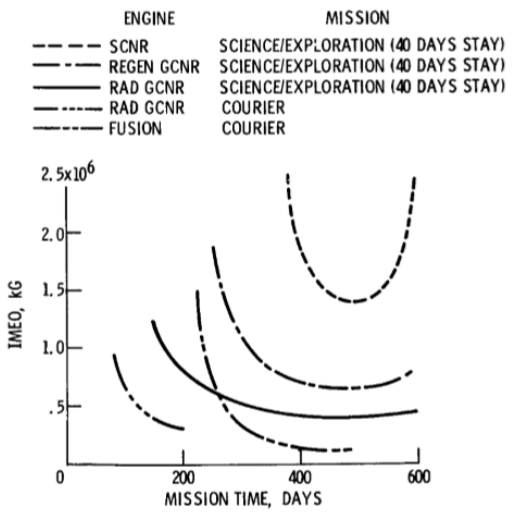

Figure 1.6: Mars round-trip mission duration for various nuclear rocket engines versus IMEO.

Studies show that the gas core nuclear rocket enables roundtrip mission times of only 80-days to Mars [15]. The faster trip times greatly reduce physiological degradation associated with long-duration space flight. If realized, the gas core rocket can become the basic architecture for human exploration of the solar system, reaching essentially all planets with round trip times of less than a decade. This attractive feature of the gas core nuclear rocket is why this engine should be developed further for enabling human exploration of space a reality.

1.5 Dissertation Overview

While the goal of chapter one was to introduce the problem being addressed by gas core reactors, subsequent chapters focus on discussing the evolution of the technology and criticality calculations. Chapter 2 overviews the state of the art in understanding the gas core nuclear rocket technology including past research and challenges to development and realization. Chapter 3 summarizes the challenges addressed by this dissertation regarding the realization of a gas core engine, which is largely addressed computationally. Chapter 4 discusses criticality calculations carried out in this dissertation work. This includes studying the material properties and conducting the neutronic analysis to obtain a critical self-sustaining engine. Chapter 5 discusses

the performance of the critical engine design including heat transfer to the propellant. Chapter 6 summarizes earlier work on liquid core engines. In this chapter, the liquid core centrifugal nuclear thermal rocket is discussed along with the neutronics of the CNTR engine. Chapter 7 summarizes the thesis work and future works needed for further development of the gas core nuclear rocket concept.

CHAPTER 2 Overview of Gas Core Nuclear Rocket Research

2.1 State of Art

The most common depiction of an open-cycle gas core nuclear rocket design is shown in Figure 2.1 [17]. Here hydrodynamically confined fissioning uranium plasma acts as the fuel element and a light gas such as hydrogen is used as the propellant. As illustrated in Figure 2.1, the hydrogen propellant flows around the engine to cool not only the nozzle but also the reflector cavity walls before passing through a porous wall into the chamber. Nuclear fuel such as uranium-233 or uranium-235 in gaseous uranium hexafluoride form is injected into the system through the fuel feed line [15]. The fissioning core transfers heat to the propellant via radiation, conduction, and convection. The high enthalpy propellant then goes through a converging-diverging nozzle to convert the random thermal energy into thrust.

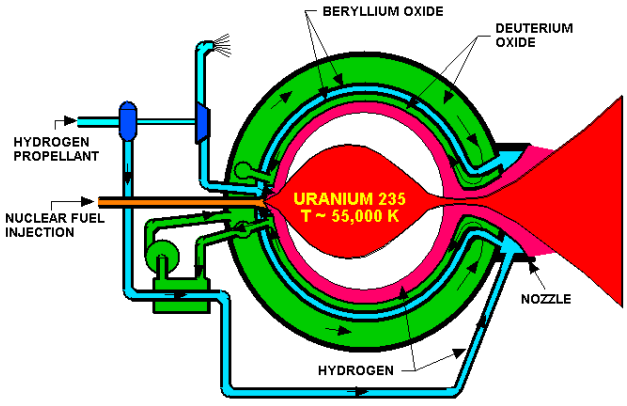

Figure 2.1: An Open Cycle Gas Core Nuclear Rocket Engine.

The gas core nuclear engine's capacity for high thrust and high specific impulse attracted a lot of attention, particularly during the period from the 1960s to the early 2000s. Although conceptually simple, implementation of this engine concept has proved quite challenging. The

chief challenges are associated with the high temperature and pressure conditions required to operate the engine long with the confinement of the core itself. These challenges have been explored both computationally and experimentally. In the following sections, the challenges to gas core nuclear rocket engine implementation are discussed alongside past research that addressed these issues.

2.2 Challenges of an Open Cycle Gas Core Nuclear Rocket Engine

While the realization of gas core nuclear rocket performance would represent a significant advance in rocket technology, many technical challenges stand in the way of its development and eventual implementation. As mentioned previously, the chief challenges include 1) stable confinement of the fissioning plasma, 2) minimization of uranium plasma erosion due to mixing and subsequent entrainment with hydrogen fuel, 3) optimization of the heat transfer from fissioning uranium plasma to the hydrogen fuel, and 4) nozzle survival. Loss of fissioning fuel can occur via hydrodynamic instabilities that can arise from the motion of hydrogen fuel around the uranium plasma core such as the Raleigh Taylor fluid instability where the heavy fissioning plasma is supported by light flowing hydrogen gas. Perturbation to the interface can grow leading to the deleterious mixing of the hydrogen gas with the uranium fuel. Hydrogen of density ρ_H and velocity v_H flowing around stationary uranium plasma of density ρ_U under the influence of acceleration ‘a’ can lead to Kelvin – Helmholtz instability as well (e.g. velocity shear which can lead to mixing and ultimately disruption of confinement), which is expressed as in Equation 2.1 [18].

$$v_H^2 > \frac{a(\rho_U^2 - \rho_H^2)}{k\rho_U\rho_H} \approx \frac{a\rho_1}{k\rho_2} \tag{2.1}$$

Here it is assumed that uranium density is much larger than the hydrogen density. 'k' is the wavenumber of the oscillation. Figure 2.2 and Figure 2.3 below show Rayleigh Taylor instability and Kelvin – Helmholtz instability respectively [19].

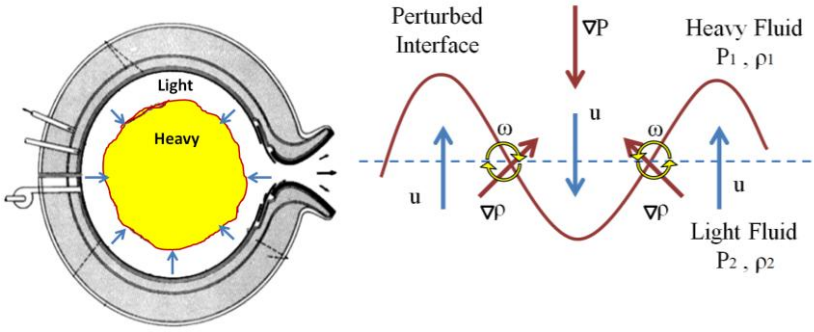

Figure 2.2: Rayleigh Taylor Instability.

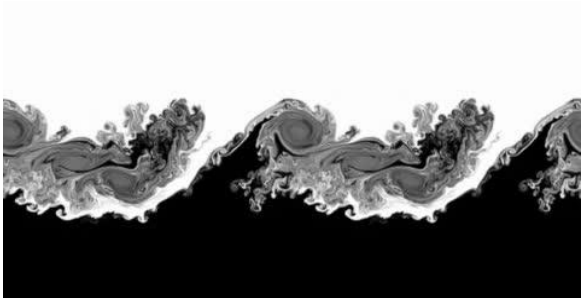

Figure 2.3: Kelvin - Helmholtz Instability.

Confinement must minimize core fissionable material loss while isolating the hydrogen fuel from the walls [20]. The stability and confinement of uranium plasma, as well as heat transfer to the fuel, are still not well understood. The design goal of a gas core engine is to maximize heat transfer to the fuel while running the core power as high as practically achievable and keeping this core in stable confinement with minimum fuel erosion.

Once the confinement problem is solved, the material challenges posed by this engine need to be addressed as well. The exhaust is extremely hot, exceeding the melting point of

known materials (>5000 K). The material with the highest known melting point is tantalum hafnium carbide with a melting point of 4263 K. Both the nozzle and chamber walls must survive these extreme conditions of thermal load in the presence of intense radiation. Research work on fusion reactor materials and hypersonic flight materials are promising work that could tackle the gas core nuclear rocket engine's material problems. For example, similar conditions exist near the walls of tokamaks albeit not at the rocket pressure envisioned but there the power flux is more than one MW per square meter. In this case, diverter technologies are used to channel hot plasmas towards a water-cooled target [21].

Demonstration of the engine performance on the ground could be a challenge as well since the exhaust will most certainly contain fission fragments and fuel. Even if the fuel core is confined to 99.9 percent, the small amount of fuel loss from the engine could make the ground test study a challenge. Ground test work for future tests of solid core and the liquid core nuclear rocket may also provide gas core engines with options for ground testing.

2.3 Past Research on Gas Core Nuclear Rocket

Significant investigation of the gaseous core rocket concept extended from the 1960s into the early 1990s. These research works can be divided into five categories: rocket operations, reactor physics, fluid mechanics, heat transfer, and gas core confinement studies. Each of these categories is reviewed further in the following sections.

2.3.1 Rocket Startup and Shutdown

The startup scenario for a gas-core nuclear rocket is not straightforward. The key is to establish confinement of the core hydrodynamically and then bring the core to criticality. This approach is expected to minimize the loss of uranium fuel from the system. One of the proposed ideas for startup featured the injection of an antiproton beam to generate the required number of

neutrons to initiate the fission reaction and thus the chain reaction [22]. In another study, it was found that a source of about 10^{22} neutrons is needed for the startup [11]. In both these studies, it is assumed that the core has already formed via fuel injection that is ultimately hydrodynamically confined and is thus ready to fission. If the confined core assembly is non-self-sustaining (i.e., sub-critical engine), then a constant source of neutrons will have to be provided for the fissioning process to continue. Another proposed concept involved the solid uranium fuel pellets injection into the cavity region where hydrogen has been pumped to a pressure of 50 MPa to 200 MPa [15]. Due to the high pressure of hydrogen propellant in the chamber, the uranium fuel will achieve criticality and rise to a power level that would allow the uranium rod to eventually vaporize giving rise to the gas core. The gaseous core is obtained by the high pressure and the fissioning process of uranium metal. In this proposed concept, the hydrogen propellant has to be pumped into the chamber and the chamber should be pressurized to desired pressure before injecting the uranium pellets into the chamber. Figure 2.4 illustrates a gas core nuclear rocket with a uranium feed system [15].

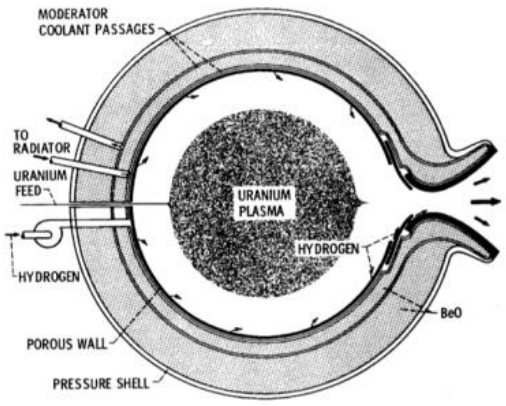

Figure 2.4: Porous gas core nuclear rocket with uranium feed system.

The engine shutdown is not straightforward either. The engine shutdown involves terminating the self-sustaining chain reaction in the core of the engine. In principle, control

drums that contain materials with a high neutron absorption cross-section can bring a critical engine to a sub-critical level thus effectively ending power production. These control drums can be used to also control the power of this engine by manipulating the neutron flux in the reactor. The core, however, must still be dealt with. One method of managing the core during the shutdown is to let the fissioning fuel exit the engine through the converging-diverging nozzle by removing the hydrodynamic confinement. This is not only an expensive method of engine shutdown but also the high temperature of the gaseous core potentially could come into contact with the converging-diverging nozzle. Another proposed method of a shutdown is to draw the gaseous uranium back into the uranium chamber that is surrounded by the control drums to prevent further fissioning. In this method, the drawing of the reactor core will also include the fission by-products being drawn back into the uranium storage chamber. Once cooled, the core materials may need reprocessing to facilitate the reuse of the fuel.

2.3.2 Reactor Physics

Reactor kinetics studies have been conducted to study the critical mass requirement of cavity reactors. Critical mass design considerations include fuel density, fuel density variation with temperature, reflector temperature, and neutron utilization as well as geometrical aspects such as core and reflector shape. Experiments were conducted for both cylindrical and spherical geometries, and for both solid and gaseous (uranium hexafluoride) nuclear fuel at Idaho-Nuclear Corporation to study the uranium fuel mass and configuration requirements [15]. The focus of the research was to calculate fuel mass, propellant pressure, cavity diameter, and reflector-moderator thickness for a gas core engine. A summary of the results from this study can be found in Reference 15. The reactivity and the criticality calculations were made using the neutron transport code TDSN (two-dimensional discrete angular segmentation transport program) with

spherical geometry [23]. Table 2.1 summarizes the notional configuration of the gas-core nuclear rocket derived from the studies in References 23 and 24.

Table 2.1: Sample Engine Specification.

Engine Parameters	**Specifications**
Impulse (s)	5000
Thrust (N)	110,000
Propellant	LH_2 seeded with Tungsten
Fuel	U-233 enriched to 98%
Reactor Power (MW)	3,750 Thermal
Total Engine Mass (kg)	91,000
Cavity Diameter (m)	2.4
Moderator Thickness (m)	0.76

Americium has also been investigated as a potential fuel. ^{242m}Am has a large thermal fission cross-section. This leads to a significantly smaller reactor (comparable fuel density as that of ^{235}U and a radial size reduction of about 70 percent) that can produce the same performance as that of a uranium-235 gas-core nuclear reactor [11]. However, it was found that thermal-hydraulics and neutronics computational study favors uranium-233 as the best fuel due to its modest epithermal fission cross sections and hydrogen as the best propellant due to its low molecular weight [25]. The neutron energy spectrum was found to be in the epithermal energy range of 0.035 eV to a few hundred eV [26]. The fast neutrons produced from the uranium

fission process are slowed down to epithermal neutrons by the hydrogen propellant which acts as a moderator as it flows around the core. Table 2.1 below includes a sample engine specification that was calculated from previous research work. It can be seen from the table that a large cavity is required for the engine to be critical.

The most recent criticality work on a gas core engine concept using modern computational tools was carried out by Poston in the early 1990s [25]. He conducted his studies on a cylindrical homogenous system as shown in Figure 2.5 below.

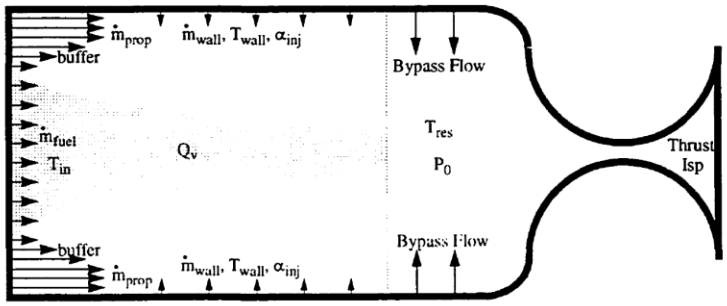

Figure 2.5: David Poston's cylindrical homogenous gas core nuclear rocket model.

The neutronics work using TWODANT software produced only a sub-critical system that required a continuous flow of uranium fuel as well as a neutron source. The best k_{eff} (multiplication factor) obtained was 0.907 using U-233 as fuel and He as the propellant. Although helium improves the criticality of the engine, it adversely affects the engine performance due to its heavier mass than hydrogen. Specific impulse will drop by a factor of two when changing from atomic hydrogen (fully dissociated) to helium due to its inversely proportional relation to the square root of the propellant mass. While this work featured modern computational tools, a non-self-sustaining engine (or reactor with k_{eff} less than one) is not a promising engine for in-space propulsion. Table 2.2 below shows the criticality values obtained by Poston for different fuel and propellants.

Table 2.2: Multiplication Factor for various fuel and propellant combinations.

Fuel	Propellant	k_{eff} (multiplication factor)
U-235	H	0.582
U-233	H	0.805
Pu-239	H	0.676
U-235	He	0.756
U-233	He	0.907
Pu-239	He	0.793

2.3.3 Fluid Mechanics

Fluid mechanics studies have also been carried out to understand the factors that govern the fission fuel loss rate as a function of hydrogen propellant flow rate/flow velocity as well as injection geometry. Isothermal flow experiments were conducted using air as both fuel and propellant in a cylindrical system as shown in Figure 2.6 [15]. One such study showed that the fuel volume consists of only 20 or 30 percent of the cavity volume. Under these conditions, less than one percent by mass of uranium is exhausted alongside hot hydrogen gas from the engine [15]. Earlier fluid mechanics works focused on conducting vortex experiments to study the separation ratio which is defined as the ratio of the mass flow rate of hydrogen propellant to the mass flow rate of uranium fuel. High separation ratios were desired and these vortex experiments showed that very small fuel volume fractions yielded high separation ratios [27]. Additional

experiments were carried out to study the confinement of the uranium fuel or methods to reduce the fuel loss. This subject is discussed further in the gas-core confinement section.

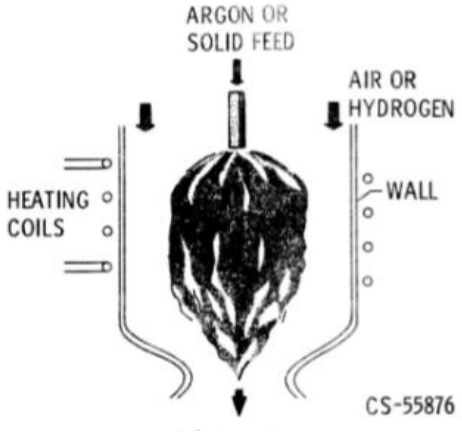

Figure 2.6: Experimental schematic to study gas core nuclear rocket using inductive heating.

Major fluid mechanics studies were conducted to understand the loss of uranium out of the engine. To calculate the uranium loss out of the engine, the plasma instabilities that contribute to the loss need to be included as well. One study that included these instabilities calculated the total uranium mass flow out of the core as the expression given below [28],

$$L_A = 8\pi r_c D_A \rho_U \tag{2.2}$$

Here L_A is the total uranium mass flow out of the core due to acoustic instabilities, r_c is the core radius, D_A is the diffusion coefficient calculated using the growth rate from the plasma instabilities, and the wave number calculated from a wavelength equal to the core radius, and ρ_U is the uranium density. This loss rate determined from the plasma instabilities helps in determining how long the fuel will be in the system before it is completely lost from the engine. This study did not include any hydrodynamic or magnetic confinement to prevent fuel loss in their calculations.

2.3.4 Heat Transfer

The heat from the uranium plasma needs to be absorbed completely by hydrogen propellant and then stored as internal energy until the heat is converted into thrust by the nozzle. The heating of the propellant occurs mostly by radiative heat transfer. Energy not absorbed by the propellant thermally loads the cavity wall and nozzle. To reduce this heat loading, studies have been carried out to optimize the energy transfer to the hydrogen gas.

Previous studies have modeled the radiative heat transfer occurring in the engine using the diffusion approximation. These studies used a conduction coefficient depending on the cubic power of the core temperature. Heat transfer with the uranium gas was assumed to occur through conduction only and by using Rosseland averaged opacity, the thermal conductivity was calculated. Rosseland averaged opacity is used in calculating the total energy absorbed over all wavelengths. Opacity quantifies how strongly the energy of an electromagnetic wave or photon is absorbed while traveling through a material. Poston's total conductivity is given as [25],

$$k = k_{cond} + k_{rad} = k_c + \frac{16\sigma T^3}{3\alpha_r} \tag{2.3}$$

Here k is the thermal conductivity, σ is the Stefan-Boltzmann constant, T_U is the uranium temperature and α_r is the Rosseland mean absorptivity. Using this diffusion approximation, uranium's opacity, and the power distribution obtained from the neutronics calculation, Poston obtained a temperature distribution within the engine as shown in Figure 2.7 [25]. Similar temperature distribution within the engine was obtained by Reference 28. This temperature distribution along with power distribution and neutron flux in the engine is shown in Figure 2.8 [28]. In both these studies, the temperature at the core center is very high and at the boundary of the uranium and hydrogen, the temperature drops significantly down to the 10,000 K to 20,000 K range. This results in the input hydrogen gas rising to temperatures between 5000 K to 15,000 K.

The power distribution and neutron flux in these studies are flat due to the long mean free path for neutrons in the gaseous uranium core.

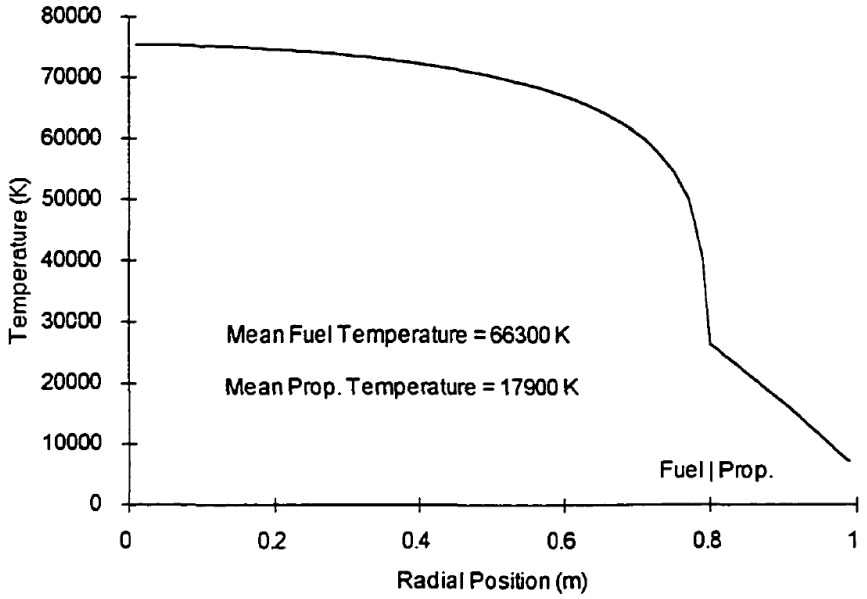

Figure 2.7: Poston's calculated radial temperature profile at core Exit.

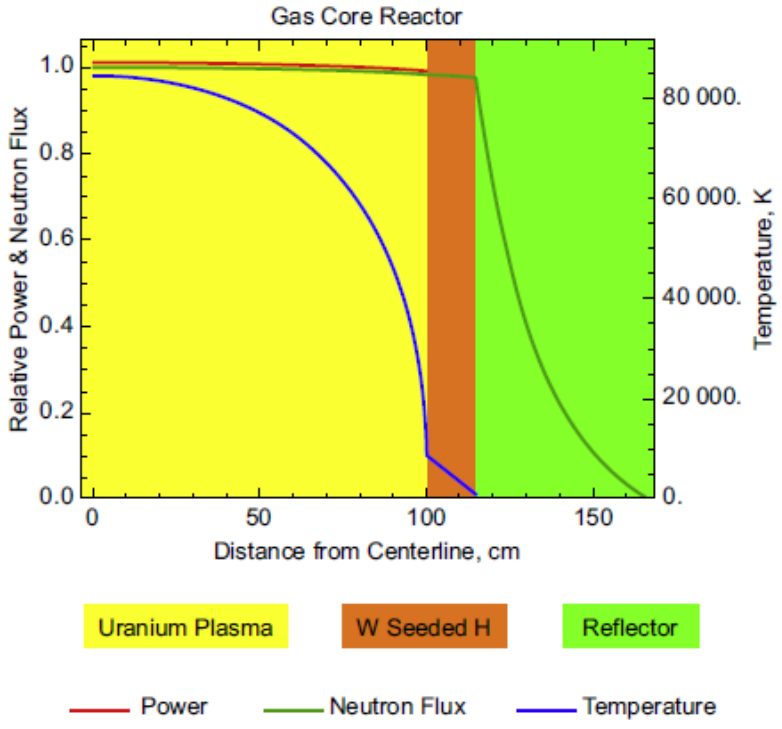

Figure 2.8: Temperature, power, and neutron distributions calculated in Reference 28.

Experiments show that adding tungsten particles (micrometer size) to hydrogen gas will produce a mixture of absorption cross-sections ranging from 2000 to 100,000 square centimeters per gram. The study also demonstrated that the absorption increases with higher pressure too [15]. However, adding tungsten particles to the hydrogen gas negatively impacts the specific impulse. At a high temperature of 7000 K, hydrogen itself becomes quite absorptive [27]. Under these conditions, tungsten seeding is no longer necessary and thus engine performance can improve greatly. In this respect, the seeded hydrogen may only be necessary at low operating core temperatures.

Keston and Krascella [29] used a semi-empirical model and Park et al. [30] used the first-principles model to obtain gas phase compositions, heat-transfer characteristics, and optical parameters of uranium over a range of temperatures from 5000 K to 110,000 K and pressures from 100 atm to 1000 atm. Similarly, Krascella [31] and Patch [32] have calculated the composition, heat-transfer characteristics, and optical parameters of hydrogen over a range of temperatures up to 50,000 K and pressures up to 1000 atm. These works conducted previously provide some key insight into the material properties and behavior of uranium and hydrogen at high temperatures and pressures which are used for gas core nuclear rocket studies. These studies showed that the uranium core is optically absorptive to its thermal radiation and that hydrogen at several hundred atmospheres pressure and temperature above 7000 K is opaque to thermal radiation.

2.3.5 Gas Core Confinement

Confining the nuclear gas core has proven to be a challenging problem. The conventional approach to gas core confinement features hydrodynamic containment. This approach was experimentally tested to assess feasibility. The geometry of this approach is shown in Figure 2.9

[33]. Here injected gas flows past a porous diffuser through which propellant is also injected. This creates a vortex in which the uranium plasma can be injected and confined. The flow through the diffuser keeps the uranium core off the surface of the diffuser – essentially the flow obstruction that generates the vortex. This study showed that a secondary injection of gas (first the uranium fuel is injected, then followed by hydrogen propellant) at the base end of the gas core would reduce the fuel loss. The recirculation region forms just downstream of the diffuser and it essentially forms a bubble into which uranium fuel can be injected. Figure 2.9 illustrates this concept [33]. This work validated the vortex trapped core concept.

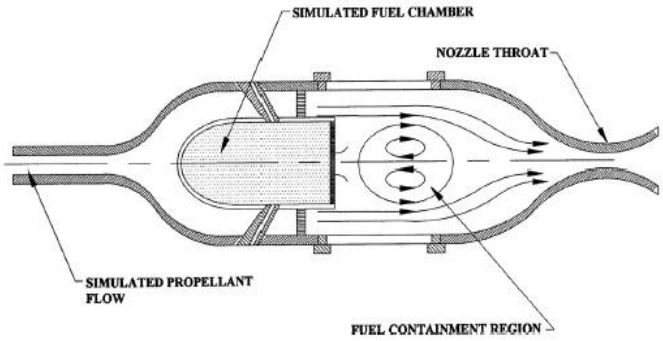

Figure 2.9: Base bleed stabilized gas core nuclear rocket.

Since the gas core operates at very high temperatures, the gas core is in a partially ionized plasma state. This ionized state, therefore, enables the use of magnetic fuel containment. Previous studies have focused on confining the plasma using “mirror geometry” in which the magnetic fields at the ends are stronger than the magnetic field at the center where the uranium plasma core is situated [18]. However, it was found that magnetic mirror confinement at practical field strengths is not feasible owing to collisions that would scatter nuclear fuel into the loss cone. Sedwick and KerrebrocK [34] used externally applied electromagnetic fields alongside hydrodynamic vortices as a uranium fuel-containment mechanism. In their study, their engine acted both as a propulsive device and/or as a power reactor. The power reactor supplied the power to drive the MHD system. Their results showed the addition of electromagnetic fields to

the hydrodynamic fuel containment made the vortex containment feasible by eliminating the wall shear force at the outside perimeter of the vortex.

One of the significant computational efforts addressing the gas core nuclear rocket problem was carried out by Poston. Figure 2.5 shows the two-dimensional model that Poston used for his neutronics and thermal-hydraulic studies. His study featured the continuous inflow of uranium into the engine at a slower rate than the hydrogen flow. As a result of the continuous inflow of uranium, no confinement of the uranium core is achieved. His study showed that increasing reactor power or rocket acceleration could severely degrade fuel containment. The maximum wall heat flux limited the specific impulse of this engine to the range of 2000 – 3000 seconds. He recommended acceleration-assisted containment for fuel containment in this engine as shown in Figure 2.10 [25].

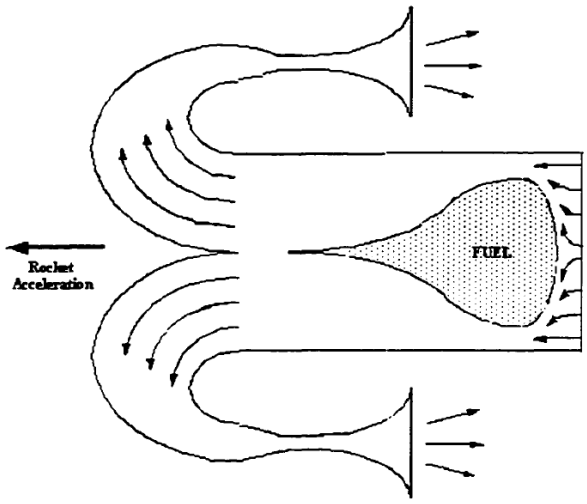

Figure 2.10: Acceleration Assisted Containment.

Thode, Cline, and Howe investigated the formation and stability of a recirculation region using a two-dimensional, axisymmetric, finite difference code [35]. Their study found that the recirculation region might provide improved confinement of the uranium fuel and the position of this recirculation depends on the inlet geometry and injection velocity, the nozzle position,

subsonic convergence angle, the base bleed injection rate, and turbulence. This shows the importance of including accurate nozzle contours in computational studies for vortex formation and stability of the system.

An alternative confinement geometry that has been considered is the counter flow toroidal configuration shown in Figure 2.11 [36]. The flow of propellant as shown in Figure 2.11 around the fuel causes a circular motion of fuel. This geometry is expected to reduce the uranium loss rate due to the centripetal force added to the uranium vortex. Additionally, the thicker layer of the hydrogen propellant will circulate the uranium to decrease the thermal loads on the walls of this engine.

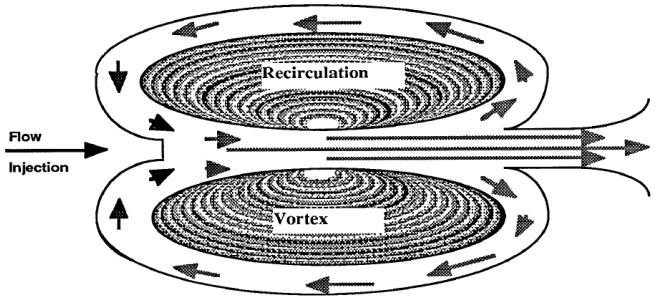

Figure 2.11: Toroidal Configuration for the Gas Core Nuclear Rocket.

CHAPTER 3 Research Approach and Model Description

3.1 Research Approach

The goal of this research work is to understand the neutronics and heat transfer within the gas core nuclear rocket engine using modern computational tools. The gas core nuclear rocket engine computational model is complex due to the high temperature and pressure at which this engine operates. Not only is the computational model complex but also the material properties of the hydrogen propellant and uranium fuel at high temperatures and pressures are not readily available.

3.1.1 Materials

The first step in this research study was to select materials that can be used to credibly assemble a gas core nuclear rocket consistent with the engine's performance envelope. Past research work on gas core nuclear rockets, advanced propulsion systems, and nuclear reactors provide some insight into the materials that can be used in a gas core nuclear rocket engine model. As seen in chapter 2, the fuel that gave the best k_{eff} (but is still sub-critical in Poston's model [25]) is uranium-233 and the propellant that gives the best engine performance is hydrogen owing to the specific impulse scales inversely with the square root of the mass. In the model, it is uranium-233 and hydrogen that are explored for engine nuclear fuel and rocket propellant respectively. Silicon carbide was selected for the hydrogen inlet porous wall and the support structure material because of its favorable neutronics such as irradiation tolerance and high-temperature properties [37]. Silicon carbide has lower neutron absorption and higher neutron moderation as compared to zirconium alloy of the same thickness [38]. Silicon carbide is

also of interest for use in advanced reactors such as high-temperature gas-cooled reactors and fusion reactors [37]. Beryllium metal will be used as the reflector and Ti-6Al-4V (Grade 5) annealed alloy as the pressure vessel (similar to Reference 23). Beryllium reflector is commonly used in nuclear applications as a reflector due to its unique combination of structural, chemical, atomic number, and neutron absorption cross-section [39]. Ti-6Al-4V features good mechanical properties at high temperatures and they are used widely in the aeronautic and aerospace industry [40]. The pressure vessel material does not have a significant impact on the neutronics of the engine due to the presence of a beryllium reflector. Materials needed in this work are shown in Table 3.1.

Table 3.1: Materials used in the computational model of a gas core nuclear rocket engine.

Material	**Description**
U-233	Fissioning fuel
Hot Hydrogen	Propellant and moderator
80% dense SiC	Porous wall [20% by volume H_2 inflow]
Hydrogen Coolant	Regenerative coolant
SiC Outer Wall	Support material if necessary
Beryllium	Reflector
Ti-6Al-4V (Grade 5)	Pressure Vessel

Once the materials are identified, their material properties at high temperatures and pressures are to be obtained from literature work or calculated. The propellant is also used for regenerative cooling of the engine and nozzle before it flows into the engine chamber. This

regenerative cooling is expected to cool the engine components considerably as inferred from past nuclear thermal propulsion experiments, particularly NERVA. The materials that are at high temperatures and require high-temperature material properties are only the heated hydrogen propellant and the fissioning uranium-233 fuel. These thermo-material properties are discussed further in the next chapter.

3.1.2 Computational Codes

For neutronics analysis, the neutronics code has to have the ability to calculate the criticality of the engine, handle the high-temperature material properties and neutron scattering, and include enough large number of energy groups to faithfully represent the reaction physics. The widely used Monte Carlo N-Particles (MCNP) [41] transport code was chosen for this research neutronics study. MCNP is a general-purpose, continuous-energy, generalized-geometry, time-dependent, Monte Carlo radiation transport code designed to track many particle types over broad ranges of energies [42]. For this research, the MCNP6.1.1 version was used. MCNP input file has three parts to it – cell cards, surface cards, and data cards. The typical input file has the form as shown in Figure 3.1.

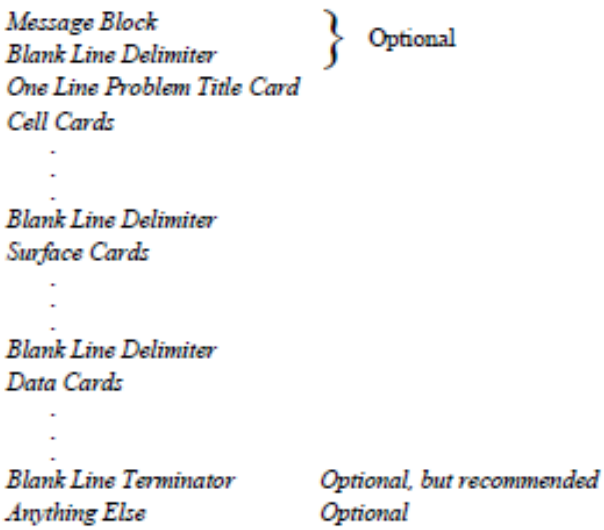

Figure 3.1: MCNP input file format.

The cell cards are an enclosure defined by the surface cards. For the gas core nuclear rocket neutronics studies, each region in the engine has its cells. Inside cells, the material properties are defined the same. Uranium fuel at 55,000 K is one cell and hydrogen propellant at 15,000 K is another cell. If temperature gradient or different properties are needed, the cells are split up accordingly. The surface cards, as the name suggests, describe the surfaces of the cells. These surfaces define the geometry of the engine. The data cards contain the material information, the particles involved, the neutron source, and the output information that specifies what is needed from these Monte Carlo calculations. A sample MCNP input file is provided in Appendix A.

For nuclear materials data, ENDF/B-VIII.0 (Evaluated Nuclear Data File) was used as the material information source for the MCNP transport code. From the MCNP input file, the code calls the material information from ENDFs which are in ACE (A Compact ENDF) format. ENDF is the United States' nuclear reaction cross-section database. They contain material information including neutron cross-sections of various materials at different temperatures. However, they do not have the high-temperature (over 3000 K) neutron cross-section

information that is needed for materials used in a gas-core nuclear rocket engine. These high-temperature neutron cross-sections have to be calculated and inputted into the MCNP data source as an ACE file. For these calculations, NJOY2016 [43] software was used. NJOY's name comes from advancing its predecessor's name – MINX. NJOY is a nuclear data processing system that is used for producing pointwise and Multigroup nuclear cross-sections and related quantities from evaluated nuclear data in the ENDF format [44]. It takes the basic data from the nuclear data library and converts it into the forms needed for applications such as using in MCNP.

The NJOY software takes the ENDF/B-VIII.0 nuclear data and Doppler broadens the material neutron cross-section for the temperature specified in the input file. A sample NJOY input file is provided in Appendix B. The output files with high-temperature cross-sections from NJOY will be in an ACE format that can be added to the MCNP data folder. In the cross-section source directory file, output file descriptors have to be provided so that MCNP can locate data and determine what files should be read to access the data if called by the MCNP input file. For the gas core nuclear rocket neutronics studies, a high-temperature neutron cross-section was calculated using NJOY for the fuel materials and the propellant materials at various temperatures. This material information was called in MCNP for the neutronic analyses and criticality calculations for a gas core nuclear rocket.

Several thermal-hydraulics computational tools such as ANSYS Fluent were considered for the fluid flow, core hydrodynamic confinement, and heat transfer. Due to the complexity of the gas core nuclear rocket engine – which includes dynamic confinement, the thermal-hydraulics solution using these tools is left to future work. Other challenges of thermal-hydraulics computational modeling are related to the high temperatures and pressures of this system, two plasma species flow, radiative heat transfer, and the severe velocity gradients/shear.

Due to these factors, no fluid flow analysis within the engine chamber was calculated and it was determined that the heat transfer modeling can be carried out using the basic heat transfer equations rather than using an already existing insufficient computational code. Here it is assumed that confinement can be achieved as suggested by past experimental studies discussed earlier.

3.1.3 Assumptions

The complexity of the gas core nuclear rocket engine calls for assumptions to be made to simplify the engine model. The assumptions made for this research work are as follows:

1. The engine is in steady-state condition – the startup of the engine and its reaching steady-state has already been achieved. At steady-state conditions, the uranium gaseous core has already been achieved and the hydrogen propellant is flowing around this core.

2. The uranium core is confined by the hydrodynamic confinement mentioned in Chapter 2 by the secondary injection of uranium fuel followed by the injection of hydrogen gas at the base of the fuel core. Although there will still be some uranium fuel loss from the system, here the assumption is that there is no fuel loss – complete confinement.

3. The hydrogen propellant efficiently cools the engine components by regenerative cooling before entering the engine chamber. This hydrogen cooling along with the radiative cooling is sufficient to keep the engine components from melting. The engine components also do not deform due to the high pressure within this engine.

4. The mixing between hydrogen and uranium is small and it does not lead to plasma instabilities as mentioned in Chapter 2.

These assumptions help in narrowing the focus of this research work to the neutronics and heat transfer happening in an ideal steady-state gas core nuclear rocket engine.

3.1.4 Research Approach Path

After obtaining the material properties, the neutronics work was carried out to achieve critical engine conditions. Various geometries and temperatures were studied to optimize the engine using neutronics with the engine. Once the critical engine was obtained, heat transfer analysis was carried out to obtain the temperatures within this critical engine. The thermal solution was then looped back into neutronics to check if the engine is still critical or not. The goal of this method was to converge the thermal and the neutronics solutions to a critical engine. Figure 3.2 illustrates the research approach flow path.

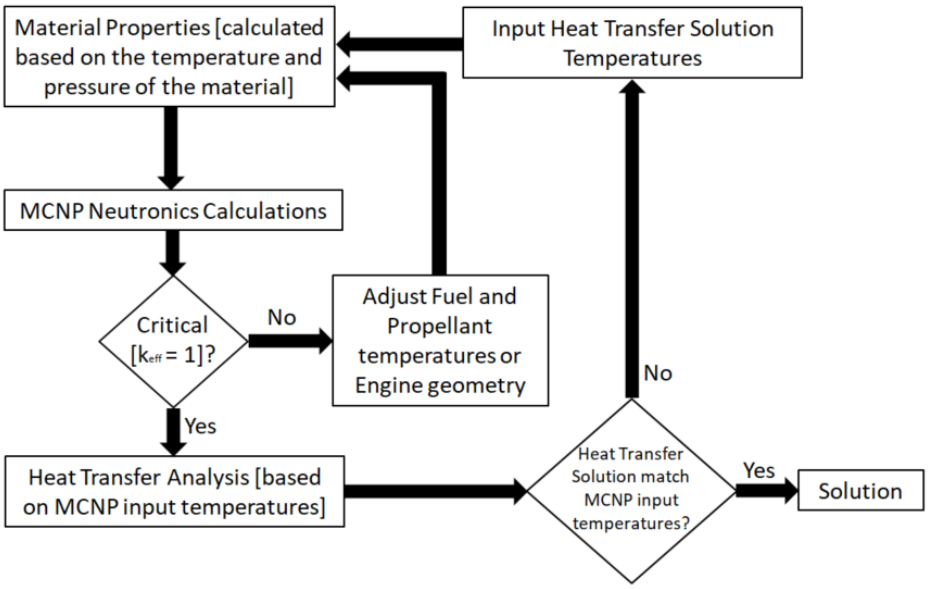

Figure 3.2: Research Approach Flow Chart.

3.2 Engine Model

The initial research work was conducted using a cylindrical gas core nuclear rocket similar to Poston's computational model [25]. In the "Gas Core Nuclear Rocket Feasibility Project" paper by S. D. Howe and his team, the cylindrical geometry for the gas core nuclear rocket was concluded to be a non-viable configuration [36]. This conclusion comes from hydrogen propellant thickness between the fuel core and the chamber wall being narrow from the

narrow annular injection. This leads to high wall heating and low propellant heating. This current research work focuses on the classic spherical fissioning gas core. The system is a spherical non-homogenous model. Figure 3.3 illustrates the spherical gas core nuclear rocket model, as modeled in MCNP.

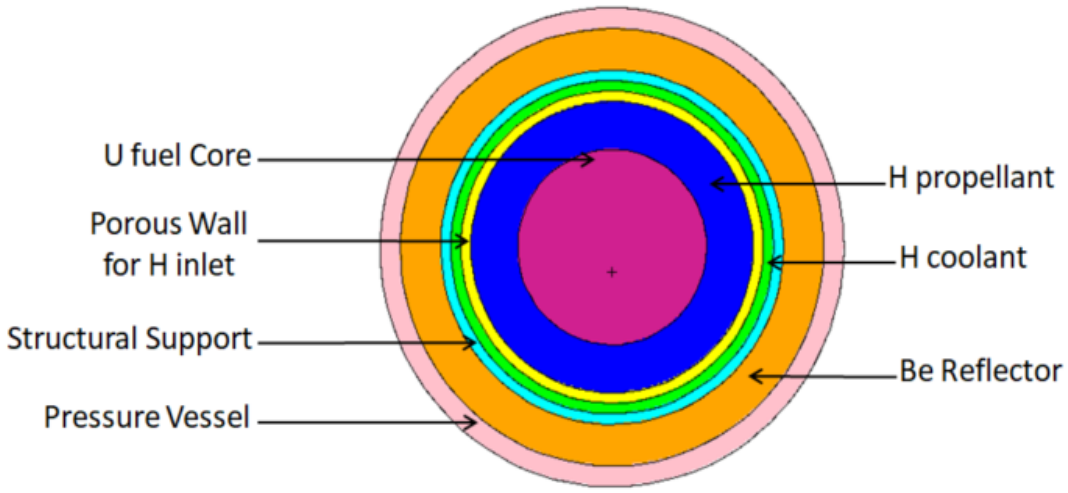

Figure 3.3: A spherical gas core nuclear rocket engine model from MCNP.

The uranium 233 fuel is at the center of the sphere with hydrogen propellant flowing around it. This hydrogen is injected into the system through the porous SiC wall. Outside this SiC porous wall is the hydrogen flow channels that cool the support structure as well as the beryllium reflector. This whole system is enclosed in a pressure vessel. The initial engine input specifications for this research work are given in Table 3.2 below. These values were obtained from previous work and these parameters were optimized with the engine's criticality and heat transfer solutions. The pressure was taken as 1000 atm with fuel core temperature around 55,000 K and hydrogen propellant temperature around 10,000 K. These pressure and temperature values were taken based on previous studies [15], [23], [25], [28]. The cavity diameter and reflector thickness were based on Reference 23. The support structure thicknesses were chosen to accommodate high pressure in the cavity. These initial values were modified with the neutronics

and heat transfer results to obtain a critical engine with the highest transfer of heat from the fuel to the propellant.

Table 3.2: Initial engine model geometry, temperature, and pressure inputs.

Parameter	**Specification**
Engine pressure (atm)	1000
Core temperature (K)	40,000 - 65,000
Propellant temperature (K)	5,000 – 15,000
80% dense SiC temperature (K)	2,500
Hydrogen coolant temperature (K)	1,200
SiC outer wall temperature (K)	1,200
Beryllium reflector temperature (K)	1,200
Pressure vessel Temperature (K)	900
Engine cavity radius (cm)	213
Core radius (cm)	157
SiC porous wall thickness (cm)	15
Hydrogen coolant thickness (cm)	15
SiC outer wall thickness (cm)	15
Beryllium reflector thickness (cm)	61
Pressure vessel thickness (cm)	30

CHAPTER 4 Criticality Studies

4.1 High-Temperature Material Properties for Neutronics

The starting point for any computational study of a gas core nuclear rocket begins with the determination of the high temperature, and pressure material properties of the propellant and the nuclear materials that make up the reactor engine. In general, these can be calculated or in cases obtained from published experimental data. In this work, the reactor is modeled with uranium fuel temperatures ranging from 10,000 K to 75,000 K and hydrogen propellant temperatures ranging from 5,000 K to 50,000 K. At such high temperatures, the uranium fuel, and hydrogen propellant are in a partially ionized state. Material properties needed to conduct neutronics analyses include both neutron cross-sections and the mass densities of engine elements. Neutron cross-sections are called into MCNP through the input file from the MCNP data folder and the mass densities are directly inputted into the MCNP input file. The material properties calculations are discussed in the following sub-sections.

4.1.1 Mass Density Calculations

At such high operating temperatures, hydrogen propellant dissociation and ionization have to be taken into consideration. Dissociation is the process in which a molecule breaks into smaller molecules or its constituent atomic species. In the case of hydrogen gas, it dissociates from diatomic hydrogen to atomic hydrogen. Ionization is the process in which an electron is removed from a molecule or atom. Hydrogen gas dissociation and subsequent ionization are given in Equation 4.1.

$$H_2 \leftrightarrow 2H \leftrightarrow 2p^+ + 2e^- \tag{4.1}$$

Dissociation and ionization of the heated hydrogen gas are calculated using the Saha equations given in Equations 4.2 and 4.3 respectively [45].

$$\frac{[n_H]}{[n_{H_2}]} = \frac{\left(2\pi\left(\frac{M_H}{2}\right)kT\right)^{\frac{3}{2}}}{h^3}\exp\left(\frac{E_2}{kT}\right) \tag{4.2}$$

$$\frac{[n_p][n_e]}{[n_H]} = \frac{(2\pi m_e kT)^{\frac{3}{2}}}{h^3}\exp\left(\frac{E_1}{kT}\right) \tag{4.3}$$

Here n_{H_2}, n_H, n_p and n_e are, respectively, the particle density (number per m^3) of hydrogen gas, atomic hydrogen, ionized hydrogen, and electrons, M_H and m_e are the molar mass of atomic hydrogen and electron, T is the propellant temperature in ^oK, k is the Boltzmann's constant, E_1 = 13.6 eV is the ionization energy of the hydrogen atom, and E_2 = 4.476 eV is the dissociation energy of the hydrogen gas. Both dissociation and ionization were taken into consideration in calculating the densities of the various species at the core temperature.

$$n_o = \frac{PV}{kT} \tag{4.4}$$

The initial particle density of hydrogen gas, n_o, entering the gas core nuclear rocket chamber can be calculated using the ideal gas law given in Equation 4.4. Let 'x' be the percentage of diatomic hydrogen particles that underwent dissociation and 'y' be the percentage of atomic hydrogen particles that underwent ionization at a particular temperature and pressure, then the particle densities of hydrogen gas, atomic hydrogen, ionized hydrogen, and electrons in that system are given in Equations 4.5 through 4.8.

$$[n_{H_2}] = (1 - x)n_o \tag{4.5}$$

$$[n_H] = 2xn_o - 2yn_o \tag{4.6}$$

$$[n_p] = 2yn_o \tag{4.7}$$

$$[n_e] = 2yn_o \tag{4.8}$$

From these particle densities and the Saha equations, the 'x' and 'y' can be calculated as the temperature increases. Here 'x' is called the dissociation factor of hydrogen and 'y' is called the ionization factor of hydrogen. It implies the percentage of hydrogen dissociated and ionized as the temperature of hydrogen goes up while keeping the pressure constant. These dissociation and ionization factor for hydrogen at 1000 atm is plotted in Figure 4.1.

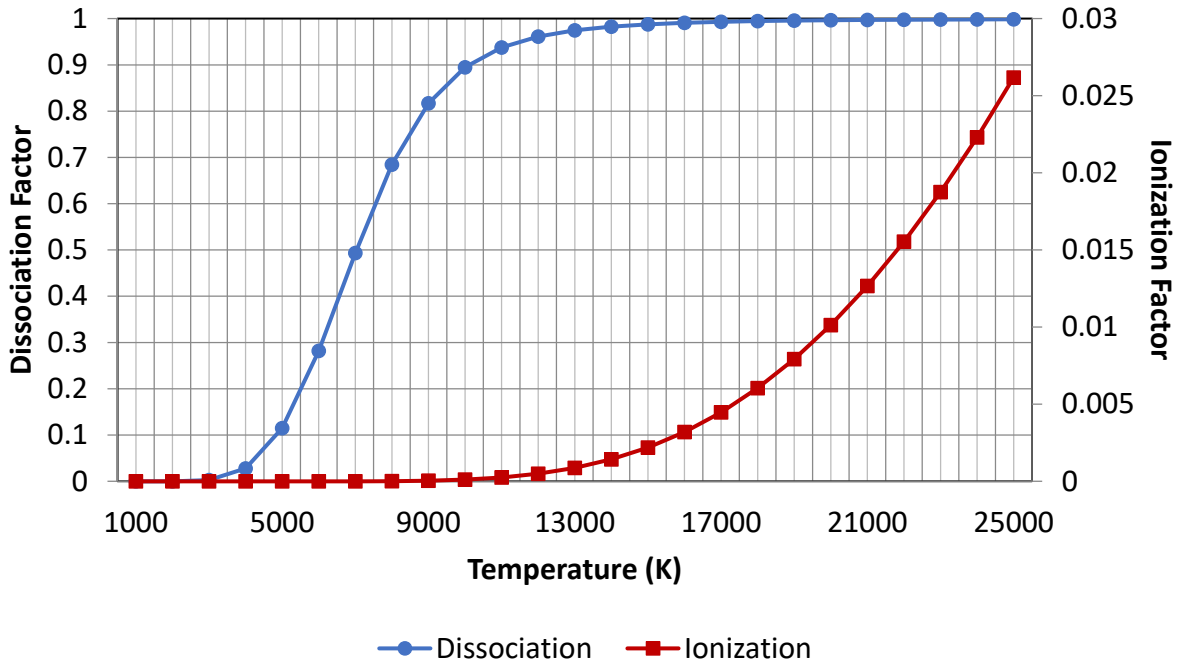

Figure 4.1: Hydrogen dissociation and ionization at 1000 atm pressure with temperature change.

Around 2500 K, the hydrogen gas starts dissociating into atomic hydrogen, and at around 17,000 K the hydrogen gas has completely been dissociated. The ionization of hydrogen at this pressure starts to happen around 21,000 K as seen in Figure 4.1. As the pressure decreases, the dissociation and ionization curves shift towards the left. This is illustrated in Figure 4.2 where the pressure is 1 atm. Here the dissociation begins around 3000 K and the hydrogen is fully

dissociated at 7500 K. Similarly, the ionization starts around 9000 K and the hydrogen is fully ionized around 25,000 K. This is largely due to a reduction in randomizing collisions. If the pressure is increased, the graph will shift towards the right.

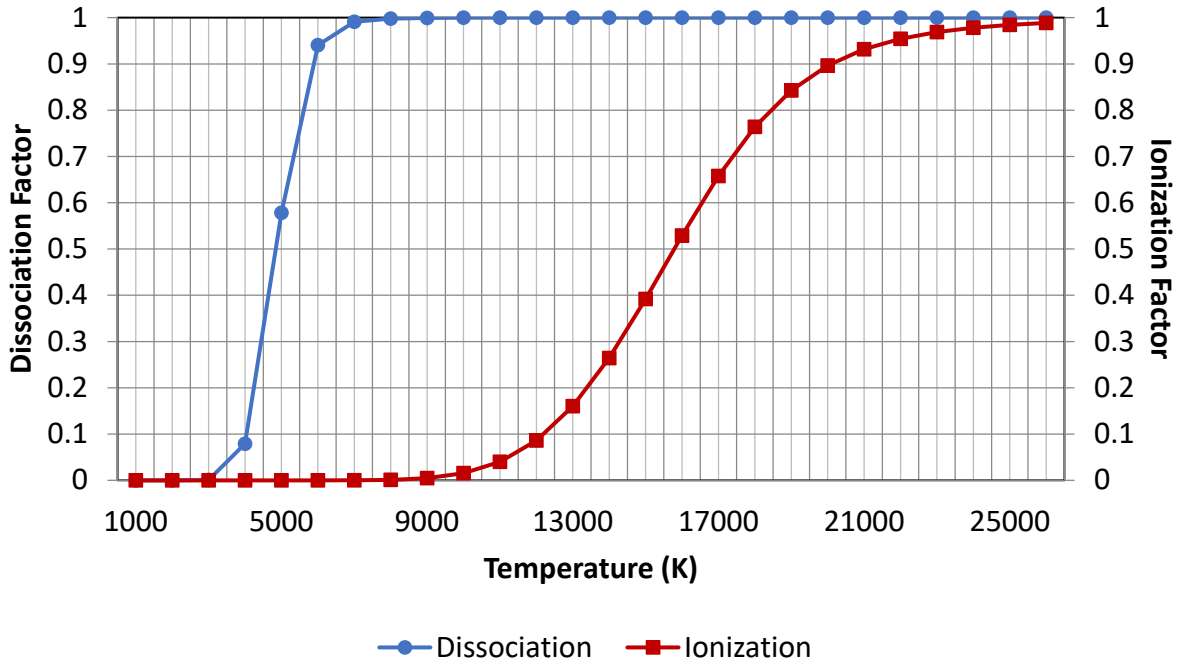

Figure 4.2: Hydrogen dissociation and ionization at 1 atm pressure with temperature change.

From these dissociation and ionization factors, the hydrogen mass observed can be calculated. Mass observed is the average molecular mass of diatomic hydrogen, atomic hydrogen, ionized hydrogen, and electrons at a particular temperature and pressure. This is calculated using Equation 4.9. Using this calculated mass, the hydrogen density can be calculated using the ideal gas law given in Equation 4.10.

$$M_{Obs} = \frac{M_{H_2}}{1 + x + y} = \frac{2.016}{1 + x + y} \tag{4.9}$$

$$\rho_{propellant} = \frac{P_{chamber} M_{Obs}}{R T_{propellant}} \tag{4.10}$$

As the temperature increase, the hydrogen gas dissociated and ionized. This resulted in hydrogen density going down since the pressure is kept constant. The hydrogen density calculated is plotted in Figure 4.3.

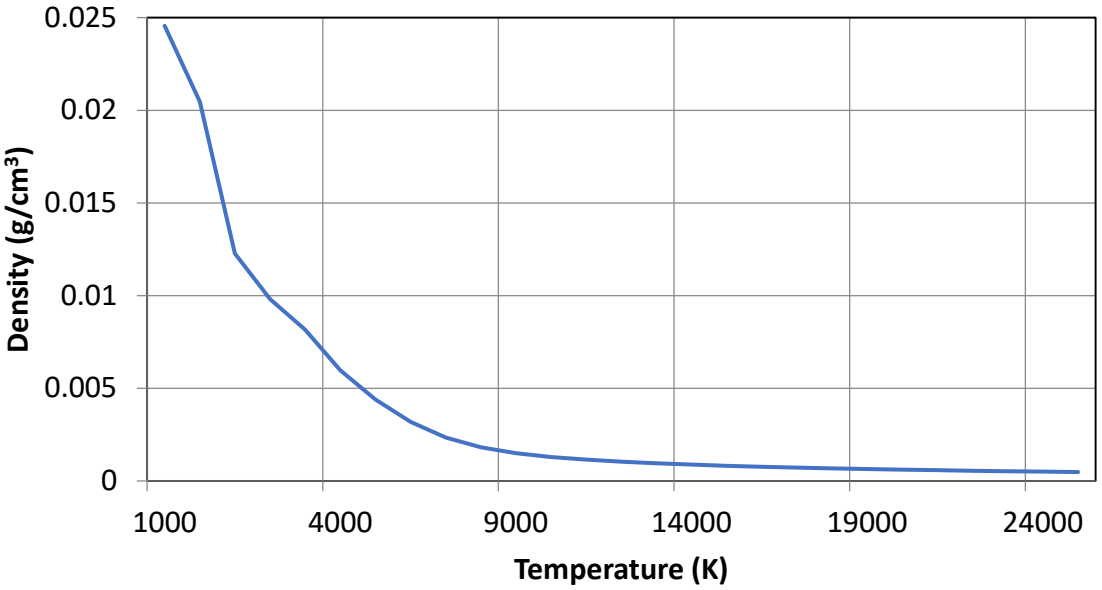

Figure 4.3: Variations in hydrogen propellant density at 1000 atm pressure with temperature.

The density of uranium fuel was also calculated using the ideal gas law. Uranium 233 in gaseous form is considered an ideal gas and since there is no dissociation associated with uranium 233, the ideal gas law was directly applied to obtain the uranium density. Uranium density calculated is plotted in Figure 4.4 below.

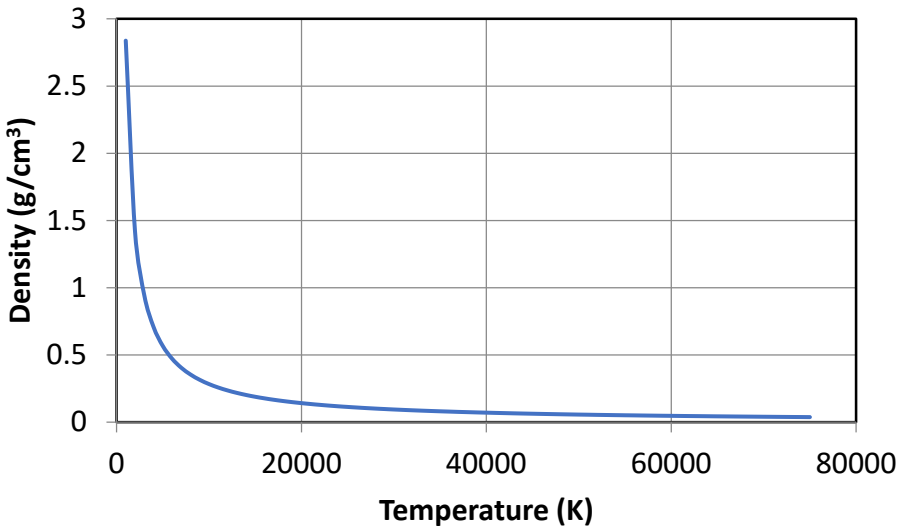

Figure 4.4: Variation in uranium 233 fuel density at 1000 atm pressure with temperature.

All the solid parts of the engine are assumed to be cooled effectively by the regenerative propellant coolant flow and radiator panels. A sample regenerative coolant flow path is illustrated in Figure 4.5. Here the propellant flow lines go around the nozzle and the engine chamber before the propellant goes into the engine cavity.

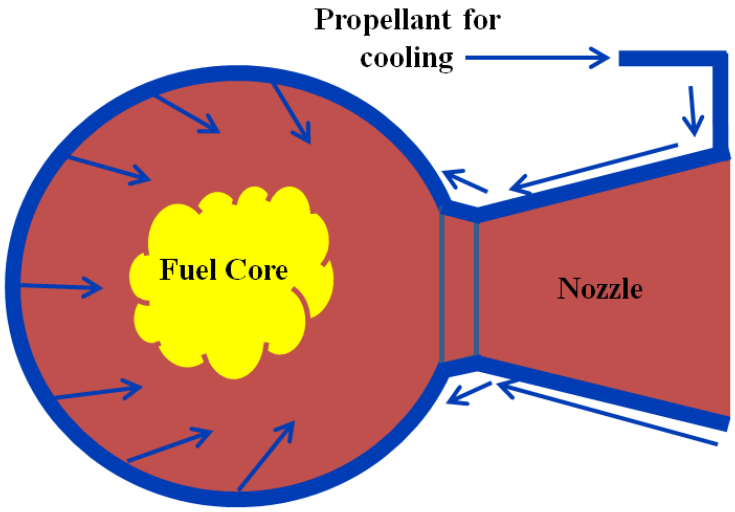

Figure 4.5: A sample regenerative cooling flow path.

This is expected to cool all the engine components. For these component materials, the densities were taken for temperatures below their melting point. Table 4.1 provides the densities used for these materials.

Table 4.1: Material densities used for solid materials in MCNP gas core nuclear rocket model.

Material	**Density (g/cm^3)**
Pressure vessel (Ti-6Al-4V)	4.43
Beryllium reflector	1.85
SiC outer wall	3.21
80% dense SiC w/ 20% H_2	2.57

4.1.2 Neutron Cross-section Calculation from NJOY

Neutron cross-sections for uranium 233 at various high temperatures ranging from 5000 K to 75,000 K are required to conduct neutronics analysis of a realistic gas core nuclear rocket engine. If there are 'n' neutrons per square cm in a beam and 'v' is the speed of neutrons, the intensity of the beam is given as,

$$I = nv \tag{4.11}$$

This intensity of neutron radiation determined by the flow of neutrons is also called the neutron flux. It is measured in neutrons/cm^2/sec. The number of collisions between the neutrons and the nuclei is directly proportional to the intensity of the beam. The number of collisions per second in the entire target can be calculated as given in Equation 4.12 which is valid for the case of a thin target [46].

$$Number\ of\ collisions\ per\ second\ in\ the\ entire\ target = \sigma INAX \tag{4.12}$$

Here σ is the proportionality constant known as the neutron cross-section, N is the atom density of the target, A is the colliding surface area and X is the thickness of the target.

In the MCNP transport code, materials neutron cross-section data up to 3000 K is readily available. For temperatures above 3000 K, the neutron cross-section data has to be added to the MCNP data folder. For this high-temperature data, the fission cross-section in the so-called resonance region is Doppler broadened. This resonance region extends from 1 eV to 2500 eV for uranium-235 at 293.15 K as shown in Figure 4.6. These peaks in the neutron cross-section of any material would be called the resonance region of that material.

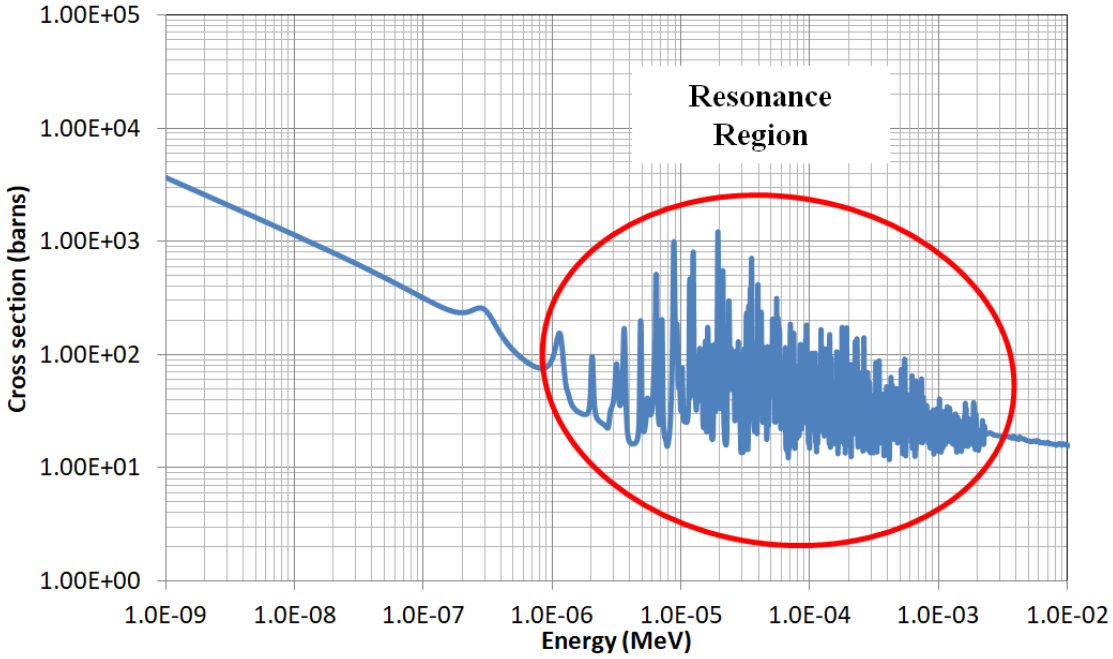

Figure 4.6: Uranium-235 total neutron cross-section at 293.15 K.

The Doppler broadening is related to neutron cross-sectional dependence on the relative velocity between the neutron and the target nucleus. The target nuclei themselves are in continuous thermal motion and they may appear to be greater or less than the neutron speed. These differences in their speeds give rise to the Doppler Effect [47]. The target nucleus thermal motion increases with the increase in the temperature. This leads to the broadening of the

resonance cross-section line shape and its peak magnitude decreasing due to the Doppler Effect. Figure 4.7 illustrates an example of Doppler Broadening at different temperatures for uranium 238 [48].

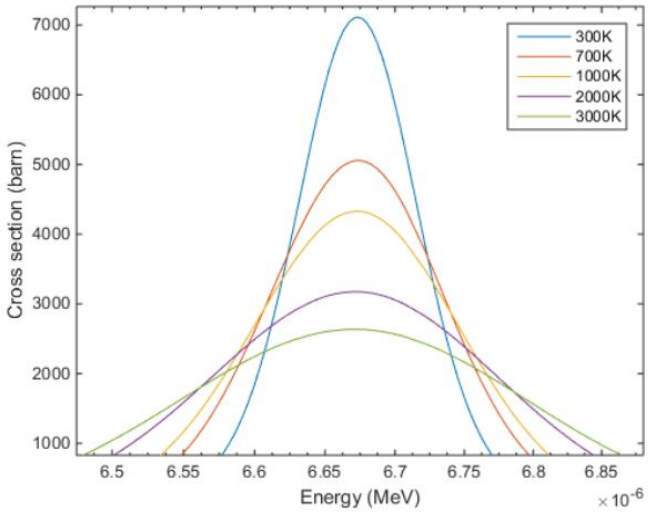

Figure 4.7: Doppler broadening of neutron capture resonance cross-section at E=6.67 eV.

The standard form of the Doppler-broadened cross-section is given in Equation 4.13 [49]. This form is also known as Solbrig's kernel. Here the target nucleus motion is isotropic and the distribution of velocities is defined by the Maxwell-Boltzmann function. This is partially integrated in terms of the relative velocity V.

$$\bar{\sigma}(v) = \frac{1}{v^2}\sqrt{\frac{\gamma}{\pi}}\int_0^\infty dV\sigma(V)V^2\{\exp(-\gamma(V-v)^2) - \exp(-\gamma(V+v)^2)\} \tag{4.13}$$

Where,

$$\gamma = \frac{AM}{2kT} \tag{4.14}$$

Here, σ(v) is the Doppler-broadened cross-section, v is the velocity of the incident neutron, V is the relative velocity of the neutron to the target given as $|v-v'|$, v' is the target velocity, M is the neutron mass, A is the atomic weight ratio of the nuclide, k is the Boltzmann's

constant, and T is the temperature of the nuclei. NJOY software uses this equation to Doppler broaden material cross-section to the specified high temperatures.

As the temperature increases, the resonance cross-section is broadened. However, the total area under the resonance spectral line remains constant. The increase in temperature also impacts the neutron absorption by the fuel core which in turn impacts the criticality of the engine. Thus, it is important to Doppler-broaden correct neutron cross-sections for the neutronics analysis of a gas core engine to obtain a realistic engine response. Figure 4.8 compares the magnitude of this broadening in the resonance region for uranium 233 total neutron cross-section at 293.6 K, corresponding to a thermal reactor typical of terrestrial power plants, and 50,000 K, the expected operating temperature of a gas core rocket.

At the higher temperature, the neutron cross-section is broadened and the peak magnitude decreased. Similarly, uranium 235 total neutron cross-section at 293.6 K and 50,000 K is illustrated in Figure 4.9. Similarly, neutron cross-sections were obtained for other fuel materials for temperatures ranging from 293.6 K to 75,000 K in this thesis study. These cross-section data were input into the MCNP data folder and called from MCNP for the neutronics calculations.

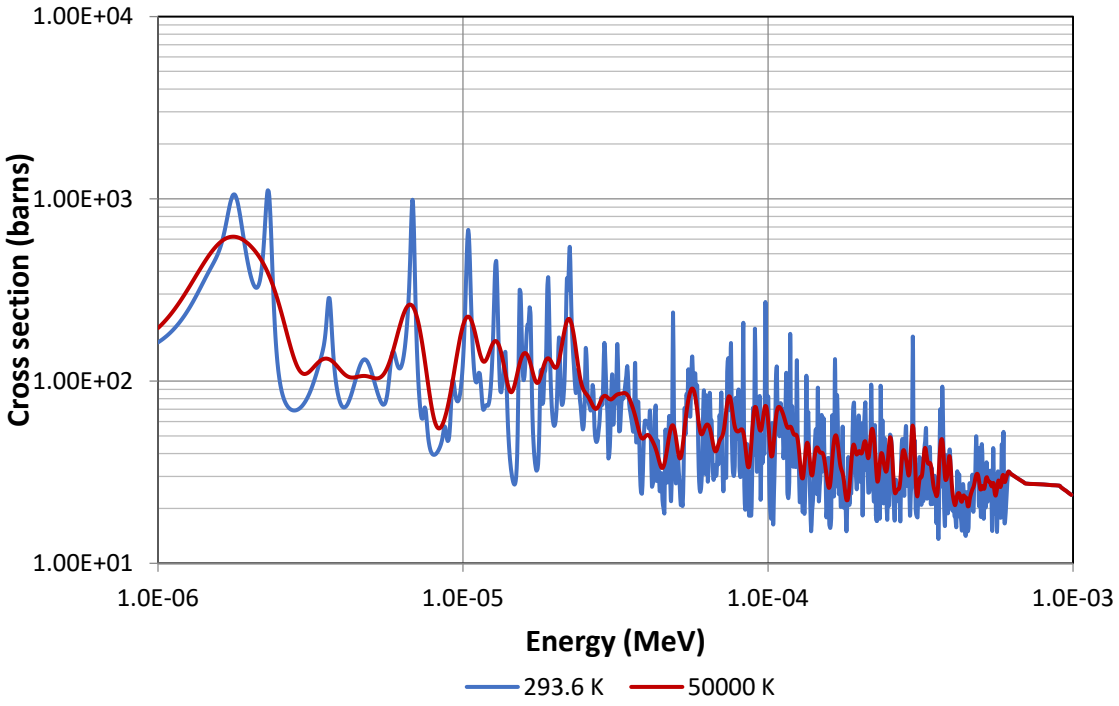

Figure 4.8: Total neutron cross-section comparison of U-233.

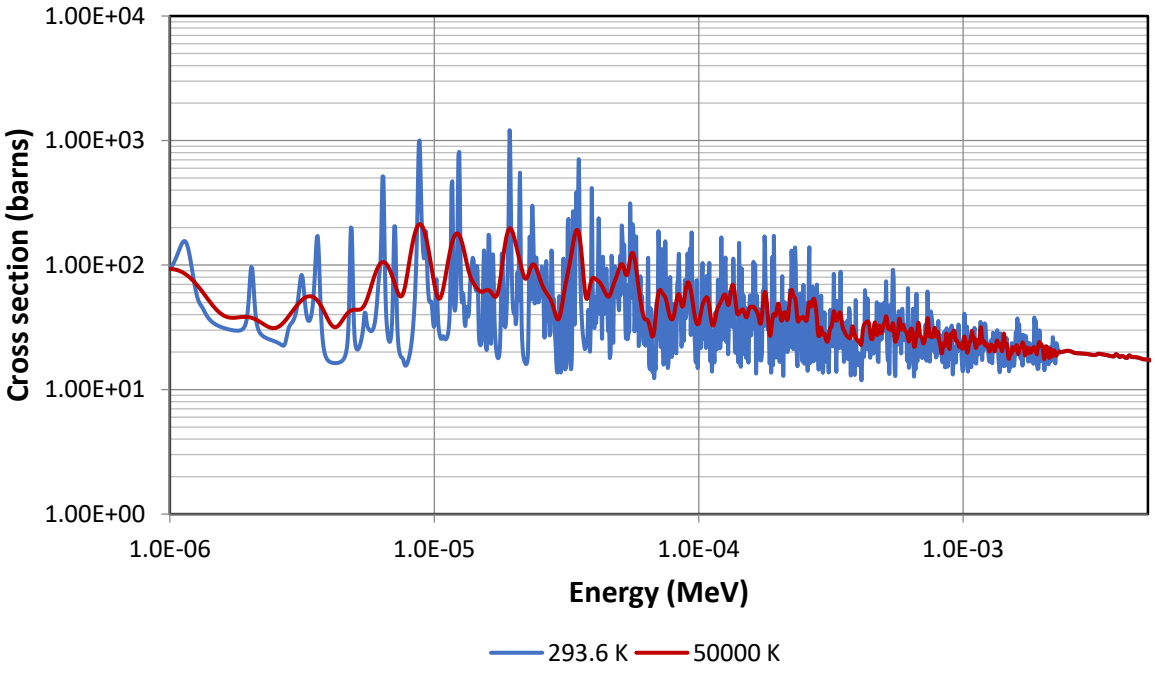

Figure 4.9: Total neutron cross-section comparison of U-235.

4.2 Neutronic Analysis of Gas Core Nuclear Rocket in MCNP

The goal of this thesis work is to achieve a critical gas core nuclear rocket. Criticality was obtained in this work for a spherical non-homogenous engine with uranium 233 as the fuel and hydrogen as the propellant. In a critical engine, the number of neutrons in one generation and the number of neutrons in the previous generation are equal. The neutron flux in the system and the power distribution in the engine can be calculated using the nuclear diffusion theory. In reference 28, the neutron flux was derived for all regions of the gas core nuclear reactor as given in Equation 4.15. In their model, three different regions are defined – the fuel core region, the propellant region, and the reflector region. The focus of this work is primarily on the reactor and those systems that maintain its criticality. In this respect, the cooling scheme, the porous wall gas distributor, and pressure vessel walls are assumed.

$$\phi(r) = \begin{cases} \dfrac{q_0 \sin(\alpha r)}{\alpha r}, & 0 \le r \le \mathrm{R_{fuel}} \\ q_0 \left\{ \left[\dfrac{\sin(\alpha R_{fuel})}{\alpha R_{fuel}} - \cos(\alpha R_{fuel}) \right] \left(\dfrac{R_{fuel}}{r} \right) + \cos(\alpha R_{fuel}) \right\}, & R_{fuel} \le r \le R_{Prop} \\ q_0 \dfrac{(\alpha T_{prop} \cos(\alpha R_{fuel}) + \sin(\alpha R_{fuel}))}{\sinh(\beta \mathrm{T}^*_{\mathrm{ref}})} \dfrac{\sinh[\beta(R^*_{Rx} - r)]}{\alpha r}, & R_{prop} \le r \le R_{ref} \end{cases} \quad (4.15)$$

Here $\phi(r)$ is the neutron flux, q_0 is the local core power density, R_{fuel} is the radius of the fuel core, R_{prop} is the propellant radius – from the center of the engine to the propellant outer edge, R_{ref} is the reflector radius – from the center of the engine to the reflector outer edge, T_{prop} is the propellant thickness calculated as ($R_{prop} - R_{fuel}$), R^*_{Rx} is the extrapolated reflector radius where the neutron flux goes to zero, T^*_{ref} is the reflector thickness including the extrapolated reflector region calculated as ($R^*_{Rx} - R_{prop}$), α is the buckling in the core given as in Equation 4.16 and β is the material buckling in the reflector given as in Equation 4.17 [28]. Material

buckling can be defined as the difference between neutron production and neutron absorption. Figure 4.10 illustrates the dimension of the engine for which this neutron flux was calculated.

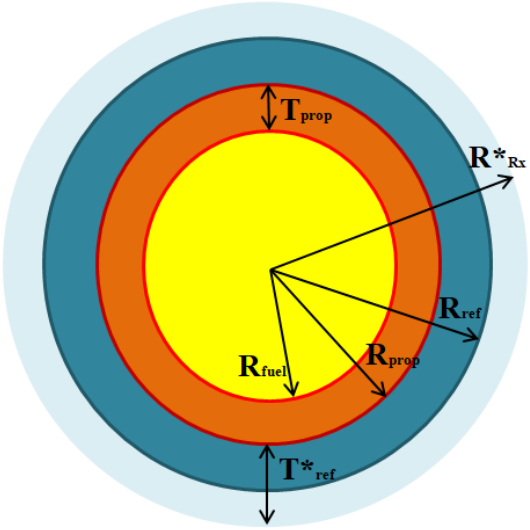

Figure 4.10: Spherical gas core nuclear rocket model with three regions.

$$\alpha = \frac{\left(\frac{\nu\Sigma_f^c}{k_{eff}} - \Sigma_a^c\right)}{D_c} = \frac{3P^2\left(\frac{\nu\sigma_f^c}{k_{eff}} - \sigma_a^c\right)\sigma_{tr}^c}{R^2T^2} \tag{4.16}$$

$$\beta = \frac{\Sigma_a^r}{D_r} \tag{4.17}$$

Here ν is the number of neutrons produced per fission, Σ^c_f and Σ^c_a are the macroscopic fission and neutron absorption cross-sections at the core respectively, k_{eff} is the multiplication factor, D_c is the diffusion coefficient at the core, P is the core pressure, T is the core temperature, R is the gas constant for the uranium gas, σ^c_f , σ^c_a, and σ^c_{tr} are the microscopic fission, neutron absorption and transport cross-sections at the core respectively [28]. Similarly, Σ^r_a and D_r are the macroscopic neutron absorption cross-section and diffusion coefficient at the reflector respectively.

The flux calculations and criticality calculations in this thesis work for continuous energy neutron diffusion are carried out by the MCNP transport code. Studies were conducted by varying the system temperatures and engine dimensions. The studies carried out and their results are discussed in the following sub-sections.

4.2.1 Pre-Heat Transfer Neutronics Analysis – Sensitivity Study

For this study, the fuel core temperature and the propellant temperature were varied to understand their impact on the engine's criticality. The engine dimensions and temperatures used for this study are given in Table 3.2 in the previous chapter. The engine studied was a non-homogenous engine – the fuel and the propellant do not mix. Criticality was obtained for an engine with uranium covering 70 to 80 percent of the cavity or chamber volume. The cavity region is the region containing the fissioning fuel core and the hydrogen propellant. In Figure 4.10, the cavity volume is the volume of the sphere with radius R_{prop}. A 4.3 m cavity diameter was needed to achieve critical condition for uranium 233 at 55,000 K. At lower uranium 233 temperatures, the criticality can be obtained at a smaller size cavity or lower uranium volume occupancy. For 10,000 K U-233, only 30 percent cavity volume of uranium was needed to yield criticality. Figure 4.11 shows the k_{eff} change with an increase in core temperature. The k_{eff} goes down as the core temperature increases due to the uranium being less dense at higher temperatures while keeping the pressure constant at 14696 psi (or 1000 atm).

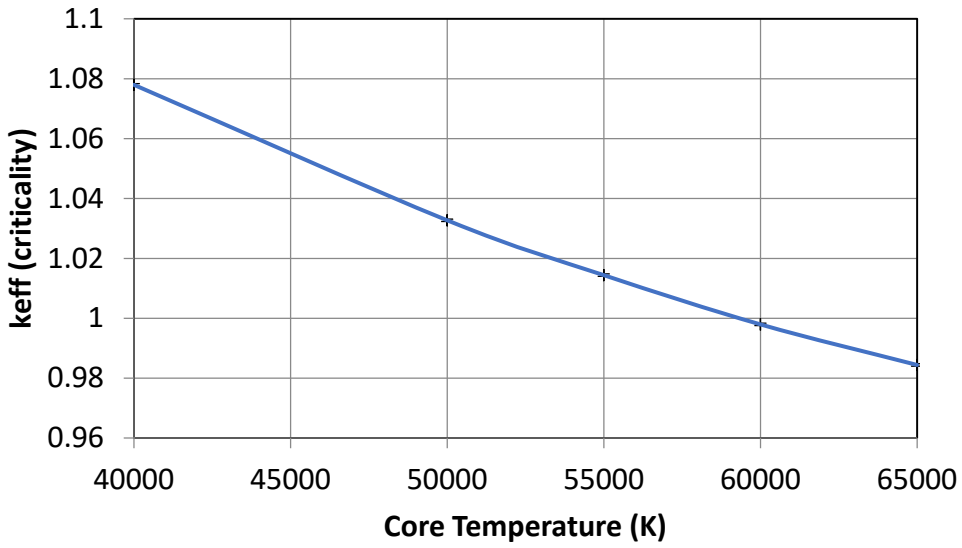

Figure 4.11: Change in k_{eff} as the core temperature increases at 1000 atm pressure.

In this first set of studies, the k_{eff} was relatively insensitive to beryllium reflector thickness (thickness of 0.61 m), suggesting that the reactor behaves as one would expect from a finite engine where most neutron scattering processes occur primarily before reaching the reflector region. Figure 4.12 shows the change in criticality with a change in uranium volume occupancy percentage for different hydrogen temperatures. Uranium volume occupancy percentage is defined as the percentage volume of uranium in the gas core nuclear rocket chamber cavity. The spherical fuel core was kept at the center of the chamber with hydrogen around it. The chamber cavity is filled with uranium and hydrogen only. Uranium volume occupancy percentage can be calculated as below,

$$U - volume\ occupancy\ \% = \frac{Volume\ of\ uranium\ in\ the\ cavity}{Total\ chamber\ cavity\ volume} * 100 \tag{4.18}$$

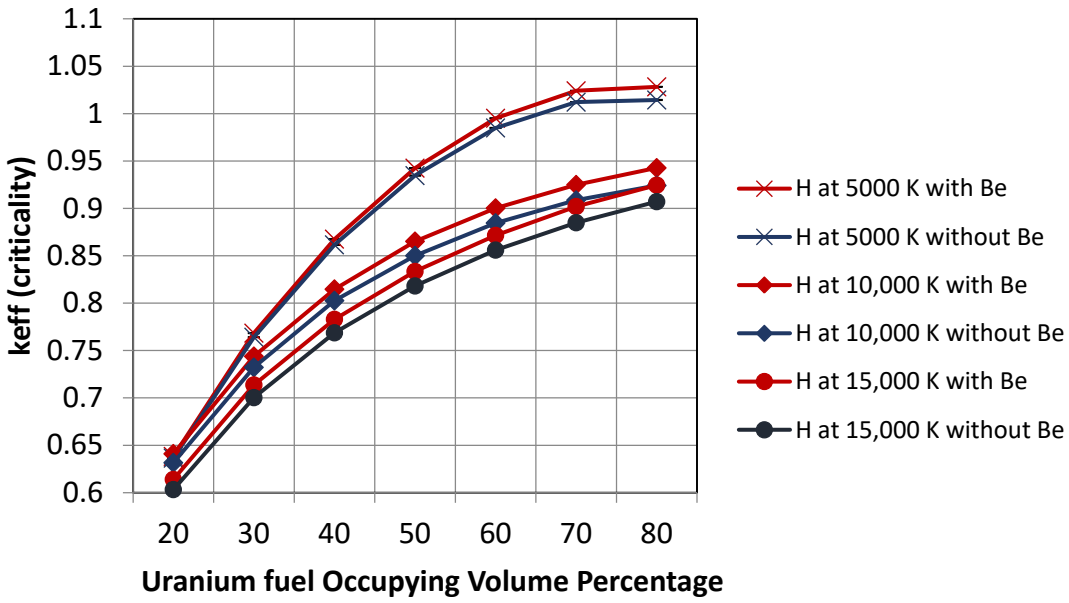

Figure 4.12: Change in k_{eff} with the change in uranium volume occupancy percentage and hydrogen temperatures.

As the uranium occupying volume percent is increased (by increasing the centrally located spherical uranium core's diameter) in the spherical cavity, the k_{eff} increases due to an increase in the amount of uranium present in the system cavity. In Figure 4.14, an increase in uranium volume-occupying percent means that the uranium core sphere gets larger while the hydrogen propellant thickness gets smaller. The cavity volume remains constant and it is the sum of the uranium sphere volume and the hydrogen hollow sphere volume. At lower uranium occupying volume percent, the beryllium reflector's impact on the criticality is negligible as compared to at higher uranium occupying volume percent. This would be due to the large distance between the uranium core outer edge and the beryllium reflector at low uranium volume occupancy percent. The neutrons will have to travel a sufficient distance in hydrogen propellant which is also acting as a moderator and in silicon carbide support structure before reaching the beryllium reflector. This renders the use of beryllium reflector in a large gas core nuclear rocket less effective. Additionally, with the hydrogen propellant temperature increase, the k_{eff} decreases

due to the lower density of hydrogen around the core to moderate the neutrons. However, the impact of beryllium is still negligible due to the presence of coolant hydrogen between the uranium core and the reflector. To understand the effect of different parts of the engine on k_{eff}, each layer of the gas core was studied. Figure 4.13 illustrates how the k_{eff} varied as layers of a gas core nuclear rocket were added as cells in MCNP and Figure 4.14 illustrates a full engine model with all layers.

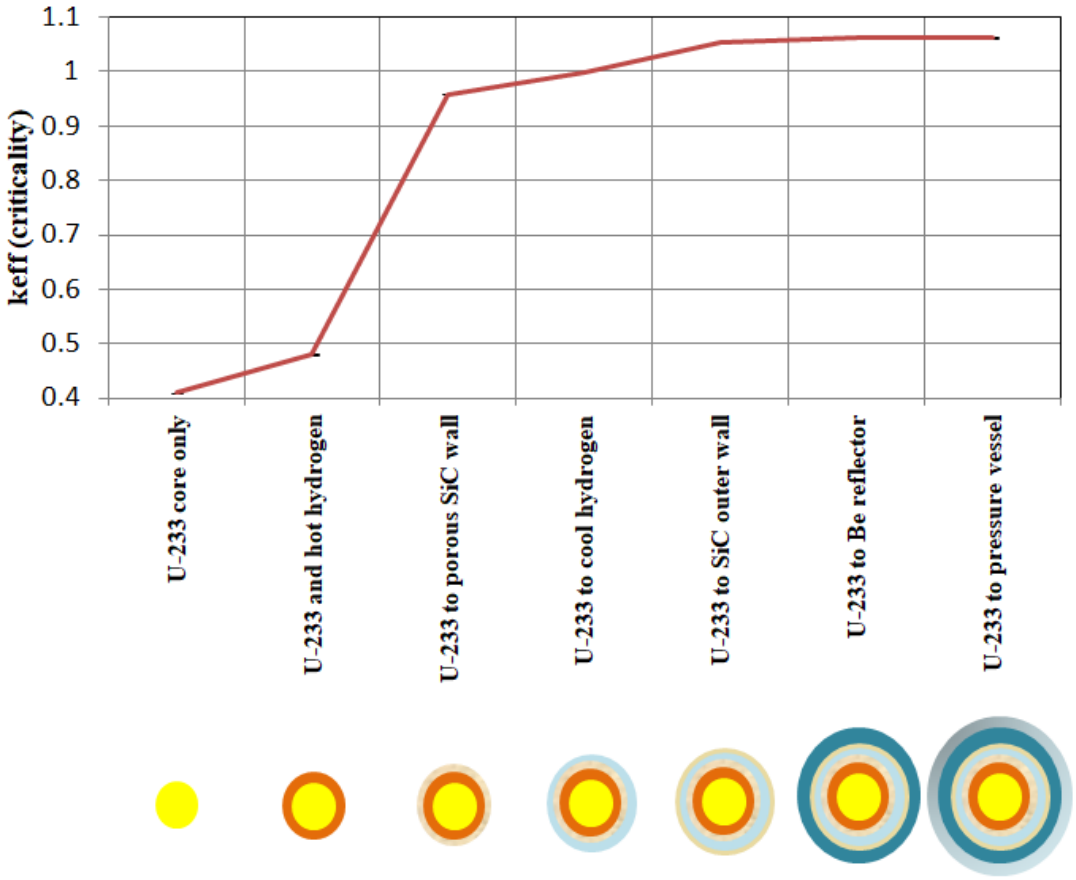

Figure 4.13: Change in k_{eff} as the engine layers were added radially outwards.

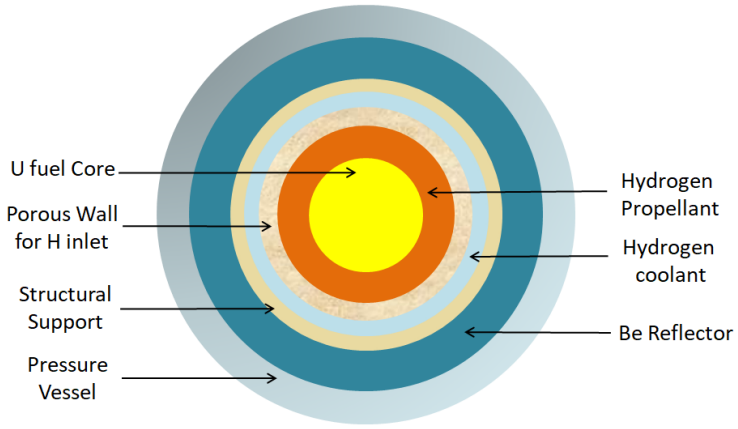

Figure 4.14: Gas core nuclear rocket engine schematic with all layers.

This layer-adding study was conducted to understand why the impact of beryllium reflector is negligible. From Figure 4.13, it can be seen that the major jump in k_{eff} happens when the SiC wall with the hydrogen inlet was added. This SiC porous wall is fairly close to the core and its neutron scattering properties could be affecting the criticality. It should also be noted that this porous wall thickness was taken as 15 cm, which could add a further distance of the core from the reflector. Therefore, the k_{eff} sensitivity to this SiC porous wall thickness was explored. Figure 4.15 shows the criticality change with the change in SiC porous wall thickness. Here 80 percent uranium volume-occupying percentage was used and the outer SiC structural support was removed to have SiC material only at the porous inlet.

The SiC porous inlet wall consists of hydrogen propellant and silicon carbide. The hydrogen present in this porous wall is cold hydrogen. This cold hydrogen was integrated into the silicon carbide material as a weight fraction at that region. Silicon carbide weight fraction was taken to be 80 percent. The weight fraction values were input in the MCNP input file for neutronics analysis. The 80 percent dense silicon carbide was used because it was the recommended weight fraction used in the centrifugal nuclear thermal rocket described in Chapter 6.

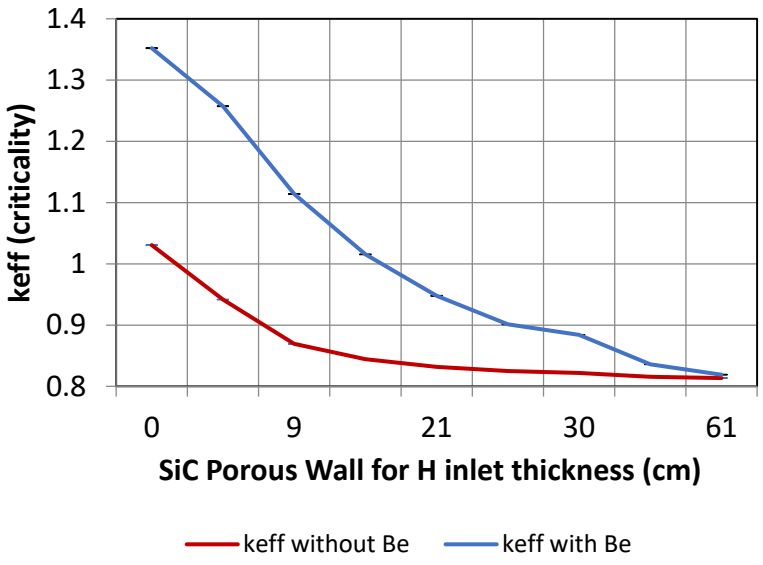

Figure 4.15: Change in k_{eff} with the change in propellant inlet wall thickness.

Increasing the SiC porous wall thickness led to the decrease in k_{eff} of the engine. At smaller SiC porous wall thickness, the impact of the beryllium reflector is higher. At larger SiC porous wall thickness, the beryllium reflector's impact is negligible and this is due to the reflector being far from the fuel core. The increase seen in Figure 4.13 in k_{eff} by the addition of SiC porous wall layer may be due to the presence of cold hydrogen with a higher density coming through this wall. The hydrogen concentration in this SiC porous wall is 20 percent by weight. From Figure 4.13, it can also be seen that the hydrogen coolant loop increased the k_{eff} of the engine. Therefore, the impact of the hydrogen coolant region thickness on criticality was explored. Figure 4.16 shows the criticality change with the change in hydrogen coolant region thickness.

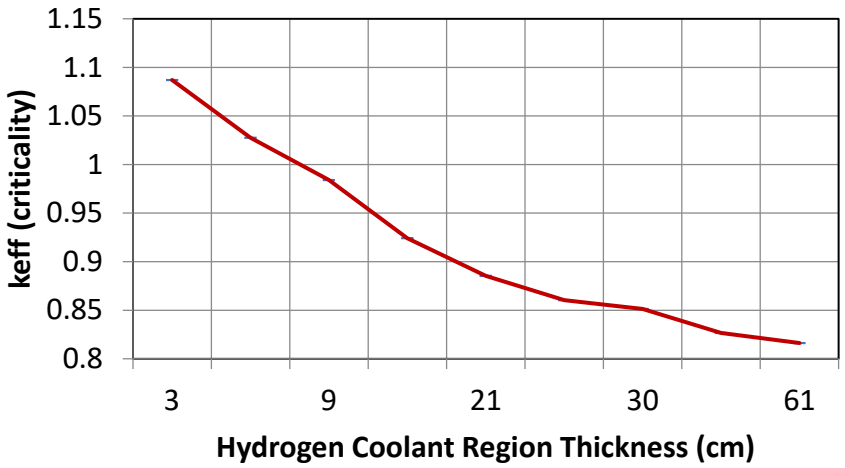

Figure 4.16: Change in k_{eff} with the change in hydrogen coolant region thickness.

Here no beryllium reflector was used and 80 percent uranium volume-occupying percentage was used. The increase in coolant region thickness led to a decrease in the criticality of the engine. It should be noted that the thicknesses of the SiC porous wall and the hydrogen coolant region were both 15 cm in the initial sensitivity studies done. These thicknesses are too large and they increase the chance of neutron escape from the system or neutron absorption by non-fuel material in this engine. To understand the change in k_{eff} to the thicknesses of coolant and the SiC inlet wall, post-heat transfer analysis studies were conducted on realistic thicknesses as used in other advanced nuclear rockets such as centrifugal nuclear thermal rockets.

4.2.2 Post-Heat Transfer Neutronics Analysis – realistic engine size considerations

The heat transfer analysis is discussed in detail in chapter 5 of this dissertation. From the heat transfer analysis, it was found that the hydrogen temperature in the system can range from 10,000 K to 50,000 K. From Figure 4.12, it was found that the k_{eff} decreases with the increase in the hydrogen temperature for the initial geometry used. With the same engine model as the initial neutronics study, a study was conducted for hydrogen at 50,000 K with varying uranium volume-

occupying percentages. Figure 4.17 shows that the k_{eff} of an engine with hydrogen at 50,000 K will not be able to achieve critical conditions with the initial geometry.

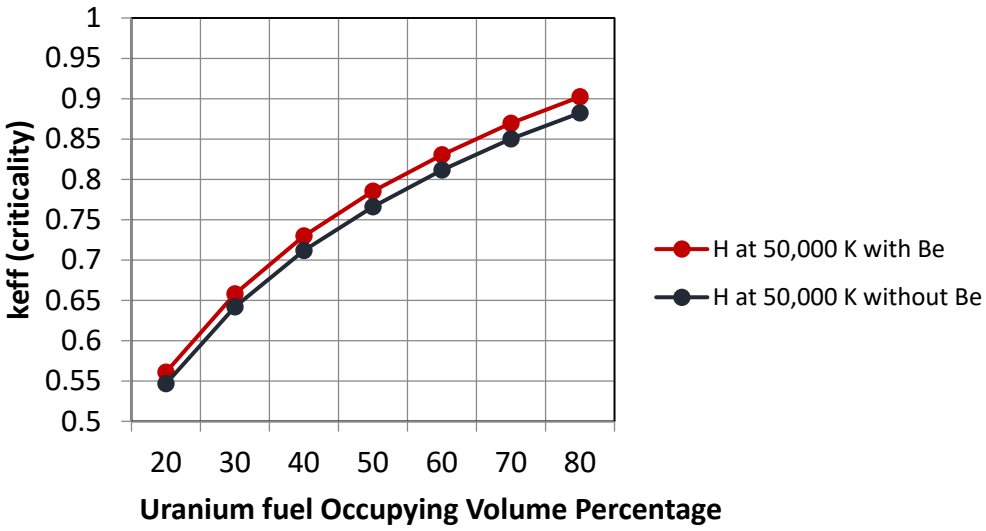

Figure 4.17: Criticality change with uranium volume-occupying percentage for hydrogen at 50,000 K.

Therefore, in this study, the thicknesses of the SiC porous wall and the hydrogen coolant region were changed from 15 cm to 0.5 cm and 1 cm respectively. This new value was taken from the SiC porous wall thickness in other advanced nuclear rockets such as the centrifugal nuclear thermal rocket (CNTR) discussed in chapter 6 of this dissertation. Along with the thickness change, the hydrogen temperature was increased from 5,000 K to 50,000 K range. The impact of the beryllium reflector on this engine was also studied.

The beryllium reflector's impact on the criticality increased considerably when realistic engine sizes were used. Figure 4.18 shows the change in k_{eff} with the change in beryllium reflector thickness as well as the change in hydrogen temperatures. For this study, 20 percent uranium volume-occupying percentage was used. No outer silicon carbide wall was used either to reduce the neutron escape or neutron absorption in non-fuel materials in the engine.

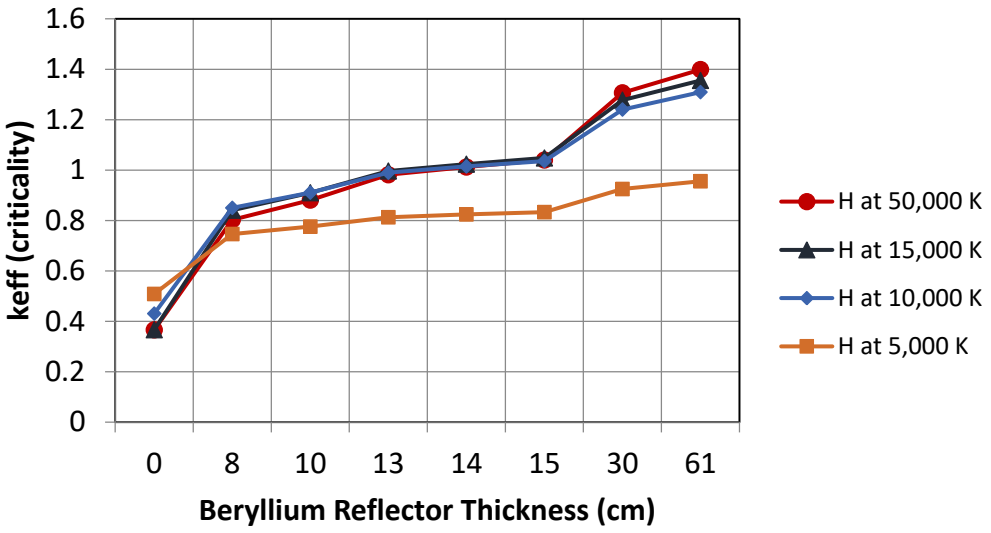

Figure 4.18: Change in k_{eff} with varying reflector thicknesses and hydrogen temperatures.

With the increase in beryllium reflector thickness, the k_{eff} increases too. The impact of beryllium is high as compared to the results in Figure 4.12. It is interesting to note that with the presence of beryllium in the system, the k_{eff} increases with the increase in the hydrogen temperature and when there is no beryllium, the k_{eff} decreases with the increase in the hydrogen temperature. In Figure 4.12, it was observed that the k_{eff} decreased with the increase in hydrogen temperature and the impact of beryllium was negligible. This is similar to the case shown in Figure 4.18 when there is no beryllium in the system.

At higher hydrogen temperatures, the hydrogen density is lower than at lower hydrogen temperatures while keeping the pressure constant. Since the uranium volume-occupying percentage is only 20 percent, the neutrons have to travel to the reflector and then back to the fuel core. With the increase in hydrogen density at lower temperatures (5000 K), there are more collisions of neutrons and the chance of neutrons escaping the system is higher, leading to lower k_{eff}. Whereas, at higher hydrogen temperatures (50,000 K), the lower hydrogen density leads to lesser collisions of neutrons and escape from the system as they make their way to the reflector

and back to the fuel core. When there is no beryllium reflector in the system, the neutrons are not reflected back and with the lower density of the high-temperature (50,000 K) hydrogen, there are not enough collisions and moderation occurring in the system, leading to lower k_{eff}. If the size of the uranium core is increased considerably, the k_{eff} should decrease with an increase in hydrogen temperature. Figure 4.19 shows the criticality change with the hydrogen propellant temperature change.

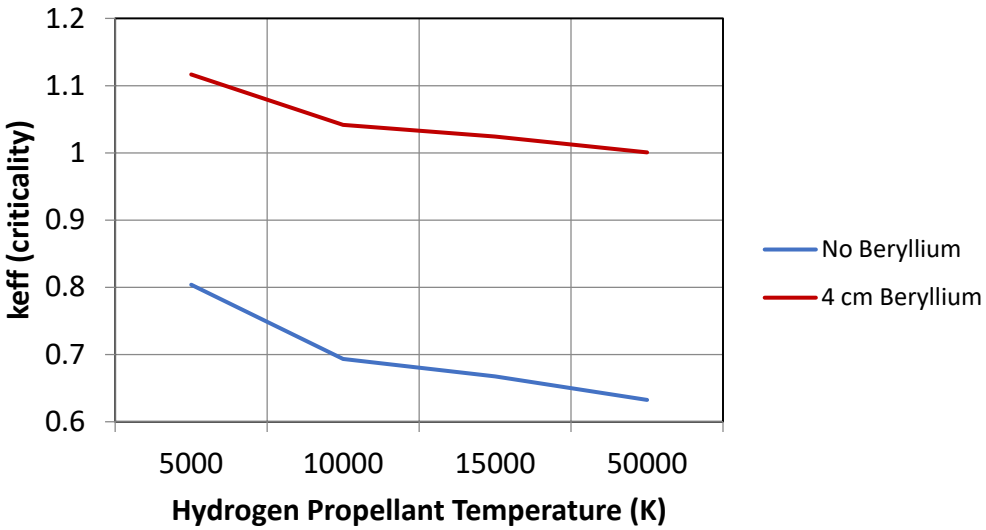

Figure 4.19: Criticality change with the hydrogen propellant temperature for 80% uranium volume-occupying percentage.

In this case, the uranium core size was increased to 80 percent uranium volume-occupying percentage. As expected, the k_{eff} decreased with the increase in hydrogen temperature. This is because now the neutron's distance to the reflector and back to the fuel core is reduced considerably. At 80 percent uranium volume-occupying percentage, more neutron collisions will lead to higher k_{eff}. With the higher hydrogen density at lower temperatures, there are more neutron collisions and slowing down (moderation) for lower temperature hydrogen propellant than at higher temperature hydrogen propellant. Again the impact of beryllium can be seen to be high in this case study too.

The mass of uranium required for this engine ranged from 420 kg at 20 percent volume-occupying percentage to 1,680 kg at 80 percent volume-occupying percentage. However, in critical conditions, the total mass of the engine is better for the 80 percent uranium volume-occupying percentage. The total mass of the engine including the reflector and the pressure vessel ranged from 98,050 kg at 80 percent uranium volume-occupying percentage to 120,500 kg at 20 percent uranium volume-occupying fraction.

From the MCNP output file, it was observed that the largest percentage of fissions is caused by neutrons in the intermediate energy level (0.625 eV to 100 keV) or the thermal energy levels (less than 0.625 eV). For example, a critical reactor with an 80 percent uranium volume-occupying percentage has 71 percent of its fission caused by intermediate energy neutrons. For a critical reactor with a 20 percent uranium volume-occupying percentage has 65 percent of its fission caused by thermal energy neutrons. This could be happening due to the moderation happening to the neutrons as it travels in hydrogen propellant. At a 20 percent uranium volume-occupying percentage, the neutrons have to travel through a larger thickness of hydrogen which leads to the neutrons being slowed down to the thermal energy levels. The energy spectrums for neutrons obtained from MCNP for the full engine are plotted in Figures 4.20 and 4.21. Figure 4.20 is for the case of 20 percent uranium volume-occupying percentage and Figure 4.21 is for the case of 80 percent uranium volume-occupying percentage.

It is interesting to note that in the 20 percent uranium volume-occupying percentage case the peak is narrower and higher in magnitude as compared to the case of 80 percent uranium volume-occupying percentage. In Figure 4.21, the spectrum is wider and it is mostly present at energies higher than 1 eV (or intermediate energy range). There is a smaller peak present in

Figure 4.20 with energy less than 1 eV corresponding to the thermal neutron energy range. These neutron flux plots provide the neutron energy range present in the complete critical engine.

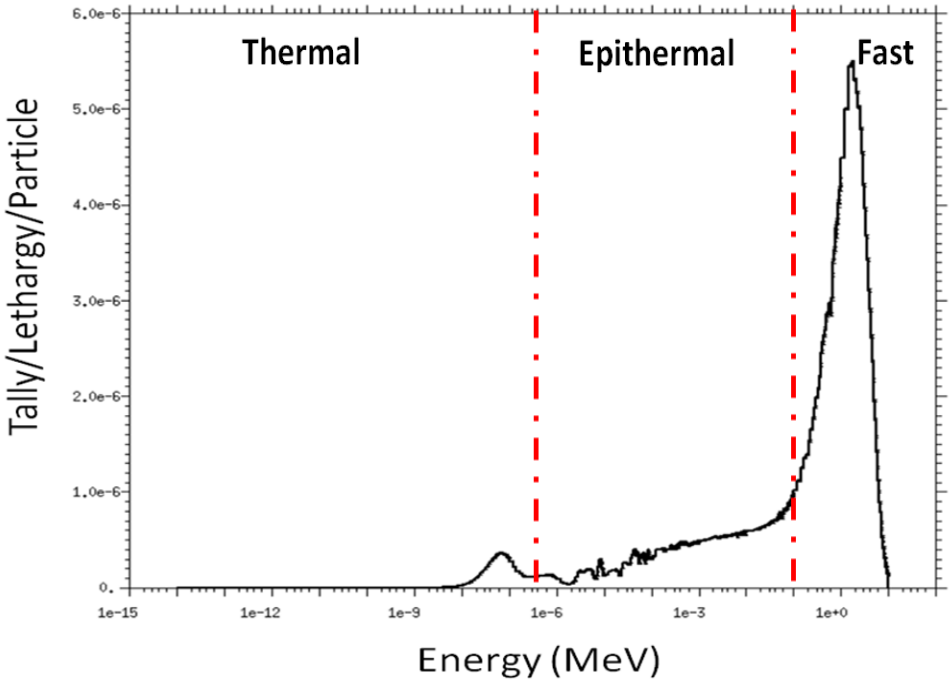

Figure 4.20: A log-linear plot of energy normalized neutron flux versus energy for neutrons in a gas core nuclear rocket with a 20 percent uranium volume-occupying percentage.

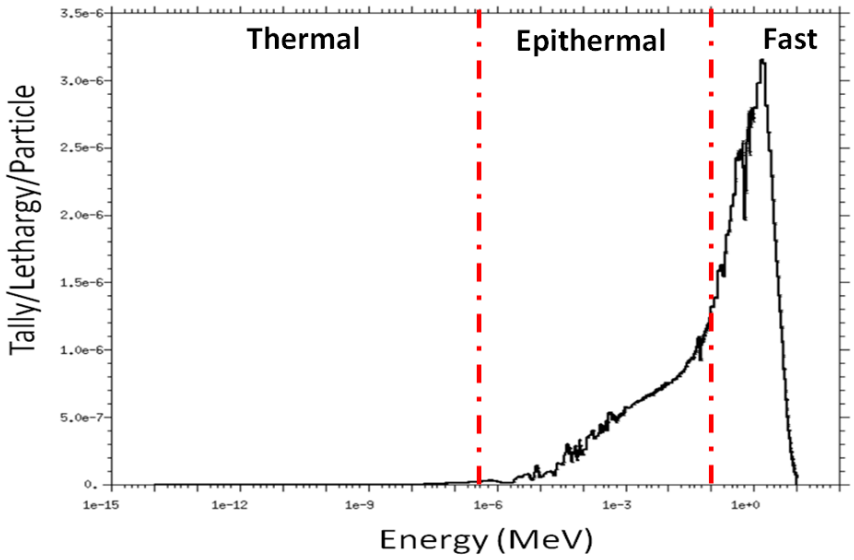

Figure 4.21: A log-linear plot of energy normalized neutron flux versus energy for neutrons in a gas core nuclear rocket with an 80 percent uranium volume-occupying percentage.

4.3 Recommendations

From all these neutronics studies, it can be concluded that a spherical gas core nuclear rocket can achieve criticality. The geometry and the temperatures of the engine impact the criticality considerably. The gas core nuclear rocket could be an epithermal or a thermal reactor depending on the uranium fuel core size. The fuel core size has to be adjusted to make sure the neutron moderation happening in the engine is optimum with reduced neutron escape from the system or neutron absorption at non-fuel materials. It is recommended to have a 20 percent uranium volume-occupying percentage with hydrogen propellant at 50,000 K. This is recommended because – (1) less uranium has to be used and confined in the engine cavity, and (2) higher hydrogen temperature means higher performance from this engine. However, the mass of the engine will be higher for this case due to the large thickness of beryllium used to achieve criticality. The full engine system description is discussed in the next chapter.

CHAPTER 5 System Description of the Engine

5.1 Heat Transfer

Heat transfer analysis of a gas core nuclear rocket was carried out using basic heat transfer equations. As the hydrogen propellant flows around the hot fissioning plasma core, both convective and radiative heat transfer will occur. The source of heat is the fissioning of uranium fuel. Some of the heat will be lost from the hydrogen propellant to the surroundings again in form of radiative and convective heat transfer. The heated hydrogen will leave the system through a converging-diverging nozzle to produce thrust. The focus of this heat transfer analysis is to determine the hydrogen propellant temperature which is used in the neutronics and engine performance calculations. Figure 5.1 below illustrates the heat transfer processes prevailing in a gas core nuclear rocket engine.

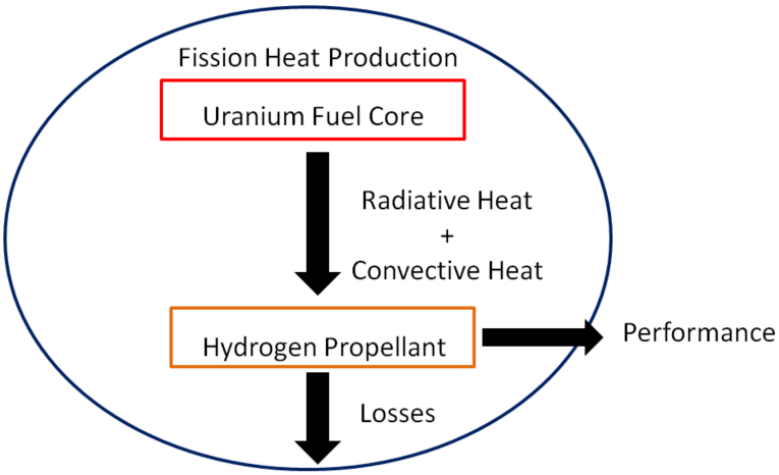

Figure 5.1: Block diagram of the heat transfer happening in a gas core nuclear rocket engine.

5.1.1 Uranium Fuel Core Heat Transfer

The uranium fuel core is the source of heat for the gas core engine. This heat is produced from the fissioning of uranium 233 to release energy. The fission of one atom of uranium 233 generates 197.9 MeV (or $3.171*10^{-11}$ J) of energy [50]. This released energy sustains the uranium core temperature. Since the uranium is in the gaseous state, it can have a higher temperature as compared to solid or liquid uranium cores. The heat produced from the uranium fission is transferred to the surroundings through radiation and convection. Thermal radiation is the transfer of energy in the form of electromagnetic waves from a hot emitter at some finite temperature to the surroundings [51]. The rate at which energy is released per unit area (W/m^2) from a surface is called the surface emissive power, E (also known as the heat flux). Stefan Boltzmann's law gives the heat flux from a surface as

$$E = \varepsilon \sigma T_s^4 \tag{5.1}$$

Here ε is the material emissivity ($0 \leq \varepsilon \leq 1$) which provides a measure of how efficiently a surface emits energy relative to a blackbody, σ is the Stefan Boltzmann constant ($\sigma = 5.67*10^{-8}$ $W/m^2.K^4$), and T_s is the absolute temperature of the surface. A blackbody is an ideal radiator of heat with emissivity being equal to one. Uranium fuel core is treated as an ideal black body emitter ($\varepsilon_{uranium} = 1$) due to its high temperature. At high temperatures, the body has to completely emit the heat to the surroundings where the temperatures are comparatively lower. As the temperature of a material increases, its emissivity increases too. The blackbody spectral intensity is determined by the Planck distribution which is given in Equation 5.2.

$$I_{\lambda,b}(\lambda, T) = \frac{2hc_o^2}{\lambda^5 \left[\exp\left(\frac{hc_o}{\lambda k_B T}\right) - 1\right]} = \frac{E_{\lambda,b}(\lambda, T)}{\pi} \tag{5.2}$$

Here $I_{\lambda,b}$ is the blackbody spectral intensity, λ is the wavelength of the energy wave emitted, T is the absolute temperature of the blackbody, h is the universal Planck's constant (h = $6.626*10^{-34}$ J.s), c_o is the speed of light ($c_o = 2.998*10^8$ m/s), k_B is the Boltzmann constant ($k_B = 1.381*10^{-23}$ J/K), and $E_{\lambda,b}$ is the blackbody spectral emissive power. This equation gives the heat radiation intensity at the surface of the uranium core surface at a particular temperature. Figure 5.2 plots the spectral radiance emitted by a blackbody at 55,000 K.

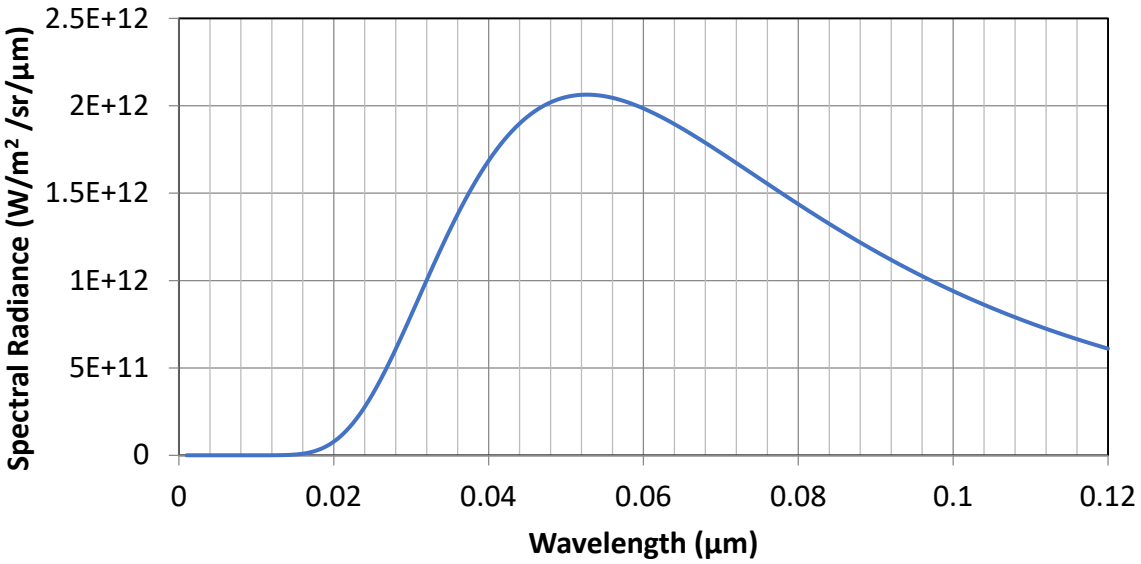

Figure 5.2: Spectral radiance of uranium 233 treated as a blackbody at 55,000 K.

Similar to the emission of heat from the surface is the absorption of radiative heat by a surface. Emission of heat from the surface is the loss of heat from the object while the absorption of heat is the gain of heat by the object. The absorption heat flux is given as

$$G = \alpha\sigma T_{sur}^4 \tag{5.3}$$

Here G is the heat flux into the system, α is the material absorptivity ($0 \leq \alpha \leq 1$), and T_{sur} is the surface temperature of the body that is emitting the heat. The absorptivity of a blackbody is one. If the absorptivity is one for a body, the reflectivity and transmissivity of that body are equal

to zero. Heat is also lost from the uranium fuel core in form of convective heat because the hydrogen propellant is flowing around the fuel core.

The convective heat transfer happens as a result of bulk or macroscopic motion of the fluid in the presence of a temperature gradient [51]. The uranium core is assumed to be in a stationary state while hydrogen is flowing around the core. The convective heat transfer equation is given as

$$q" = \bar{h}\,(T_U - T_{Hs-s}) \tag{5.4}$$

Here q" is the convective heat flux (W/m^2), T_U is the uranium surface temperature and $T_{Hs\text{-}s}$ is the steady-state hydrogen propellant surface temperature.

Globally under steady-state conditions, the heat loss from the system is equal to the heat entering the surroundings. The heat added to the uranium core is the fission heat produced and the radiative heat coming from hydrogen propellant and other materials. The heat leaving the system is the radiatively emitted heat from the uranium surface and the convective heat loss from the uranium to the hydrogen propellant. This heat transfer equation in units of power [W] for uranium is given in Equation 5.5.

$$Fission\ thermal\ Power + (A_s\sigma T_{Hs-s}^4) = (A_s\sigma T_U^4) + \bar{h}A_s(T_U - T_{Hs-s}) \tag{5.5}$$

Here A_s is the uranium spherical core surface area. This heat transfer flow schematic is given in Figure 5.3 below.

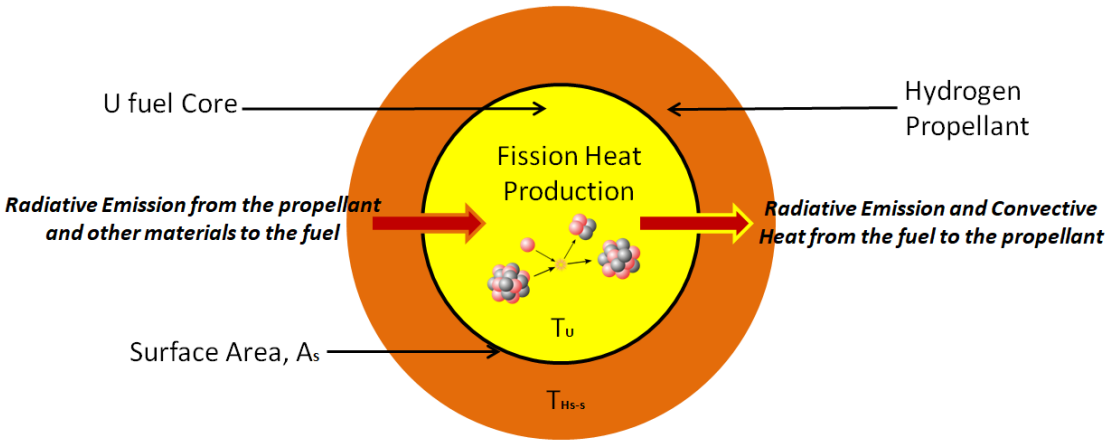

Figure 5.3: Heat flow diagram to and from the uranium fuel core.

From Equation 5.5 and the fission power produced, the temperature of the uranium core can be calculated. The power produced in the uranium core can be throttled using the control drums located at the periphery of this spherical engine. The fission power required out of this fuel core depends on the temperature it needs to maintain at the spherical surface of the core. There are two ways the heat transfer analysis can be conducted – (1) by assuming the fuel core is maintained at a constant temperature throughout the core or (2) by assuming the center of the fuel core is at the highest temperature and the heat is transferred from the center to the outer surface of the core through conduction and radiation. The second way of heat transfer within the uranium core is calculated in Reference 28 and Poston's thesis [25]. The thermal conductivity calculated in Poston's thesis is given in Equation 2.3 in chapter 2. The temperature and the power distributions for this case are also illustrated in chapter 2 Figure 2.8. The fission power required to maintain the temperatures in both heat transfer analysis are given in Table 5.1.

Table 5.1: Reactor power requirements in a gas core nuclear rocket engine.

Case	Temperature (K)	Power (MW)

Constant Temperature throughout the core (20% uranium volume occupancy percentage)	55,000	$7.6*10^6$
	10,000	8266
Highest Temperature at the center of the core	[Ref x] 84,598 (center) and 10,000 (core surface)	4188
	[Poston] 75,000 (center) and 30,000 (core surface)	3000

The huge difference in the reactor power seen in Table 5.1 is due to the size of the engine taken for analysis. The power calculated for constant temperature throughout the fuel core is based on a core diameter of 2.5 m. This is the diameter used for the neutronics analysis that gave a critical engine. This large diameter resulted in a higher power requirement to maintain a high uranium core surface temperature at steady-state conditions. For the case of the highest temperature at the center of the core, the reactor powers were obtained from the indicated references. Since the surface temperature of the uranium core is what affects the temperature of the hydrogen propellant, the surface temperature ranging from 10,000 K to 55,000 K was taken for further heat transfer analysis.

5.1.2 Hydrogen Propellant Heat Transfer

Figure 5.4 illustrates heat transfer into the hydrogen propellant. Hydrogen gas enters the chamber cavity at a mass flow rate of $\dot{m}$, and with an inflow temperature given as T_{Hi}. The heat transfer into the hydrogen is given in Equation 5.6.

$$\dot{m}C_{p_H}\left(T_{H_f} - T_{H_i}\right) = \alpha_H(A_{IS}\sigma T_U^4) + \bar{h}A_{IS}\left(T_U - T_{H_f}\right) - \varepsilon_H(A_{IS} + A_{OS})\sigma T_{H_f}^4 \quad (5.6)$$

Here C_{PH} is the specific heat capacity of hydrogen at the final temperature, α_H is the absorptivity of hydrogen, ε_H is the emissivity of hydrogen, A_{IS} is the inner hydrogen surface area, A_{OS} is the outer hydrogen surface area, σ is the Stefan Boltzmann constant, $\bar{h}$ is the convective heat coefficient, T_U is the uranium core surface temperature, T_{Hi} is the inflow hydrogen temperature and T_{Hf} is the final hydrogen temperature before exiting out of the chamber.

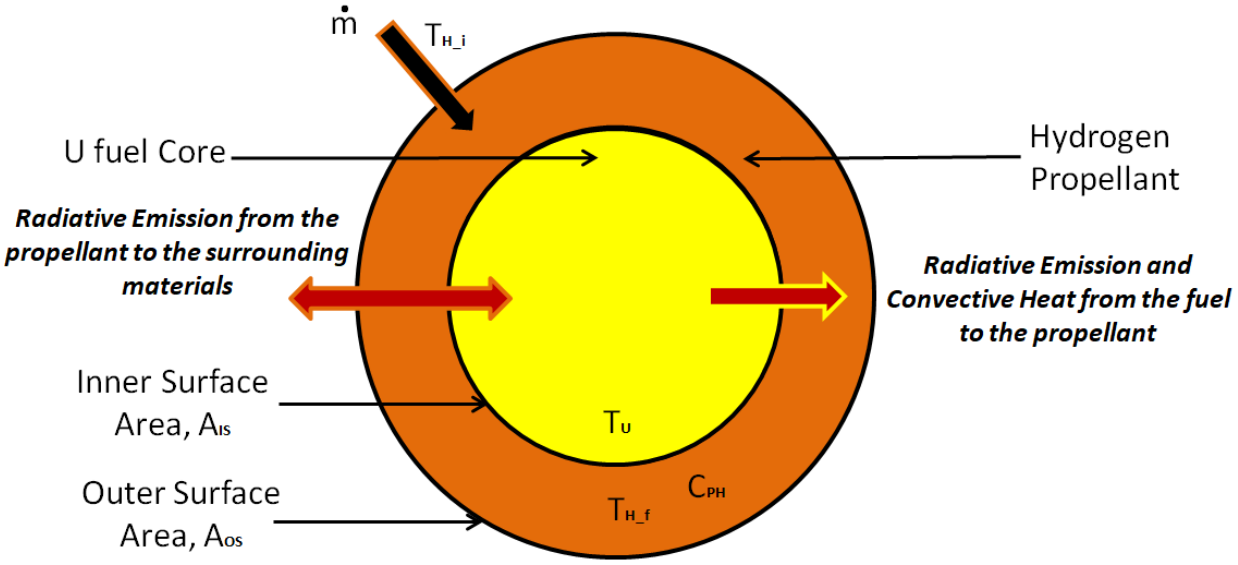

Figure 5.4: Heat flow diagram to and from the hydrogen propellant.

The final hydrogen temperature was calculated from Equation 5.6. The inner surface area, which was taken to be the uranium core surface area at 20 percent uranium volume-occupying percentage, was approximately 20 m^2. The outer surface area is the chamber wall surface area for a chamber of 4.3 m diameter in size. This outer area is approximately 77 m^2. As mentioned before the uranium temperature varied from 10,000 K to 55,000 K range. The mass flow rate of hydrogen was calculated from previously estimated engine performance. Using the range of thrust and specific impulses performance requirements given in the literature [15] [23] [25], the range of mass flow rate of hydrogen into the system was calculated from Equation 5.7.

$$\dot{m} = \frac{T}{I_{sp} g} \tag{5.7}$$

Here I_{sp} is the specific impulses from the literature ranging from 2000 s to 7000 s, T is the thrust from the literature [23] ranging from 20,000 N to 400,000 N, and g is the acceleration due to gravity – 9.806 m/s^2. From this, the mass flow rate of hydrogen into a gas core nuclear rocket was calculated to be in a range of 0.5 kg/s to 15 kg/s. The specific heat at constant pressure for hydrogen at various temperatures was obtained from Reference 52. The specific heat value depends on the pressure and the temperature of hydrogen. The inflow hydrogen temperature depends on the final hydrogen temperature and how much heat is absorbed by this inflow hydrogen while making its way into the cavity chamber. The unknown terms in Equation 5.6 are absorptivity, emissivity, and the convection heat transfer coefficient.

The emissivities of hydrogen for temperatures ranging from 8400 K to 12,600 K and for pressures ranging from 10 atm to 200 atm are calculated in Reference 53. Table 5.2 below provides the emissivity found in this reference. These emissivity values had to be extrapolated to obtain emissivity of hydrogen at 1000 atm and for higher temperatures. It was found that the emissivity of hydrogen over 600 atm pressure and 10,000 K temperature is equal to 1.

Table 5.2: Emissivity of atomic hydrogen as a function of temperature and pressure.

P_T (atmos)	8400°K ϵ	9200°K ϵ	10 080°K ϵ	11 300°K ϵ	12 600°K ϵ
10	0.014	0.037	0.085	0.26	0.48
20	0.030	0.071	0.16	0.35	0.66
40	0.063	0 14	0.28	0.57	0.83
70	0.11	0.24	0.43	0.74	0.92
100	0.15	0.32	0.55	0.82	0.96
150	0.22	0.44	0.69	0.89	
200	0.30	0.54	0.75		

The absorptivity was calculated from the absorption coefficient obtained from Reference 54. For various temperatures and pressures, the absorption coefficient is calculated as a function of wavelength in this paper. Figure 5.5 is the absorption coefficient plotted using the data for 8889 K and 11,111 K from Reference 54 along with the interpolated 10,000 K plot.

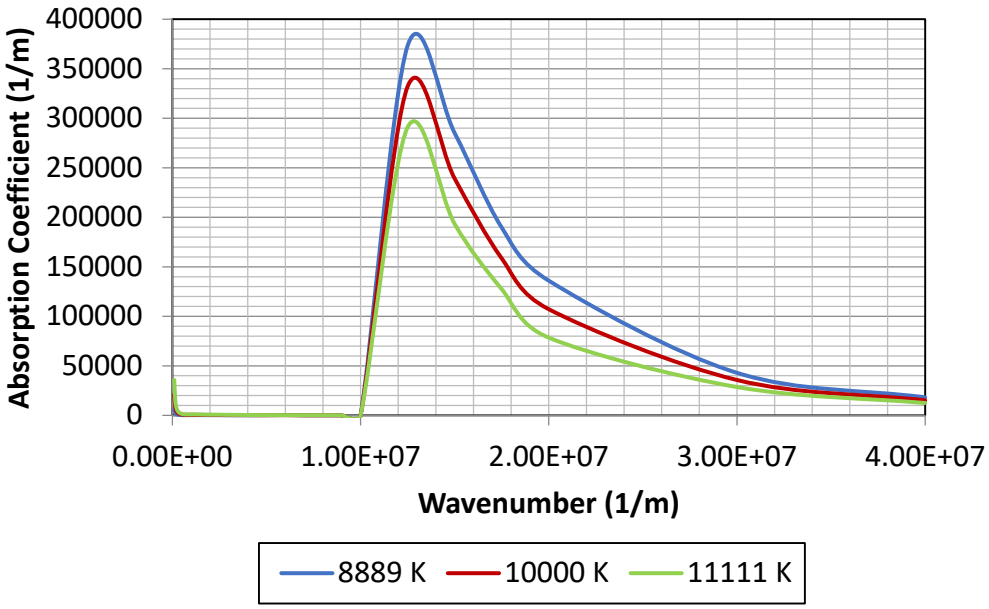

Figure 5.5: Absorption coefficient spectrum as a function of wavenumber for hydrogen at 1000 atm pressure.

The weighted average of this absorption coefficient with wave number was calculated by integrating the spectrum obtained. This weighted average absorption coefficient was inputted into the Beer's law equation given in Equation 5.7 to obtain the absorptivity of hydrogen at that particular temperature. Beer's law relates the attenuation of light to the properties of the material through which the light is traveling. In this case, the photons particles coming from the blackbody uranium core will be attenuated by the hydrogen molecules leading to an increase in the temperature of hydrogen.

$$\alpha_H = 1 - \exp(\alpha_{literature} t_H) \tag{5.7}$$

Here α_H is the absorptivity of hydrogen, $\alpha_{literature}$ is the weighted average absorption coefficient calculated from the literature data, and t_H is the thickness of hydrogen propellant in the cavity chamber. This provides the absorptivity of hydrogen at 1000 atm for various temperatures. The absorptivity calculated for hydrogen is given in Table 5.3.

Table 5.3: Absorptivity of Hydrogen at 1000 atm.

Temperature (K)	**Absorptivity**
5000	0.036
10,000	0.070
15000	0.763
20000	0.999
50000	1.000

At lower values of hydrogen temperature, the absorptivity of hydrogen is very small. This is the reason for the suggestion of adding tungsten particles to hydrogen propellant to improve its absorptivity [15]. However, adding tungsten to hydrogen propellant negatively impacts the engine performance by reducing the specific impulse. Interestingly, the absorptivity of hydrogen increases considerably as the temperature goes up. At temperatures over 20,000 K, hydrogen will not need any tungsten particles to improve its opacity. The hydrogen's opacity was calculated to increase with both temperature and pressure [54].

The convective heat transfer coefficient depends on the hydrogen flow regime and problem geometry. The convective heat transfer coefficient is given as,

$$\bar{h} = \frac{\overline{N_{u_D}} k}{D} \tag{5.8}$$

Here N_{uD} is the dimensionless parameter called Nusselt Number, k is the thermal conductivity and D is the diameter of the sphere around which the fluid is flowing. Nusselt number can be defined as the ratio of convective to conductive heat transfer at a boundary in a fluid. For a flow around a sphere, the Nusselt number can be calculated using Equation 5.9 [51].

$$\overline{N_{u_D}} = 2 + \left(0.4 Re_D^{\frac{1}{2}} + 0.06 Re_D^{\frac{2}{3}}\right) (\mathrm{Pr})^{0.4} \left(\frac{\mu}{\mu_s}\right)^{\frac{1}{4}} \qquad \begin{cases} 0.71 \leq (Pr) \leq 380 \\ 3.5 \leq Re_D \leq 7.6 * 10^4 \\ 1.0 \leq (\frac{\mu}{\mu_s}) \leq 3.2 \end{cases} \tag{5.9}$$

This Nusselt number depends on the Reynolds number, Re_D, Prandtl number, Pr, and the viscosity, μ. Reynolds number is defined as the ratio of inertia to viscous force. Reynolds number for a sphere can be calculated using Equation 5.10. Prandtl number is defined as the ratio of the momentum to the thermal diffusivities. Prandtl number can be calculated using Equation 5.11. The viscosity, μ, is evaluated at hydrogen's final temperature while μ_s is evaluated at the sphere's surface temperature (or uranium core temperature).

$$Re_D = \frac{\rho v D}{\mu} \tag{5.10}$$

$$Pr = \frac{C_{p_H} \mu}{k} \tag{5.11}$$

Here ρ is the hydrogen density, v is the velocity calculated from the mass flow rate, D is the diameter of the sphere, μ is the viscosity of hydrogen, C_{PH} is the specific heat of hydrogen at constant pressure and k is the thermal conductivity of hydrogen. The thermal conductivity, viscosity, and specific heat of hydrogen depend on the hydrogen's temperature and pressure. These values were obtained from the literature for 1000 atm pressure [25] [52]. The density of hydrogen was calculated as mentioned in chapter 4 and the diameter of the uranium core was

chosen for the 20 percent uranium volume occupancy percentage sphere. Reynolds number, Prandtl number, and the ratio of viscosities stayed within the range given in Equation 5.9. Using these numbers, the convective coefficient of hydrogen flow around the uranium core was calculated. Table 5.4 provides the numbers calculated for the convective heat transfer coefficient for hydrogen temperatures from 5000 K to 20,000 K.

Table 5.4: Convective Heat Transfer Parameters.

Hydrogen Temperature (K) / Parameters	**5000**	**10000**	**15000**	**20000**	**50000**
Density (kg/m^3)	4.41	1.30	0.82	0.61	0.22
Viscosity ($N\text{-}s/m^2$)	6.58E-5	1.07E-4	1.16E-4	9.93E-5	8.15E-5
Thermal Conductivity (W/m-K)	0.74	2.05	2.39	2.27	3.19
Specific Heat (J/kg-K)	47294	34538	36709	76224	52300
Reynolds Number	5.24E+3	3.22E+3	2.97E+3	3.47E+3	4.23E+3
Prandtl Number	4.19	1.80	1.78	3.33	1.34
μ/μ_s	0.81	1.31	1.42	1.21	1.00
Nusselt Number	81.10	50.50	49.08	65.48	48.83
Convective HT coefficient, h ($W/m^2\text{-}K$)	24.15	41.48	47.00	59.56	62.43

Now with all the parameters calculated based on a final hydrogen temperature, Equation 5.6 can be solved by an iterative process. To conduct the iterative calculation, first, a final hydrogen temperature was assumed. Then the properties of hydrogen at this assumed final temperature were obtained from the literature or were calculated using equations given earlier in this chapter. Using only these properties, the heat transfer Equation 5.6 was solved for the final hydrogen temperature. If the guessed final hydrogen temperature matched the obtained hydrogen temperature to a difference of 1 percent, the iteration was concluded. This iterative process is illustrated in Figure 5.6 below.

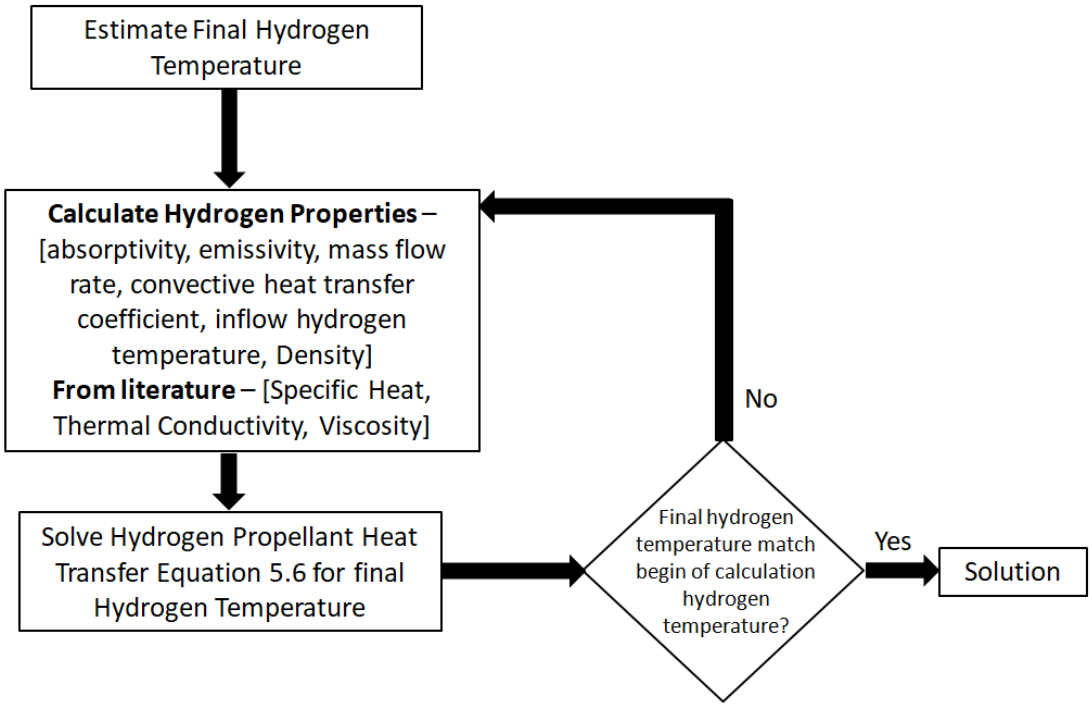

Figure 5.6: Hydrogen final temperature calculation flow chart.

From this iteration process, the final temperature of hydrogen was calculated for different cases given in the next sub-section.

5.1.3 Heat Transfer Results

The hydrogen temperature was calculated for the cases ranging from 10,000 K to 55,000 K uranium surface temperature. The estimated initial temperature for hydrogen varied from 1000 K to 20,000 K depending on the uranium surface temperature. Figure 5.7 plots the change in hydrogen temperature with the change in uranium core surface temperature. As expected, with the increase in the uranium surface temperature, the hydrogen propellant temperature increases as well.

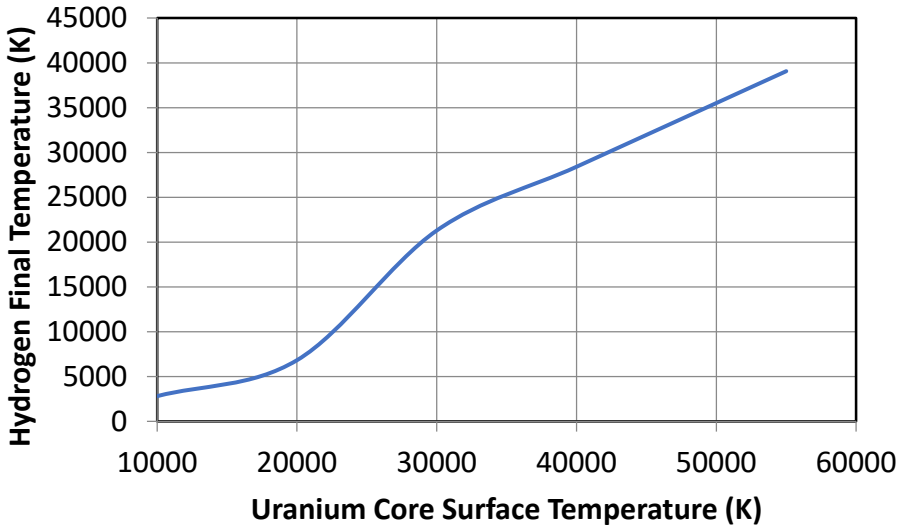

Figure 5.7: Hydrogen final temperature change with the uranium surface temperature.

It was also found that the impact of convective heat transfer is small in this gas core nuclear rocket engine. This is due to the fourth power impact of radiation temperature seen in Equation 5.6. The differences in the final temperatures calculated using the full heat transfer equation versus using just the radiative heat transfer equation are given in Table 5.5 below.

Table 5.5: The differences between the final hydrogen temperature calculated using the full heat transfer equation and using the radiation equation only.

Uranium Surface	**Hydrogen Final Temperature (K)**

Temperature (K)	Full Equation	Only Radiative Equation	% Difference
10,000	2,816	3,318	17.83
20,000	6,824	6940	1.70
30,000	21,292	21,315	0.11
40,000	28,405	28,420	0.05
50,000	35,514	35,525	0.03
55,000	39,068	39,078	0.03

The difference is predominant at the lower temperatures because the absorptivity of hydrogen at a lower temperature is very small. The full equation gave a lower final hydrogen temperature as compared to just the radiative heat transfer equation due to the mass flow rate impact on the heat transfer. As the hydrogen flows out of the chamber cavity, there is lesser time the hydrogen gets to heat up from radiation. For the lower temperature of hydrogen, the absorptivity of hydrogen is low and it will need more time in the presence of the uranium core to get heat up. The mass flow rate impact on the final hydrogen temperature is given in Table 5.6. Here the uranium surface temperature is at 55,000 K.

Table 5.6: Final hydrogen temperature change with the mass flow rate.

Mass Flow Rate (kg/s)	Hydrogen Final Temperature (K)
1	39,077
5	39,071
10	39,065
15	39,059
100	38,951

1000	37,799

From this heat transfer analysis, it can be concluded that the radiation's impact on hydrogen temperature is higher as the uranium surface temperature increases. At 1000 atm pressure and temperatures above 20,000 K, hydrogen can be considered a blackbody itself. The mass flow rates impact on the temperature is negligible but not on the engine performance. These hydrogen temperatures will be used in the calculation of the engine performances in the next sections.

5.2 Nozzle

Nozzle designed was optimized for a gas core nuclear rocket by using the chamber temperature and pressure. Hydrogen propellant temperature is taken as the chamber temperature for this calculation. The pressure was taken as 1000 atm. A converging-diverging nozzle was designed using basic rocket nozzle equations. The role of a nozzle in a rocket is to convert the random thermal energy of the hot propellant into directed kinetic energy. Figure 5.8 illustrates a converging-diverging nozzle configuration with the flow direction [55].

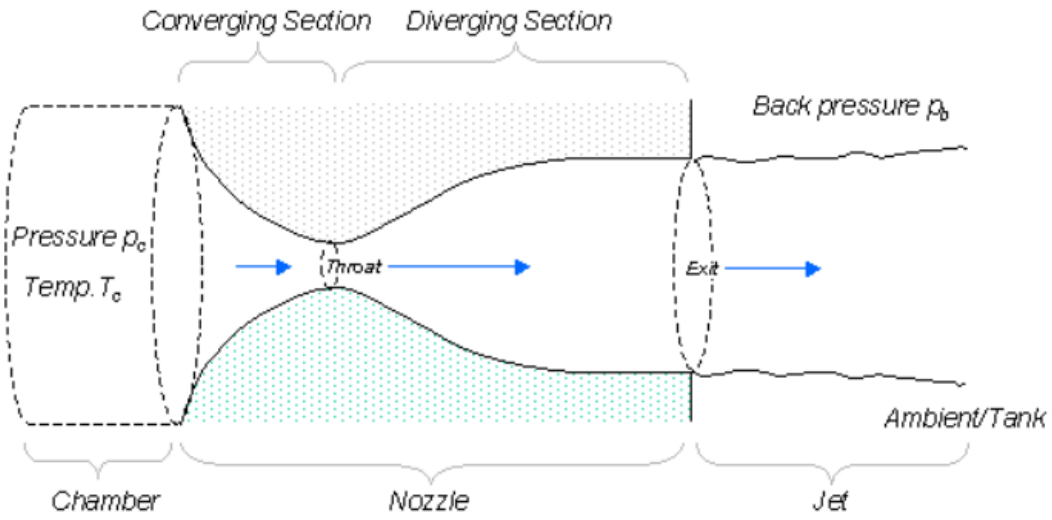

Figure 5.8: A converging-diverging nozzle configuration.

To achieve high speed supersonic exhaust velocities, the nozzle must be designed to achieve Mach 1 (so-called choked flow) at the throat. This also determines the maximum flow rate. The throat area can be found using the isentropic relations using the chamber pressure, chamber temperature, and mass flow rate. The throat area equation is given as,

$$A^* = \frac{\dot{m}}{P_c}\sqrt{\frac{RT_c}{\gamma}}\left(\frac{\gamma+1}{2}\right)^{\frac{\gamma+1}{2(\gamma-1)}} \tag{5.12}$$

Here A^* is the throat area, $\dot{m}$ is the mass flow rate, P_c is the chamber pressure, T_c is the chamber temperature and γ is the specific heat ratio. As the specific heat of hydrogen at constant pressure was obtained from the literature for the heat transfer analysis, the specific heat ratio for hydrogen at high temperature was obtained from Reference 25. The specific heat ratio can also be calculated using Equation 5.13 where specific heat constant is temperature dependent.

$$\gamma = \left(1 - \frac{\bar{R}}{\bar{m}C_{p_H}(T)}\right)^{-1} \tag{5.13}$$

Here $\bar{R}$ is the gas constant, C_{pH} is the specific heat at constant pressure and $\bar{m}$ is the atomic mass of the hydrogen gas. The throat area was calculated for various hydrogen temperatures ranging from 3000 K to 40,000 K. For a mass flow rate of 5 kg/s, the throat radius ranged from 0.93 cm to 1.80 cm. This throat radius is very small to maintain 1000 atm pressure in a 4.3 m cavity diameter. If the pressure that needs to be maintained was 10 atm, the throat radius would have ranged from 9.3 cm to 18.0 cm. From this throat radius and area calculated, the area ratio of the nozzle can be calculated. Area ratio is the ratio of the exit area of a nozzle to the throat area of a nozzle. The area ratio can be calculated using Equation 5.14.

$$\frac{A_e}{A^*} = \frac{1}{M_e}\left(\frac{2}{\gamma+1}\left(1+\frac{\gamma-1}{2}M_e^2\right)\right)^{\frac{\gamma+1}{2(\gamma-1)}} \tag{5.14}$$

Here A_e is the nozzle exit area and M_e is the exit Mach number. The exit Mach number is the ratio of exit velocity to the speed of sound in that medium. As a general rule, the area ratio needs to be at least greater than 4. From Equation 5.15, it can be seen that the maximum thrust is achieved when exit pressure is equal to the free stream pressure or the pressure outside the nozzle. The larger the area ratio, the higher the thrust will be. However, the mass increase from increasing the area ratio has to be taken into consideration. Given both the engine weight and thrust requirements, the nozzle's area ratio is adjusted accordingly. In Poston's thesis, the area ratio used was 100:1 [25] and in Reference 56 an area ratio of 300:1 was used for the nuclear thermal propulsion system. Here the nozzle design was conducted to achieve a Mach number of 4. This Mach number change is varied as per the mission requirement. For a Mach number of 4, the area ratio ranged from 13:1 to 54:1 for different hydrogen temperatures. From this range of area ratios calculated, the nozzle exit radius was calculated to be in the range of 6.60 cm to 12.65 cm. For the 300:1 area ratio, the exit radius goes up to 31 cm.

Nozzle design impacts the thrust level that can be achieved from this nuclear rocket engine. The thrust equation along with the correction fraction is given as

$$T = \lambda \dot{m} v_e + (P_e - P_o) A_e \tag{5.15}$$

Here λ is the correction factor, v_e is the exit velocity, P_e is the pressure at the exit, and P_o is the free stream pressure or the pressure outside the nozzle. The correction factor can be found using Equation 5.16.

$$\lambda = 0.5(1 + \cos\theta) \tag{5.16}$$

Here θ is the angle of nozzle expansion. Best case scenario for best thrust is $\lambda = 1$ or $\theta = 0$. But the trade is the mass of the engine versus performance. At smaller angles, the efficiency is higher but the nozzle will have to be narrower and longer. At higher angles the efficiency is

lower. The optimum angle is between 12^0 and 18^0. At 15^0, the efficiency is 98 percentage (λ = 0.98). This is the range for nozzle expansion angle used in conventional rockets where it is a good balance between the engine mass and performance. Figure 5.9 obtained from Reference 57 shows an example of nozzle design using normalized throat radius. For high altitude and better correction factor, the bell contour is used for the nozzle design.

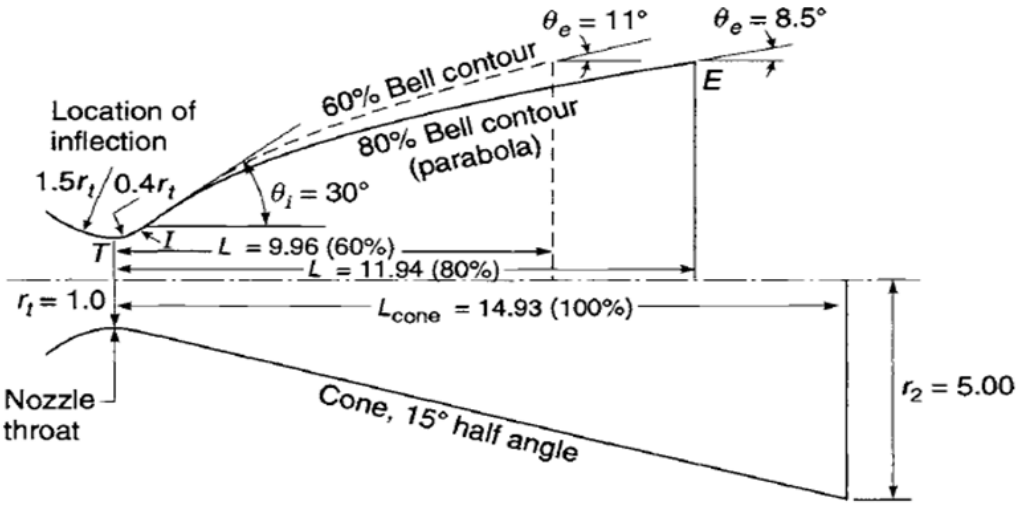

Figure 5.9: Example of nozzle designing using normalized throat radius.

In Figure 5.9, the dimension of the location of injection right before the throat depends on the throat radius calculated. The length of the nozzle is calculated as [57]

$$L_{cone} = \frac{r_t\left(\sqrt{\epsilon} - 1\right) - 0.4r_t(\sec\theta - 1)}{\tan\theta} \tag{5.17}$$

The initial, θ_i, and exit angle, θ_e, of the parabola contour of the nozzle can be found in Figure 5.10 from Reference 57. Here the length of the nozzle can be taken from 60 percent to 100 percent of the L_{cone} calculated above. As the length increases, the mass increases. So the length taken for the nozzle design was 90 percent – hardly losing any efficiency at this length.

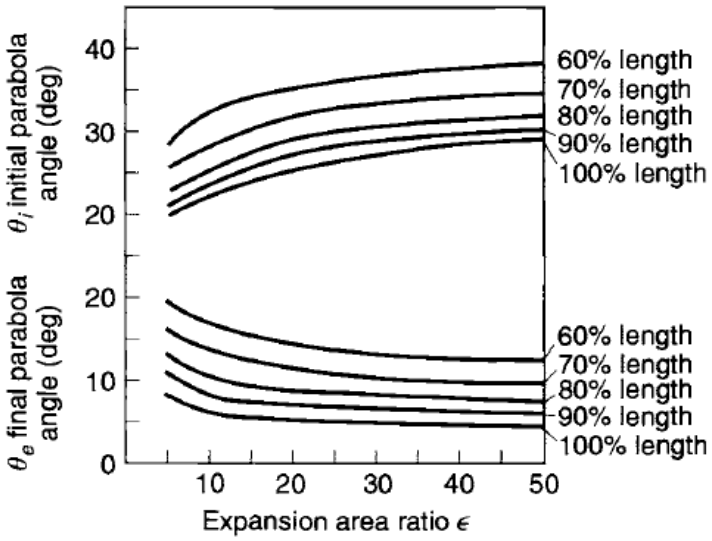

Figure 5.10: Inlet and exit angles as a function of expansion area ratio.

The nozzle length was calculated to be 0.44 m for an expansion ratio of 300:1. The inlet and exit angles obtained from Figure 5.10 were 30 degrees and 6 degrees. The throat radius and exit radius were also calculated for these conditions and a mass flow rate of 3 kg/s. The angle of nozzle expansion was chosen to be 15^0. This gave a correction factor for thrust calculation as 0.983. A nozzle was designed for these nozzle dimensions in ANSYS software. This nozzle design is shown in Figure 5.11.

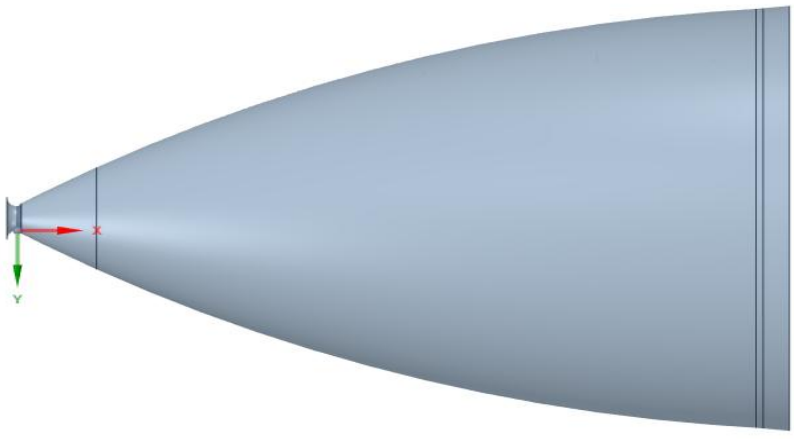

Figure 5.11: An optimized nozzle design for a gas core nuclear rocket engine.

5.3 Confinement

The confinement of the uranium core was assumed in this thesis work using the hydrodynamic confinement technique. Figure 5.12 shows the base bleed hydrodynamic study conducted to see if a vortex can be made at the base of the uranium core in cylindrical geometry [33].

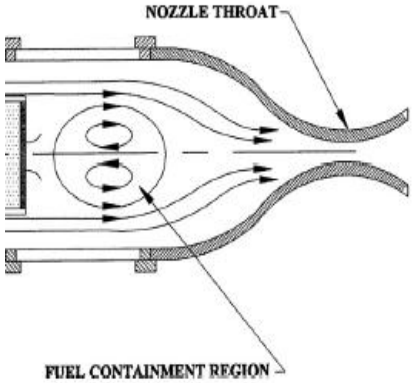

Figure 5.12: Base bleed hydrodynamic confinement.

This experimental study did show that a vortex region can be created to confine the uranium core or minimize the uranium loss considerably. This was tested on ANSYS Fluent software using Poston's cylindrical engine model (shown in Figure 2.5 in chapter 2) to see if a vortex region can be produced at the core base if uranium is injected at the core base along with the propellant flows from the side. Figure 5.13 shows the result obtained from ANSYS Fluent for this test conducted for a single uranium injection at the core base.

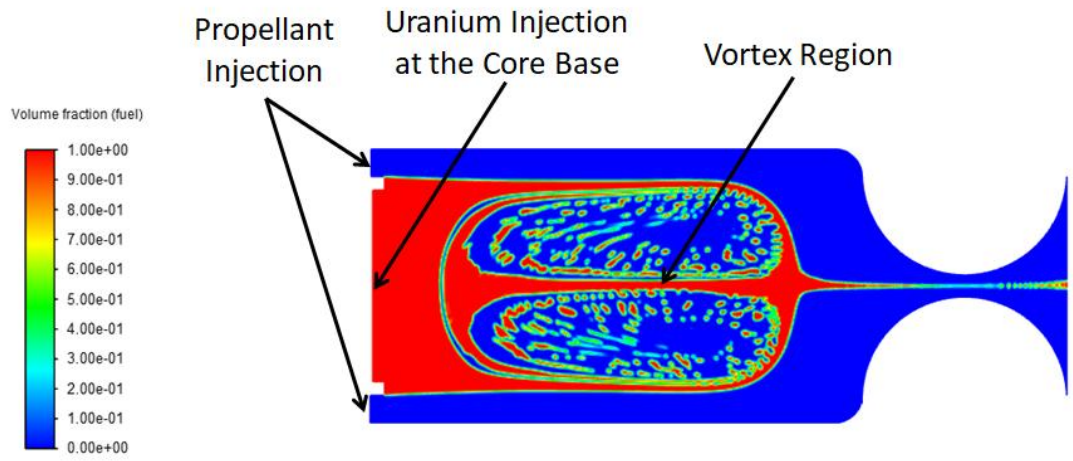

Figure 5.13: Vortex formation at the core base with single uranium injection at the core base.

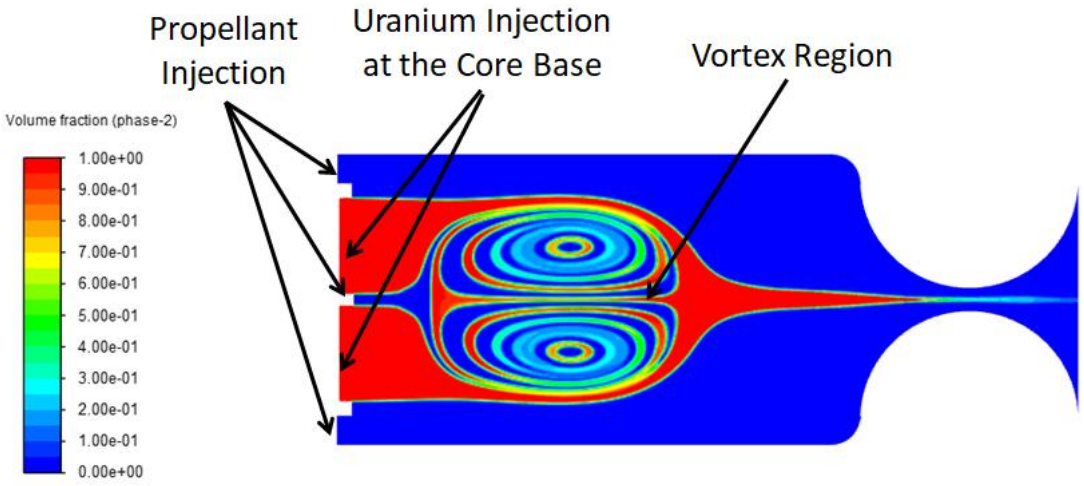

Figure 5.14: Vortex formation at the core base with two uranium injections.

Figure 5.14 shows the case of two uranium injections and one hydrogen injection at the core base. In this analysis, it can also be seen that there are mixed regions where there is some volume of hydrogen and uranium present. The vortex formation can be found in both forms of injection at the core base. This is the confinement assumed in this thesis work to confine the uranium core or minimize the uranium loss from the system.

5.4 Rocket Performance

The thrust and impulse were calculated for various hydrogen temperatures with the nozzle designed. The thrust equation given in Equation 5.15 was used to calculate the thrust. The exit velocity was calculated using Equation 5.18 for a Mach of 4. The exit temperature and pressure were calculated using Equations 5.19 and 5.20 respectively.

$$v_e = M_e\sqrt{\gamma R_H T_e} \tag{5.18}$$

$$T_e = T_c\left(1 + \frac{\gamma - 1}{2}M_e^2\right)^{-1} \tag{5.19}$$

$$P_e = P_c\left(1 + \frac{\gamma - 1}{2}M_e^2\right)^{-\frac{\gamma}{\gamma-1}} \tag{5.20}$$

Here v_e, T_e, and P_e are the exit velocity, temperature, and pressure respectively, T_c and P_c are the chamber temperature and pressure, γ is the ratio of specific heat, R_H is the gas constant for hydrogen, and M_e is the Mach number. The specific impulse was calculated using Equation 5.21.

$$I_{sp} = \frac{T}{\dot{m}g} \tag{5.21}$$

Here T is the thrust, $\dot{m}$ is the mass flow rate and g is the acceleration due to gravity. The results obtained for thrust and specific impulse are plotted against hydrogen temperature in Figure 5.15 and Figure 5.16. This is the case for mass flow rate at 5 kg/s and area ratio at 50:1. The thrust ranged from 51,000 N to 190,000 N while specific impulse ranged from 1058 s to 3891 s. If the area ratio of the nozzle is increased to 300:1, the thrust ranged from 85,000 N to 305,000 N and the specific impulse ranged from 1743 s to 6218 s. These numbers fall within the range of thrust and specific impulses estimated or calculated by past research work on gas core nuclear rocket engines [15] [23].

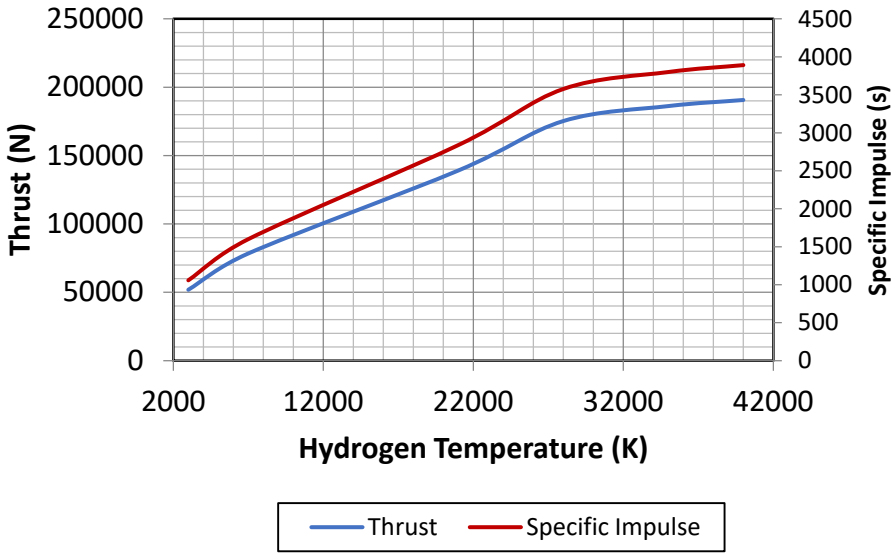

Figure 5.15: Calculated thrust and impulse of a gas core nuclear rocket engine with a nozzle area ratio of 50:1.

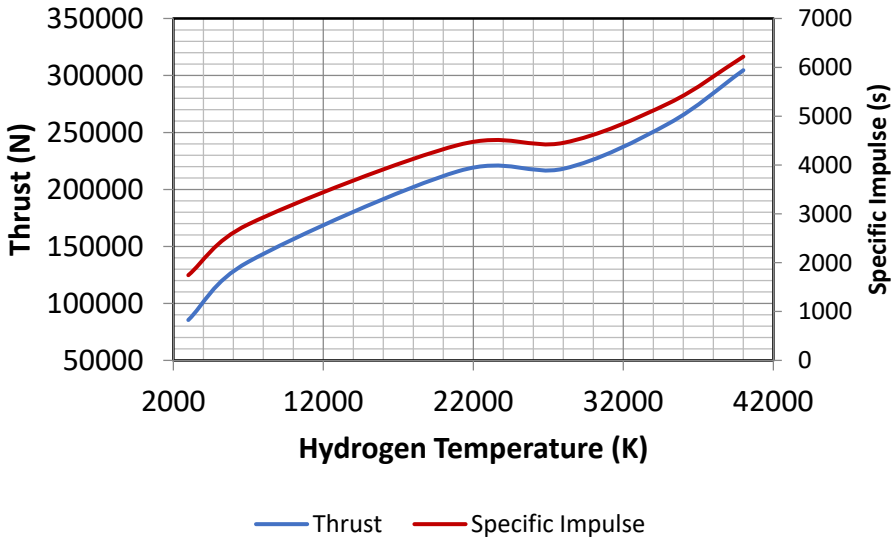

Figure 5.16: Calculated thrust and impulse of a gas core nuclear rocket engine with a nozzle area ratio of 300:1.

Table 5.7 provides the calculated engine performance for a gas core nuclear rocket. The total mass of the engine will be approximately 100,000 kg to 122,000 kg. This includes the weight of the reactor calculated in Chapter 4 and the mass of the nozzle.

Table 5.7: Gas core nuclear rocket performance specification.

Hydrogen Temperature (K)	Exit Velocity (m/s)	Thrust (N)	Specific Impulse (s)	Thrust-to-Weight
40,000	34156	304693	6218	3.05
35,000	24979	257743	5260	2.58
28,000	33916	218213	4453	2.18
21,000	25173	216069	4410	2.16
7000	13596	136463	2785	1.36
3000	9190	85429	1743	0.85

Compared to a solid core nuclear rocket, the specific impulse and thrust are much higher. The specific impulse estimated for the solid core nuclear rocket is between 850 to 1000 s with a thrust of 100,000 N. Gas core nuclear rocket's high thrust and impulse make them an attractive candidate for in-space human exploration to Mars and beyond. A full gas core engine model is shown in Figure 5.17.

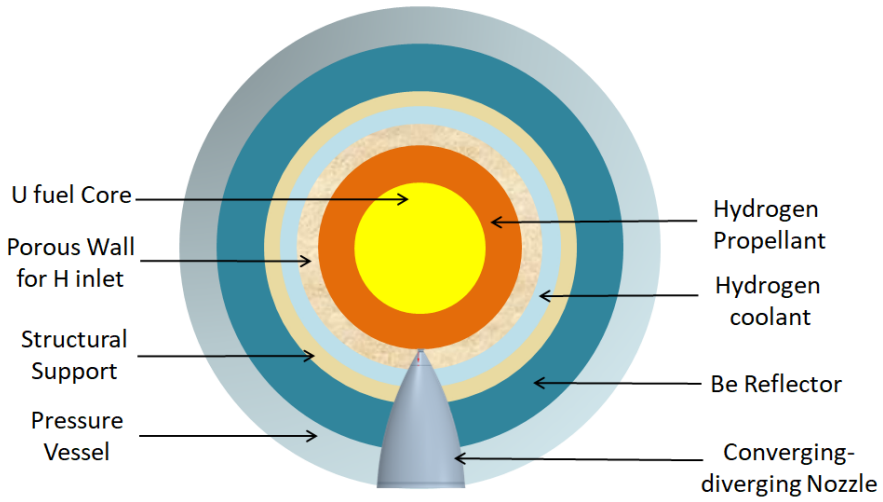

Figure 5.17: Full Gas Core Nuclear Rocket Schematic.

Table 5.8 is the performance comparison between various rocket engines. It can be seen that the gas core nuclear rocket performance is higher compared to other engines. The centrifugal nuclear thermal rocket performance needs to be calculated once the heat transfer analysis of the engine is carried out.

Table 5.8: Rocket Performance Comparison

Propulsion System	**Specific Impulse (s)**	**Thrust (N)**	**Thrust-to-Weight**
Chemical Propulsion (Space X Falcon Heavy)[58]	311	8,200,000	5.8
NERVA[59]	~710	1,000,000	3.0 – 4.0
Centrifugal Nuclear Thermal Rocket	850 – 1600		
Nuclear Light Bulb[60]	1870	409,000	1.3
Gas Core Nuclear Rocket	1000 - 6200	50,000 – 1,340,000	0.5 – 13.0

CHAPTER 6 Analysis of Centrifugal Nuclear Thermal Rocket (CNTR)

The centrifugal nuclear thermal rocket (CNTR) has been investigated in the past and is of current interest to NASA. This engine, featuring a liquid core, is a natural intermediate development step along the way to a gas core engine. The CNTR engine is attractive because its performance goal is high thrust at a specific impulse of 1800 seconds using hydrogen propellant [61], and at a specific impulse up to 900 seconds using passively storable propellants such as ammonia (dissociated). The CNTR enables a roundtrip mission to Mars in 420 days [12]. Currently, both computational and non-nuclear experimental work is being carried out on this engine to advance its technology readiness level.

6.1 Engine Design Concept

The centrifuge nuclear thermal rocket engine, unlike the gas core nuclear rocket engine uses metallic liquid uranium fuel to heat the incoming hydrogen propellant. As the name suggests, the concept behind this engine involves centrifugal confinement of molten uranium. Such confinement is achieved using rapidly spinning fuel elements. In this manner, the molten fuel is kept attached to the inner surface of the rotating element. In a CNTR, there are multiple cylindrical spinning fuel elements called centrifuge fuel elements (CFEs) which are anchored to the system by bearings in the core block. The typical rotational speed is above 25,000 RPM. These CFEs are located within a moderator block that gives CFEs the necessary structural and neutronics support. Surrounding the moderator block are the neutron reflector block such as beryllium and control drums to control the reactivity of the engine. Figure 6.1 illustrate the

CNTR engine's top view with 19 CFEs and also the radial propellant flow path into the center of the CFE [12].

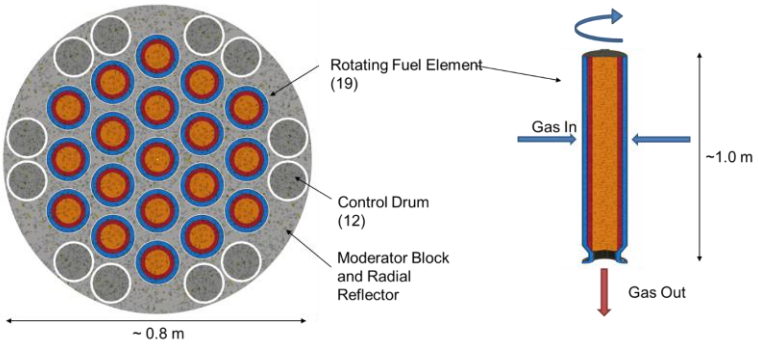

Figure 6.1: Centrifugal Nuclear Thermal Rocket schematic with 19 CFEs and radial propellant inflow schematic.

In this engine, any volatile material can be used as a propellant. The propellant is used for regenerative cooling of the engine parts before entering the CFEs. The propellant flows first through the neutron reflector and the nozzle before flowing through the moderator block material. Then the propellant flows radially into the porous cylindrical rotating CFEs' walls. Inside the CFE, the propellant passes through the liquid uranium fuel and moves towards the center of the spinning cylinders. Due to the centrifuge force and the propellant incoming pressure into the CFEs, the lighter propellant moves towards the center of the cylinder while the heavier liquid uranium fuel moves towards the walls of the cylinder. Upon effusing through the molten fuel, the heated propellant is expelled out axially through a common plenum before being accelerated through a converging-diverging nozzle. This flow path is illustrated in Figure 6.2 below [12].

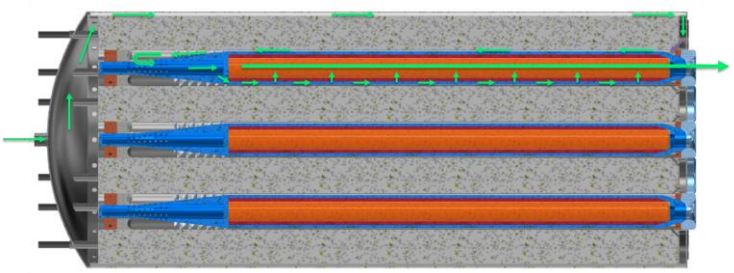

Figure 6.2: CNTR Propellant Flow Path.

It is estimated that the hydrogen at the center of CFE can reach temperatures around 5,500 K in this engine while the moderator block will be at a modest temperature of around 600 K. The heat transfer within this engine will be a combination of conduction and convectional heat transfer. All solid materials in the engine are maintained at less than 800 K except for the metallic uranium and a coating on the inside of the CFE [12]. The heat transfer from the liquid uranium to the propellant bubbles as it passes through the uranium fuel will have to be evaluated further to understand this engine's performance better. Figure 6.3 illustrates the CFE cross-section alongside the estimated temperatures of different regions in a CNTR engine [12].

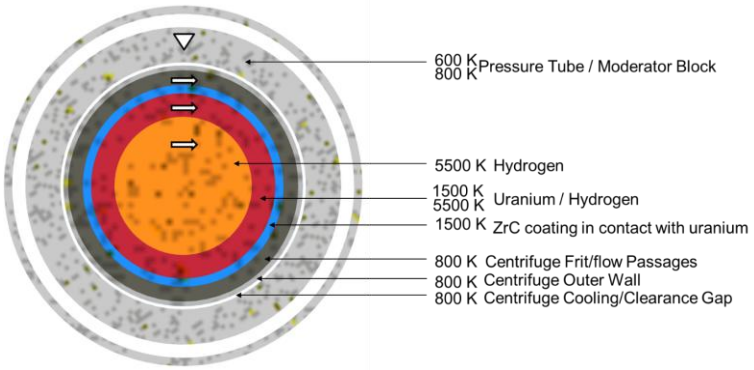

Figure 6.3: Rotating Centrifuge Fuel Element cross-section and estimated temperatures.

6.2 Challenges of a Centrifugal Nuclear Thermal Rocket Engine

A number of technical challenges must be addressed before a CNTR-based concept is viable as a propulsion option. These challenges include

1. CNTR technology involves machinery which adds to the overall system complexity. Failure analysis aimed at assessing the impact of the failure of one or more fuel elements on the neutronics and the overall engine stability has to be carried out.

2. Reliable engine startup and shutdown methods have to be developed that minimize uranium fuel losses.

3. Similar to a gas core nuclear rocket, the loss of uranium from the engine has to be minimized. Confinement techniques have to be implemented to confine the liquid uranium from exiting the engine. If there is a loss of uranium in the engine, methods to replenish the uranium fuel have to be designed.

4. A porous cylinder wall has to be developed that allows hydrogen propellant into the cylinder while preventing the molten uranium fuel out of the cylinder. This wall should have adequate cooling to prevent melting alongside uranium.

5. A coating within the CFE wall has to be developed that is compatible with liquid uranium and all propellants at high-temperature conditions [12].

6. Heat transfer between the hydrogen propellant flowing through the uranium fuel and the molten uranium has to be understood to predict hydrogen temperatures and properties at the center of CFE. The bubble flow inside a molten metal and the surface interactions need to be understood better.

7. Similar to the gas core engine, the ground testing of this engine will be a challenge due to the inevitable loss of some uranium fuel through the nozzle.

8. The engine needs to be optimized to have a critical engine that is self-sustaining even with a small loss of uranium fuel from the system. Neutronics studies along with heat transfer work can give a better picture of the reactor’s criticality and stability. Experimental work

has to be conducted to validate the computation results obtained for heat transfer and neutronics within a CNTR.

The purpose of this chapter is to tackle the neutronics challenge of this engine. Can CNTR be a critical engine and what is the minimum mass required for this critical engine? These questions will be answered in the following sections.

6.3 Neutronic Analysis of Centrifugal Nuclear Thermal Rocket in MCNP

Neutronics analyses were conducted using the MCNP code. When necessary, NJOY was used to calculate high-temperature neutronics cross-section for both fuel and propellant. Uranium was kept at 3000 K and hydrogen at 2500 K with a pressure of 500 psi. These studies were carried out for 19 CFEs and 37 CFEs CNTR models. These CFEs were placed within a hexagonal core block that is surrounded by a beryllium radial reflector. Axial beryllium reflector of 5 cm thickness was added to the top of the engine and Inconel 718 of 1 cm thickness was added to the bottom of the engine as a support plate. The side view of a 19 CFEs CNTR engine is illustrated in Figure 6.4.

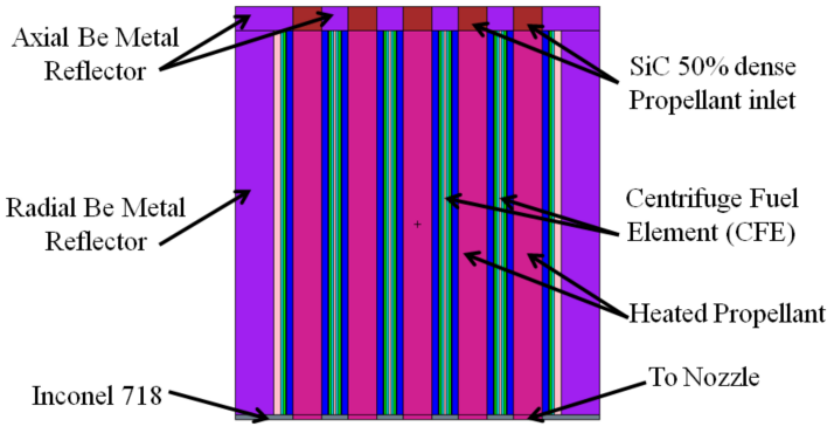

Figure 6.4: Centrifuge Nuclear Thermal Rocket engine side view produced from MCNP.

Five neutronics studies were carried out to optimize the CNTR engine. The two major goals of these studies were to have a critical engine and to have a small mass engine. From these

studies, the engine criticality's sensitivity to the engine geometry and materials was understood. These five studies are discussed in the following sub-sections.

6.3.1 Uranium Volume Fraction Sensitivity Study

In this study, the uranium fuel volume fraction was varied to understand its impact on the CNTR engine. The uranium volume fraction is defined as the ratio of the uranium fuel occupying volume present in the CFE fuel region to the total CFE fuel volume. Since hydrogen propellant gas is passing through the fuel radially to get to the CFE center, a percentage of volume in the uranium fuel region will be occupied by the propellant gas. Varying the hydrogen flow rate and the pressure of the hydrogen flow into the CFE, the hydrogen volume present in the uranium region can be varied. The total fuel region (illustrated in Figure 6.5 in blue as the molten uranium region) volume would be the sum of hydrogen volume and uranium volume in this region. This is given in equation 6.1 below.

$$VF_U = \frac{Volume\ of\ molten\ uranium\ at\ CFE\ fuel\ region}{(Volume\ of\ Molten\ uranium + Volume\ of\ propellant) at\ fuel\ region} \quad \text{(CHAPTER 6.2)}$$

The 19 CFEs were placed within SiC hexagonal core block. $ZrH_{1.87}$ moderator material cylinders were added in between the CFEs. Figure 6.5 illustrates the engine model used in this study and Table 6.1 provides the dimensions and materials used in this engine in detail.

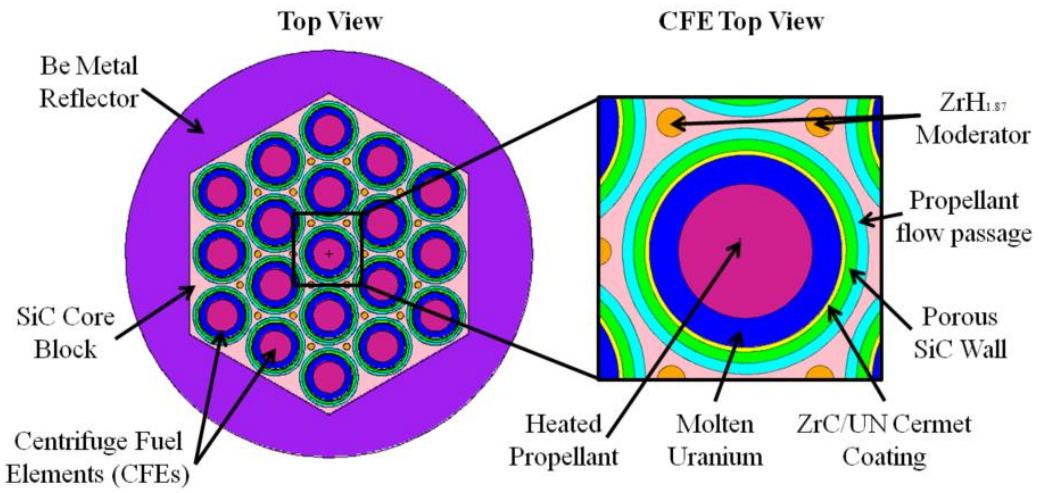

Figure 6.5: CNTR 19 CFEs model in SiC core block top view and CFE cross-section view.

Table 6.1: Model dimensions and materials going radially outward from the CFE center.

Parameter	Dimensions (cm)	Type
Central 100% propellant region	3.0	OR
19.75% Enriched Uranium	4.3	OR
50% dense ZrC/UN coating	4.5	OR
80% dense SiC inlet wall	5.0	OR
100% propellant inlet	5.5	OR
SiC core block Hexagonal Radius	25.1	OR
CFE Pitch	11.2	Pitch
$ZrH_{1.87}$ moderator cylinder	0.64	OR
Number of CFEs	19	No.

Number of $ZrH_{1.87}$ cylinders	24	No.
Beryllium radial reflector	8	T
Core height	80	H
Top Beryllium reflector	5	T
Axial 50% dense SiC for propellant inlet	3	OR
Bottom Inconel 718 support	1	T

OR = Outer Radius; T = Thickness; H = Height; No. = Number

Table 6.1 parameters go from hot propellant at CFE center to outward. The remainder of the percentage dense materials in Table 6.1 is occupied by hydrogen flowing towards the center of CFE (80% dense SiC wall region has 20% volume fraction filled by hydrogen propellant gas). The k_{eff} and mass of the engine increased with the increase in volume fraction of uranium in the system. The results obtained from this study are shown in Figure 6.6 and Figure 6.7,

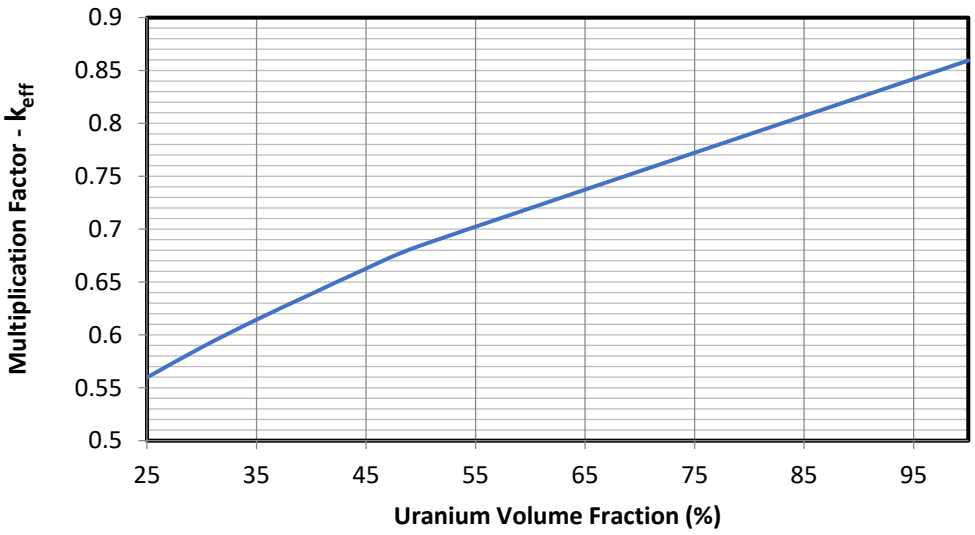

Figure 6.6: Criticality change of CNTR with the change in uranium volume fraction.

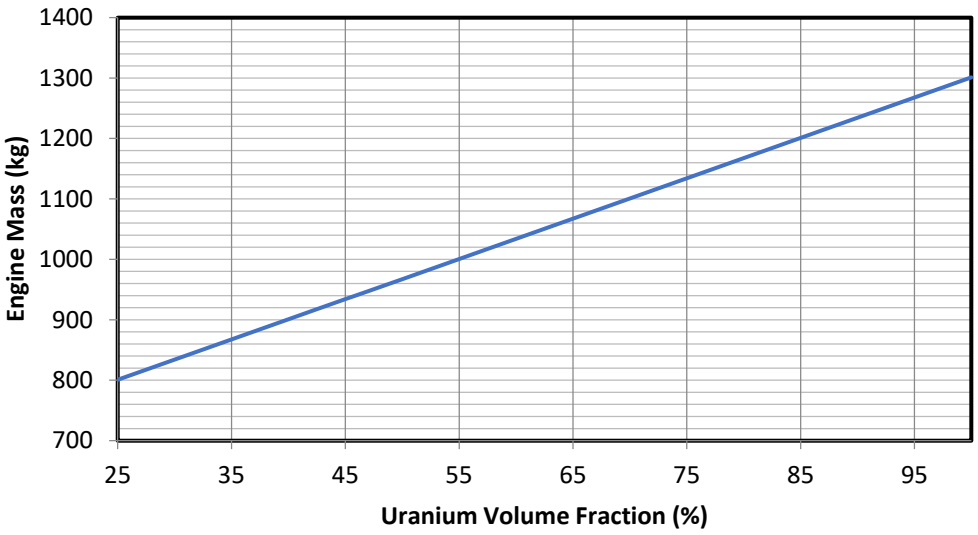

Figure 6.7: Engine mass change of CNTR with the change in uranium volume fraction.

These results were expected since the amount of fissioning uranium in the system increases with the increase in the uranium volume fraction. This results in the engine mass and k_{eff} of the engine to increase. With this engine configuration, criticality was not achieved. This led to the second study discussed in the next section.

6.3.2 Russian "Topaz" Reactor Model and CFE Pitch Sensitivity Study

In this study, the volume fraction of uranium was kept at 50% and two model changes were made to the CNTR engine. First, the SiC core block was replaced by a $ZrH_{1.87}$ moderator core block which is patterned after the Russian "Topaz" reactor model [62]. Since the core block itself is a $ZrH_{1.87}$ moderator, the moderator cylinders were removed from this model while still keeping the 19 CFEs. It is estimated that this moderator block will be maintained at around 600 degrees Celsius. Secondly, cylindrical SiC solid walls were added outside of the CFEs as support. In this study, the CFE pitch size was varied to understand its impact on the criticality and mass of the engine. CFE pitch is defined as the distance between the centers of two

neighboring CFEs. The web thickness between the cylinders was varied to change the CFE pitch. Figure 6.8 illustrates the CFE pitch and web thickness in this engine.

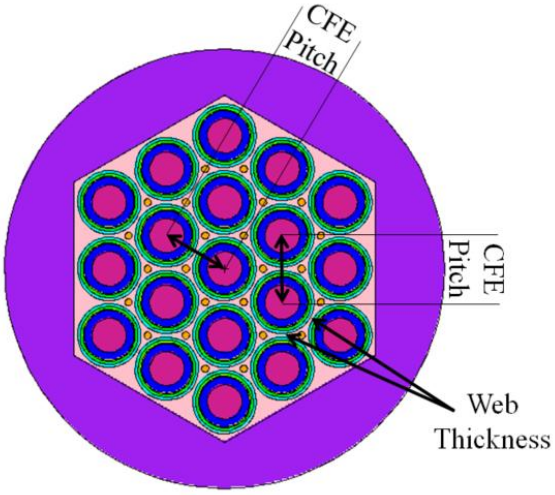

Figure 6.8: CFE Pitch and web thickness in a CNTR Engine.

Other dimensional changes in this engine are listed in Table 6.2. Everything else in the model is kept similar to the uranium volume fraction sensitivity study model.

Table 6.2: Model dimensional changes made in this study.

Parameter	Dimensions (cm)	Type
Central 100% propellant region	3.00	OR
19.75% Enriched Uranium at 50% VF	4.50	OR
50% dense ZrC/UN coating	4.55	OR
80% dense SiC inlet wall	4.90	OR
100% propellant inlet	5.10	OR
SiC outer wall	5.50	OR
$ZrH_{1.87}$ hexagonal moderator block	25.1 to 26.5	OR

CFE Pitch	11.2 to 11.7	Pitch

OR = Outer Radius

The result of this study is shown in Figure 6.9. As the CFE pitch is increased, the criticality of the engine increased too. This is due to the presence of more $ZrH_{1.87}$ moderators in the engine. More neutrons are moderated to thermal energies resulting in more fission happening in the engine. This results in the criticality of the engine to increase. By increasing the web thickness, the overall engine size also increased to accommodate 19 CFEs while keeping the size of everything similar to the uranium fraction sensitivity study model. This led to the increase in the engine mass with the increasing CFE pitch. In this study, the CNTR engine achieved critical conditions. Using this material and model configuration, the next goal is to optimize the engine geometry.

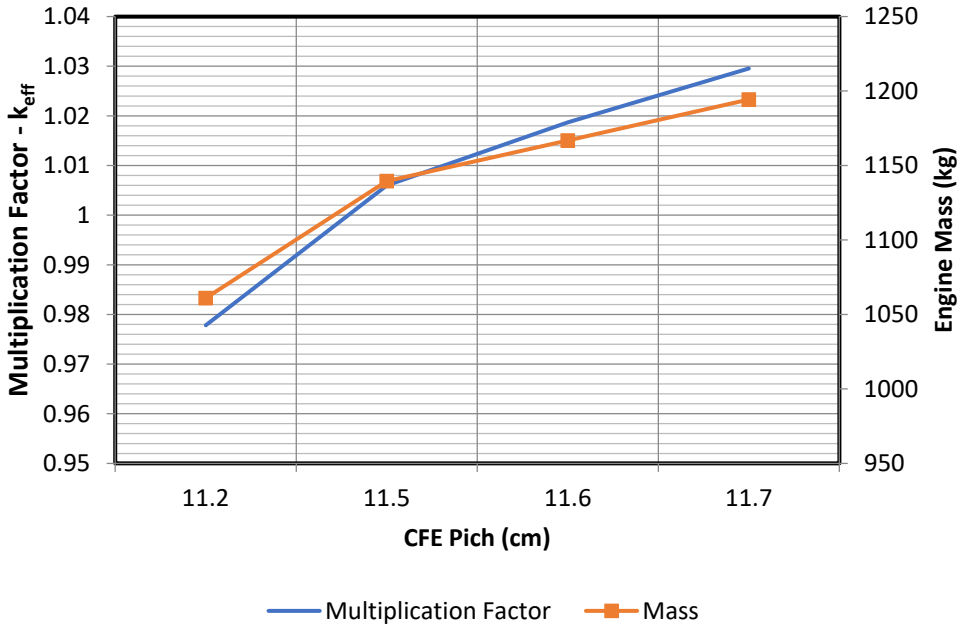

Figure 6.9: Criticality and engine mass change with the CFE Pitch in a CNTR engine.

6.3.3 Reflector Thickness and Core Length Sensitivity Study

In this study, the CFE pitch was kept at 11.7 cm ($ZrH_{1.87}$ hexagonal moderator block outer radius was kept at 25.5 cm) and the uranium volume fraction was kept at 50 percent. The radial beryllium thickness varied from 8 cm to 9.44 cm and the core length varied from 80 cm to 84 cm. The results obtained from this geometry sensitivity study are given in Table 6.3.

Table 6.3: Criticality and engine mass for various reflector thicknesses and core lengths.

Radial Be Thickness (cm)	**Core Length (cm)**	**k_{eff}**	**Engine Mass (kg)**
8.00	80	1.02954±0.00118	1194.30
9.00	80	1.03979±0.00117	-
9.00	84	1.04996±0.00115	1292.57
9.00	94	1.06831±0.00117	1436.83
9.10	84	1.04984±0.00122	-
9.44	80	1.04687±0.00117	-
9.44	82	1.04792±0.00113	-
9.44	83	1.05328±0.00120	1296.97
9.44	84	1.05353±0.00125	-

Increasing the radial beryllium thickness results in more neutrons reflected into the engine. The increase in neutron population in the engine increases the criticality of this model CNTR. The increase in core length not only increases the uranium fuel in the system available

for fission but also increases the amount of moderator and reflector mass in this engine. As a result of increased materials, the criticality of the engine increases too. Both reflector thickness increase and core length increase lead to mass increase which is also observed in the results calculated. A potential design solution is a 19 CFE CNTR engine with an approximate mass of 1300 kg and an approximate k_{eff} of 1.05. The next study examined the 37 CFEs CNTR engine model.

6.3.4 Thirty-Seven CFEs CNTR Engine

In this study, everything was kept similar to the reflector thickness and core length used in the sensitivity study. The beryllium reflector thickness was kept at 9 cm and the core length was kept at 84 cm. The number of CFEs increased to 37. To accommodate all 37 CFEs in the hexagonal core block, the core block radius was increased to 37 cm. Figure 6.10 illustrates a 37 CFEs CNTR engine.

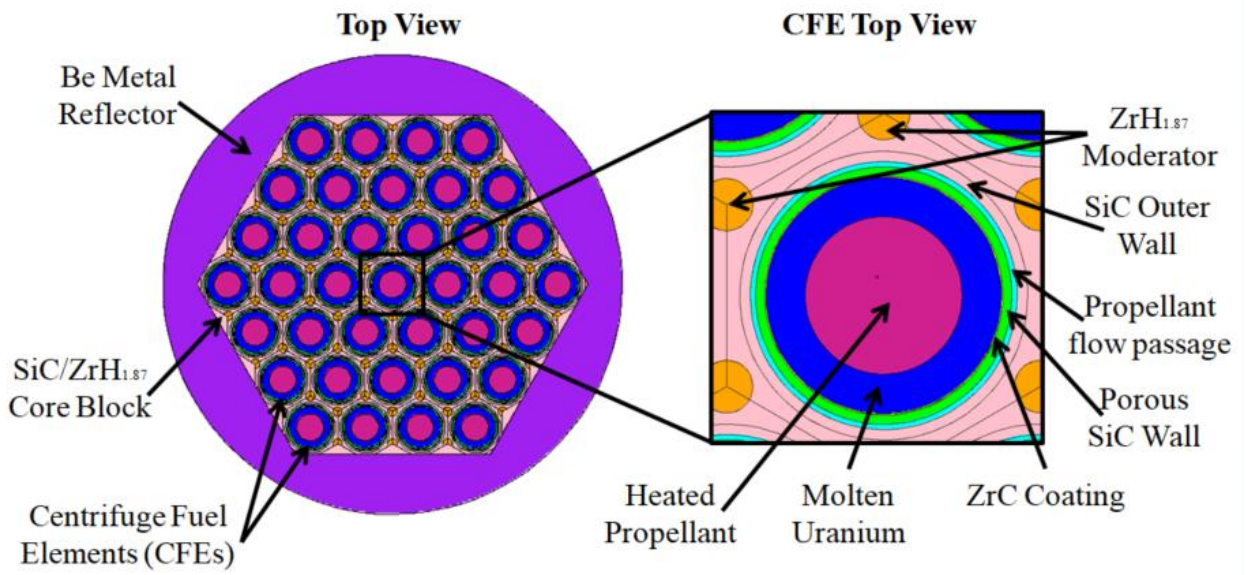

Figure 6.10: CNTR engine model with 37 CFEs top view and CFE cross-section view.

Three sub-studies were conducted on this engine model. The major changes in these three studies were the hexagonal core block and the beryllium reflector thickness. These three studies and their results are given in Table 6.4 below.

Table 6.4: Criticality of 37 CFEs CNTR engine with varying core block and reflector thicknesses.

Core Block Material	**Moderator Cylinders with 1 cm outer radius**	**Radial Be reflector thickness (cm)**	**k_{eff}**
SiC	$ZrH_{1.87}$	9	0.90713±0.00107
$ZrH_{1.87}$	None	9	1.15410±0.00111
$ZrH_{1.87}$	None	1	1.07281±0.00120

The increased amount of moderator material in the engine increased the criticality due to the moderation of neutrons in the system. As seen before, the larger beryllium reflector gave higher k_{eff} due to the reflection of neutrons back into the engine. The 37 CFEs model achieved supercritical conditions due to the higher amount of uranium in this system. With the increased number of CFEs, the mass of this system is approximately 3750 kg.

The increased mass of this 37 CFEs engine model makes it less attractive as compared to the 19 CFEs model. This 37 CFEs engine model is attractive when the mission requires higher thrust. The goal of current CNTR work is to achieve critical reactor conditions with the mass of the engine around 1000 kg. The next study was conducted to obtain criticality while keeping the engine mass at approximately 1000 kg.

6.3.5 Mass Reduction Study

The mass reduction study was conducted on 19 CFEs CNTR model by reducing the uranium fuel density. In this study, all dimensions and materials were kept similar to that used in the reflector thickness and core length sensitivity study. The reflector thickness was kept at 9 cm and the core length was kept at 84 cm. The uranium fuel density was reduced from 7.36 g/cm^3 to 1 and 2 g/cm^3. The uranium fuel temperature was dropped from 2500 K to 1200 and 1500 K to increase the neutron cross-section of uranium fuel. The result of this study is shown in Figure 6.11.

The temperature drop only provided a small increase in the k_{eff} value. However, the fuel density drop reduced the k_{eff} considerably. This is because the amount of uranium available for fission in the same volume has gone down. The lower amount of uranium in the system results in lower k_{eff} values. Reducing the mass of the engine by reducing the uranium fuel density proved unsuccessful. As the continuation of this study, other parameters were varied while keeping the uranium fuel density at 2 g/cm^3. The results of this study are shown in Table 6.5.

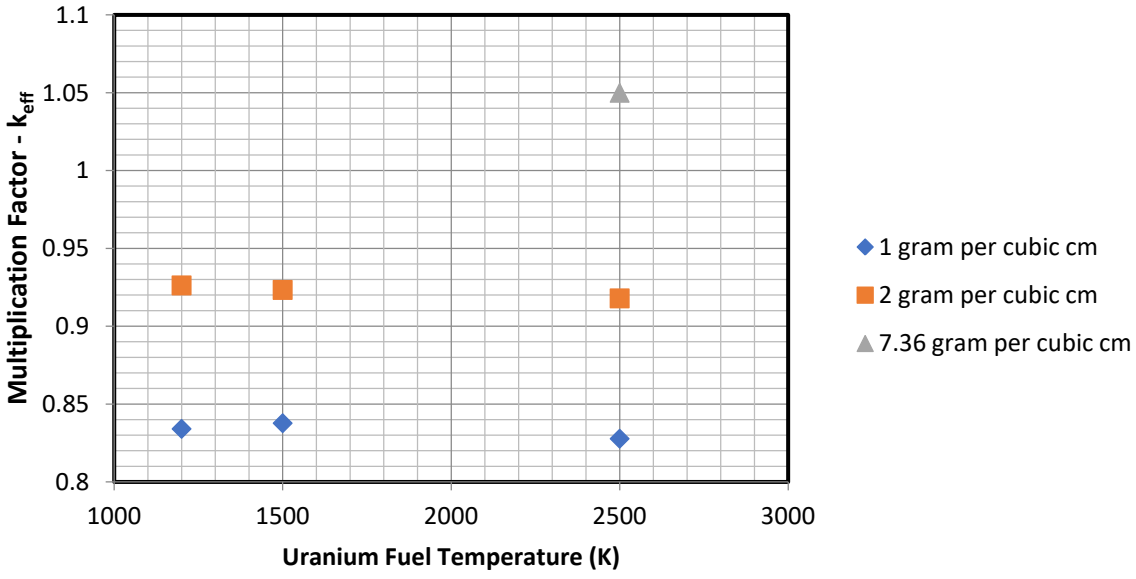

Figure 6.11: Change in criticality with uranium fuel density and temperature change.

Table 6.5: Mass reduction study results of CNTR engine with 2 g/cm^3 uranium fuel density.

CFE Pitch (cm)	**Engine Radius (cm)**	**Core Length (cm)**	**k_{eff} (±0.00120)**	**Mass (kg)**
11.8	40	84	0.92609	1015.42
11.8	45	84	0.97099	1243.53
11.8	40.95	84	0.92294	-
12.0	40.95	84	0.94176	1091.07
12.0	45	84	0.97118	1278.09
12.5	45	84	0.96239	1365.13
11.7	45	84	0.96466	1226.30
11.5	45	84	0.95859	1192.25
11.5	45	94	0.98765	1394.28
12	45	94	0.99684	1433.43
12	50	94	1.01964	1718.71
12	45	100	1.00755	1518.16
12	50	100	1.0308	1819.98

The best result for criticality still gave a mass of approximately 1518 kg. Reducing the fuel density method of mass reduction did not provide a critical self-sustaining engine. If the uranium temperatures are kept at 1200 K, the hydrogen temperature will be lower than this

which will lead to lower specific impulse in the range of 500 s to 600 s. Future heat transfer analysis can help in providing an accurate hydrogen temperature and specific impulse for the case of 1200 K uranium temperature.

From all these studies, it was calculated that the CNTR engine can achieve criticality while keeping the mass of the engine around 1300 kg and the hydrogen propellant temperature in the chamber around 3000 K. This will provide a specific impulse in the range of 850 s to 1000 s. These results are promising as it proves the feasibility of the CNTR engine in terms of just neutronics.

CHAPTER 7 Conclusion and Future Works

7.1 Neutronic Analysis Conclusion

7.1.1 Gas Core Nuclear Rocket

A criticality analysis of an open cycle gas core nuclear rocket was conducted using the MCNP transport code. The material properties of hydrogen and uranium at high temperatures were calculated for input into the MCNP. The density of hydrogen was calculated using the Saha equation taking into consideration both dissociation and ionization at constant pressure as a function of temperature. Calculations suggest that the dissociation of hydrogen at 1000 atm is 0.2 percent around 3000 K and is fully dissociated by 15,000 K. It follows also that at constant pressure in accordance with the ideal gas law, hydrogen density drops with increasing temperature. The density of gaseous core uranium was also determined using the ideal gas law and likewise was found to decrease with increasing temperature at constant pressure due to expansion. This analysis included the Doppler broadening of the resonance region owing to the high nuclear fuel temperature. At higher temperatures, the resonance cross-section spectrum flattens out and leading to a reduction in peak value. MCNP capability increased with the addition of high temperature neutron cross-sections.

The gas core nuclear rocket's criticality work showed that the engine can achieve critical conditions for a spherical non-homogenous engine of 4.3 m in diameter. This engine's criticality dropped as the core temperature increased. Analysis was conducted for uranium core temperatures up to 65,000 K. With the introduction of more uranium into the core, the criticality increases. The impact of the beryllium reflector on the engine was significant for realistic engine

geometries, particularly when the beryllium reflector is closer to the uranium core. It was also found that the criticality increases with the increase in hydrogen temperature at larger than 5 cm beryllium reflector thicknesses. This is promising as it improves the engine performance as the hydrogen temperature goes up. However, the downside is the mass of the engine increases considerably with the addition of more beryllium into the system. From the criticality study, it was concluded that an 80 percent uranium volume-occupying percentage and hydrogen at 50,000 K can give a critical engine with a mass of 98,000 kg.

The criticality of the engine was very sensitive to the inlet porous wall and the hydrogen coolant region. Additionally, the energy spectrum of the neutrons is very depended on the size of the uranium core. At smaller uranium size, the reactor is a thermal reactor and at larger uranium size, the reactor is an epithermal reactor.

7.1.2 Centrifugal Nuclear Thermal Rocket

The CNTR engine concept was also studied. This geometry was optimized to have a critical engine configuration in a low-mass package. Studies carried out in this thesis work featured 19 centrifuge fuel elements (CFEs) engines and showed that the engine is sub-critical when a core block of silicon carbide is used to hold the 19 CFEs in place. When the silicon carbide was replaced with $ZrH_{1.87}$ and with larger web thicknesses, the engine achieved critical condition. An engine of approximately 84 cm core length with a radial beryllium reflector of 9 cm thickness gave a k_{eff} of 1.05 with a mass of approximately 1,300 kg. However, the mass couldn't further be reduced by changing the material composition or geometry without losing criticality. The engine's specific impulse was calculated to be around 900 s.

7.2 Heat Transfer and Engine Performances Conclusion

Heat transfer calculations on the gas core nuclear rocket were carried out using basic heat transfer equations. Radiative and convective heat transfer analysis was carried out initially. The heat source is the fission heat production in the fuel region. The heat travels out of the uranium fuel due to radiation and convection. At high temperatures of uranium, uranium was taken as a blackbody whose emissivity and absorptivity are taken as one. The temperature of hydrogen depended on the uranium sphere's surface temperature. Depending on the surface temperature, the power within this uranium reactor ranged from 3000 MW to 7.6 TW.

Hydrogen absorbed the heat that came from the uranium fissioning core to raise its internal energy. From the iterative process, it was calculated that hydrogen's temperature can range from around 3000 K to 39,000 K for uranium core surface temperatures ranging from 10,000 K to 55,000 K. It was also observed that the contribution of convective heat transfer is very small in the heating of hydrogen at higher uranium surface temperature. It was also calculated that with the increase in mass flow rate, the hydrogen's temperature decreases due to the less time it spends in contact with the uranium core. This hydrogen goes to a converging-diverging nozzle to convert its thermal energy into kinetic energy.

A nozzle design was optimized for the gas core nuclear rocket engine with the high chamber temperatures calculated at a constant high pressure of 1000 atm. To get a choked flow, the throat radius has to range from 0.93 cm to 1.80 cm for this 1000 atm chamber pressure condition. The larger area ratio improves the engine performance but it adds extra weight to the gas core nuclear rocket. With the nozzle design and exit temperature and velocity known, the thrust and specific impulse were calculated. The mass of the engine was calculated to be in the range of 100,000 kg to 122,000 kg. The thrust of this engine ranged from 51,000 N to 305,000 N

with a specific impulse ranging from 1058 s to 6218 s. This finding proves this engine's ability to give high thrust and specific impulses.

7.3 Future Works

7.3.1 Gas core Nuclear Rocket Engine

There are still multiple challenges for the gas core nuclear rocket that needs to be tackled before this engine can take humans to Mars and beyond. Challenges like the confinement of the uranium core, engine components cooling, startup and shutdown, and ground testing have to be further researched and developed. Further computational work using modern computational tools to study the confinement of the gas core nuclear rocket by hydrodynamic confinement will enable an understanding of the best ways to confine this fuel core. Thermodynamic properties of materials at high temperatures need to be researched further. The sensitivity of the neutronics and heat transfer results to the change in thermodynamic properties needs to be understood better. Material cooling has to be done efficiently to reduce the engine components' temperature. Materials have to be developed that can withstand high temperature, pressure, and radiation from the uranium core. More work has to be conducted to come up with efficient ways to handle the spent fuel or by-products of fission present in this engine. The coupling mechanism between heat transfer and the neutronics can be in parallel. Other future work includes engine components such as hydrogen propellant storage and pressurizing the engine to the desired pressure. Throttling the power level in this engine and the shutdown of the engine has to be studied further too.

At these high temperatures, the fuel and propellant are in the plasma state. The plasma instabilities arising from plasma interaction with heavy plasma supported by light flowing plasma have to be studied and controlled to make this fuel core stable. The nozzle design

engineering challenge has to be looked into further due to its narrow throat area. All these works have to be both computationally and experimentally studied further. A simple experimental test that can be the next step for the gas core study is to have a gas such as argon flow around elevated ionic salt with secondary injection at its base. A model of this experimental setup is shown in Figure 7.1.

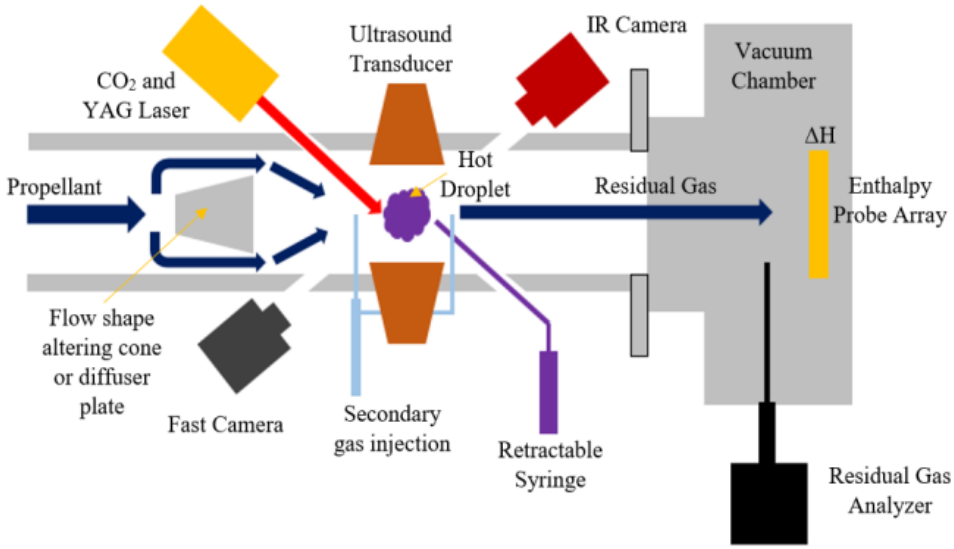

Figure 7.1: Next step experimental work for a gas core nuclear rocket engine.

Here the goal is to study the confinement of the plasma as the propellant gas flows around it. The ionic salt has to be elevated both in static and gas flow conditions. Thermal imaging can be used to quantify the laser heating of the ionic salt. The fast camera and PIC laser will help to study the instabilities at the interface and will provide an understanding of the overall stability of the droplet. The differential pumped RGA can help to assess the erosion of salt in presence of the propellant gas. From this experimental study, the surface instabilities, fuel erosion, heat transfer to the fluid via enthalpy probe, and the thermal profile can be studied. This experimental setup will help as the next step in making gas core nuclear rockets a reality.

7.3.2 Centrifugal Nuclear Thermal Rocket

Additional research needs to be carried out before CNTR becomes a reality for space flight. Many challenges are still left to be tackled for a CNTR engine. Heat transfer, fluid flow, uranium confinement, and hydrogen flow within the molten uranium studies have to be carried out to better understand the dynamics of this engine. Startup and shutdown of the engine and the ground testing of the engine before the flight has to be researched further. More experimental work needs to be conducted to validate the future computational findings. These include both non-nuclear and nuclear testing and fuel fabrication. The other engine components such as the turbomachinery and rotating cylinders have to be further analyzed. This includes analyzing the bearing lifetime, radiation tolerant blades, and other engineering components that help in achieving high RPMs for the CFEs.

The immediate next step of experimental work includes understanding the flow of and heat transfer of hydrogen bubbles in heated liquid metal. An infrared camera can be used to study the flow of bubbles in this experiment. Current experimental and computational studies are being carried out at the University of Alabama –Huntsville [63] [64]. These studies can be expanded to include heating in their bubble study. Though there are daunting challenges to the development of this engine concept, this engine has the potential to transcend solid core nuclear rockets in terms of performance.

7.4 Final Words

The studies performed in this dissertation demonstrate that the gas core nuclear rocket engine is potentially a promising engine for human exploration to Mars and beyond in a shorter time. This engine is capable of providing both high thrust and high specific impulses needed for shorter trip times. A critical engine with a very small amount of uranium loss from the system

can make this engine the next-generation nuclear rocket for space travel. To revive this engine, more research, development, and funding need to go in. With support and focus, the gas core nuclear rocket can indeed become a viable propulsion approach.

APPENDIX A MCNP Input File

A sample MCNP input file for calculating the criticality of a gas core nuclear rocket is provided below.

```
c Gas Core Nuclear Thermal Rocket MCNP Transport Code Input File
c
c Defining Cell Cards
c
c Plasma Gaseous Fuel Core at 55,000 K
1 10 -0.05160890 -100         imp:n=1 imp:p=1
c
c Hydrogen Propellant at 15,000 K
3 12 -0.000822693 100 -300     imp:n=1 imp:p=1
c
c SiC 80% dense porous Wall with H at 2,500 K
4 13 -2.56996364 300 -400      imp:n=1 imp:p=1
c
c Hydrogen Coolant at 1,200 K
5 14 -0.02046285 400 -500      imp:n=1 imp:p=1
c
c Be reflector at 1,200 K
```

```
8 17 -1.84800000 500 -700     imp:n=1 imp:p=1
c
c Pressure Vessel at 900 K
9 18 -4.43000000 700 -800     imp:n=1 imp:p=1
c
c Void Outside
10 0 800                      imp:n=0 imp:p=0 $ Union of all the regions outside the reactor


c
c Defining Surface Cards
c
c Spherical Uranium Core Gases region
100 so   124.7736849
c
c Cavity of 14 ft or 213.36 cm radius
300 so   213.36000
c
c SiC/Hydrogen inflow region of 0.5 cm thickness
400 so   213.86000
c
c Hydrogen Inflow Region of 1 cm thickness
500 so   214.86000
c
```

```
c Be reflector of 1 ft or 30.48 cm thickness
700 so   245.34000
c
c Outer Pressure Vessel Wall Cylinder
800 so   275.82000 $ Pressure Vessel wall of 30.48 cm thickness


c
c Data Cards
c
c Defining materials
c
c Central Uranium Fuel Core
m10 92233.94c -1.00 $ U-233 100% at 55,000 K
c
c Hydrogen Propellant
m12 1001.93c -1.0 $ Hydrogen at 15000 K
c
c SiC wall with hydrogen inflow 80% dense at 2500 K
m13 14028.74c -0.699917497 6000.74c -0.299318121 &
    1001.74c -0.000764382
c
c Hydrogen Coolant
m14 1001.73c -1.0 $ Hydrogen at 1200 K
```

```
c
c Be reflector at 1200 K
m17 4009.73c -1.0
c
c Ti-6Al-4V (Grade 5) Annealed Pressure Vessel at 900 K
m18  8016.72c -0.002000 13027.72c -0.060000 &
     23000.72c -0.040000 26056.72c -0.002500 &
     22048.72c -0.895500
c
c physics mode having both neutrons and photons
c
mode n p
c
c kcode and kcode soure cards to calculate keff
c source at 0 0 0
kcode 10000 1 50 500
ksrc 0 0 0
c
c total nuclear fission card
c
totnu
print
c
```

```
c Tally Specification
c
c Neutron Flux Calculation for the cells specified
F4:n 1 3 4 5 8 9
c Energy bins for the flux plotting
E4 1E-9 40I 1E-8 40I 1E-7 40I 1E-6 40I 1E-5
     40I 1E-4 40I 1E-3 40I 1E-2 40I 1E-1 40I 1 40I 10
c
c End of the Code
```

APPENDIX B NJOY Input File

A sample NJOY input code used to Doppler broaden uranium neutron cross-section for 55,000 K is given below.

```
‘ Neutron Cross-section Calculation for uranium-233 at 55,000 K
‘
‘ Converting ENDF tapers back and forth to ASCII and Blocked Binary Modes
moder
  20 -30 /
‘
‘ Resonance Reconstruction of uranium-233
reconr
  -30  -31 /
9222 0 0 /
0.001 0.0 0.01 5.0000000000000004e-08 /
0 /
moder
  -31 21 /
moder
  -31 -41 /
‘
```

‘ Doppler Broadening

broadr

-30 -31 -32 /

9222 1 0 0 0.0 /

0.001 1000000.0 0.01 5.0000000000000004e-08 /

55000 /

0 /

broadr

-30 -41 -42 /

9222 1 0 0 0.0 /

0.001 -1000000.0 0.01 5.0000000000000004e-08 /

55000 /

0 /

‘

‘ Heat Production Cross-section and radiation damage production cross-section

heatr

-30 -32 -33 /

9222 3 0 0 0 2 /

442

443

444

heatr

-30 -42 -43 /

```
 9222 3 0 0 0 2 /
 442
 443
 444
'
' Generating gas production cross-section
gaspr
 -30 -33 -34 /
gaspr
 -30 -43 -44 /
'
' Scattering in thermal energy range
thermr
 0 -34 -35 /
 0 9222 16 1 1 0 0 1 221 2 /
 55000 /
 0.001 10.0 /
thermr
 0 -44 -45 /
 0 9222 16 1 1 0 0 1 221 2 /
 55000 /
 0.001 10.0 /
moder
```

```
  -35 22 /
moder
  -45 23 /
‘
‘ Unresolved region probability tables for MCNP
purr
  20 22 24 /
  9222 1 1 16 64 1 /
  55000 /
  10000000000.0 /
  0 /
‘
‘ ACE creation for MCNP
acer
  20 24 0 25 26 /
  1 0 1 0.94000 /
  'U233 at 55,000 K' /
  9222 55000 /
  1 1 /
  /
acer
  0 25 27 28 29 /
  7 1 1 0.94000 /
```

```
  'U233 at 55,000 K' /
'
' Color Postscripts plots
viewr
  27 47/
stop
'
' End of code
```

BIBLIOGRAPHY

[1] "Ideal Rocket Equation," *NASA GRC,* NASA, Online, 2021.

[2] L. J Abadie, N. Cranford, C. W. Lloyd, *et al*., " The Human Body in Space," *NASA Human Research Program,* NASA, Online, 2021.

[3] "What is space radiation?" *Space Radiation Analysis Group*, Johnson Space Center, NASA, Online, 2022.

[4] "Radiation Sources and Doses," Radiation Protection, United States Environmental Protection Agency, Online, 2021.

[5] C. W. Lloyd, S. Townsend, and K. K. Reeves, "Space Radiation," *NASA Human Research Program Engagement and Communication,* NASA, Radiation iBook.

[6] "TA2: In-Space Propulsion Technologies," *NASA Technology Roadmaps*, NASA, 2015.

[7] N. Lewis, "Nuclear-powered rocket could get astronauts to Mars faster," *Where the Possibilities are Endless,* CNN World, News, Online, 2021.

[8] D. Fiehler, and S. Oleson, "A Comparison of Electric Propulsion Systems for Mars Exploration," *39th Joint Propulsion Conference and Exhibit*, Huntsville, AL, 2003.

[9] G. P. Sutton, and O. Biblarz, "Typical Performance Values," *Rocket Propulsion Elements,* 7th Edition, John Wiley & Sons, pp. 39 – 40, 2001.

[10] "Nuclear Thermal Propulsion: Game Changing Technology for Deep Space Exploration," NASA, Online, 2018.

[11] T. Kammash, D. L. Galbraith, and T. Jan, "An Americium-Fueled Gas Core Nuclear Rocket," American Institute of Physics, 1993.

[12] J. Allen, M. Johns, M. Patterson, *et al.*, "Overview of High-Performance Centrifugal Nuclear Thermal Rocket Propulsion System," *ANS Virtual Winter Meeting*, Virtual, 2020.

[13] R. Frisbee, "Advanced Space Propulsion for the 21st Century," *Journal of Propulsion and Power,* Vol. 19, No. 6, 2003.

[14] C. Bruno, "Nuclear Space Power and Propulsion Systems – Progress in Astronautics and Aeronautics," *American Institute of Aeronautics and Astronautics*, Vol. 225, pp. 34, 2008.

[15] R. G. Ragsdale and E. A. Willis, Jr., "Gas-Core Rocket Reactors – A New Look," *Seventh Propulsion Joint Specialist Conference*, AIAA, NASA TM X-67823, Salt Lake City, Utah, 1971.

[16] M. M. Gurfink, "Gas Core Nuclear Thermal Rocket Engine Research and Development in the Former USSR," *Idaho LDRD Program*, U.S. Department of Energy, 1992.

[17] B. Palaszewski, "High Power Electric and Advanced Space Propulsion: Making the Impossible Possible," *NASA Glenn Research Center*, Lewis Field, OH, 2005.

[18] T. Kammash, and D. L. Galbraith, "Magnetic Fuel Containment in the Gas Core Nuclear Rocket," *29th Joint Propulsion Conference and Exhibit*, AIAA 93-2368, Monterey, CA, 1993.

[19] "Kelvin-Helmholtz Instability," *Wikipedia*, Online, 2020.

[20] P. M. Sforza *et al*., "Recirculation Containment for Gas Core Fission Rockets," *AIAA*, 94-2899, 1994.

[21] R. Nayama, M. Toyota, and S. Tsujimura, "Diverter Structure," *International Nuclear Information System*, IAEA, Vol. 27, Issue 13, Patent, Ref. No. 27046701, Japan, 1995.

[22] T. R. Jan, and T. Kammash, "An Antiproton-Initiated Startup Scenario for the Gas Core Nuclear Rocket," *Proc. Nuclear Technologies for Space Exploration*, Jackson Hole, WY, 1992.

[23] M. F. Taylor, *et al*., "The Open-Cycle Gas-core Nuclear Rocket Engine – Some Engineering Considerations," *NASA Technical Memorandum*, NASA 0 X-67932, Atlanta, GA, 1971.

[24] R. G. Ragsdale, " High Specific-Impulse Gas-Core Reactors," *NASA Technical Memorandum*, NASA TM X-2243, OH, 1971.

[25] D. I. Poston, "A Computational Model for an Open-Cycle Gas Core Nuclear Rocket," *Ph.D. Thesis*, the University of Michigan, Ann Arbor, MI, 1994.

[26] L. Heilbronn, "Neutron Properties and Definitions," *NASA Summer School*, 2015.

[27] J. D. Clement, and J. R. Williams, "Gas-Core Reactor Technology," *Reactor Technology*, Vol. 13, No. 3, pp. 226 – 251, 1970.

[28] W. Emrich, "Advanced Nuclear Rocket Concepts," *Principles of Nuclear Rocket Propulsion*, Butterworth-Heinemann, ISBN 9780128044742, pp. 259 – 304, 2016.

[29] A. S. Keston, and N. L. Krascella, "Theoretical Investigation of Radiant Heat Transfer in the Fuel Region of a Gaseous Nuclear Rocket Engine," *Report NASA-CR-695,* United Aircraft Corporation, 1967.

[30] D. E. Parks, *et al*., "Optical Constants of Uranium Plasma," *Report NASA-CR-72348,* Gulf General Atomic Incorporated, 1968.

[31] N. L. Krascella, "Tables of the Composition, Opacity and Thermodynamic Properties of Hydrogen at High Temperatures," *Report B-910168-1,* United Aircraft Corporation, 1963.

[32] R. W. Patch, "Components of a Hydrogen Plasma Including Minor Species," *Report NASA-TN-D-4993,* 1969.

[33] P. M. Sforza, R. J. Cresci, and F. Girlea, "Fuel Efficient Hydrodynamic Containment for Gas Core Fission Reactor Rocket Propulsion," *44th International Astronautical Federation Congress*, IAF93-R.1.427, Graz, 1993.

[34] R. J. Sedwick, and J. L. Kerrebrock, "MHD enhanced vortex containment concept for a gas core nuclear rocket," *34th Aerospace Science Meeting and Exhibit*, AIAA, Reno, NV, 1996.

[35] L. E. Thode, M. C. Cline, and S. D. Howe, "Vortex Formation and Stability in a Scaled Gas-Core Nuclear Rocket Configuration," *Journal of Propulsion and Power,* Vol. 14, No. 4, 1998.

[36] S. D. Howe, *et al*., "Gas Core Nuclear Rocket Feasibility Project," *Los Alamos National Laboratory,* Los Alamos, NM, 1997.

[37] Y. Katoh, and L. Snead, "Silicon carbide and its composites for nuclear applications – historical overview," *Journal of Nuclear Materials,* Vol. 526, ISSN 0022-3115, 2019.

[38] K. Yueh, "SiC Composite for Fuel Structure Applications," *Electric Power Research Institute,* DOE-EPRI-0000539, 2017.

[39] T. A. Tomberlin, "Beryllium – A Unique Material in Nuclear Applications," *36th International SAMPE Technical Conference,* San Diego, CA, 2004.

[40] M. Boivineau, C. Cagran, *et al*., "Thermophysical Properties of Solid and Liquid Ti-6Al-4V (TA6V) Alloy," *International Journal of Thermophysics 27*, pp. 507 – 529, 2006.

[41] T. Goorley, "MCNP6.1.1-Beta Release Notes," LA-UR-14-24680, 2014.

[42] C. J. Werner, *et al*., "MCNP User's Manual," Code Version 6.2, LA-UR-17-29981, Los Alamos National Security, 2017.

[43] "NJOY16," *Los Alamos National Laboratory,* LA-CC-15-092, 2016.

[44] R. E. MacFarlane, *et al*., "The NJOY Nuclear Data Processing System, Version 2016," *Los Alamos National Laboratory,* LA-UR-17-20093, 2016.

[45] F. F. Chen, "Introduction," *Introduction to Plasma Physics and Controlled Fusion,* 3rd Edition, Springer, ISBN 978-3-319-22308-7, pp. 1 – 18, 2016.

[46] J. R. Lamarsh, and A. J. Baratta, "Interaction of Radiation with Matter," *Introduction to Nuclear Engineering,* 3rd Edition, Prentice Hall, ISBN 0-201-82498-1, pp. 52 – 116, 2001.

[47] "Doppler Broadening – Doppler Effect," *Nuclear Power*, Online, 2022.

[48] K. Ju, and Y. Kim, "A Comparative Investigation of Doppler broadening of Neutron absorption and Photon-induced Nuclear Resonance Fluorescence Reactions," *The Korean Nuclear Society Autumn Meeting,* Gyeongju, Korea, 2017.

[49] D. E. Cullen, and C. R. Weisbin, "Exact Doppler broadening of tabulated cross sections," *Nuclear Science and Engineering,* Vol. 60, No. 3, pp. 199 – 229, 1976.

[50] "Physics of Uranium and Nuclear Energy," *World Nuclear Association,* Online, 2022.

[51] T. L. Bergman, A. S. Lavine, F. P. Incropera, and D. P. Dewitt, "Fundamentals of Heat and Mass Transfer," 7th Edition, John Wiley & Sons, ISBN 978-0470-50197-9, 2011.

[52] R. F. Kubin, and L. L. Presley, "Thermodynamic properties and Mollier chart for hydrogen from 300° K to 20,000° K," *Scientific and Technical Information Division,* NASA, 1964.

[53] H. Aroeste, and W. C. Benton, "Emissivity of Hydrogen Atoms at High Temperatures," *Journal of Applied Physics*, Vol. 27, No. 2, 1956.

[54] R. W. Patch, "Interim Absorption Coefficients and Opacities for Hydrogen Plasma at High Pressure," *NASA TM X-1902,* NASA, 1969.

[55] W. J. Devenport, "Nozzle Applet," *Kevin T. Crofton Department of Aerospace and Ocean Engineering,* Virginia Polytechnic Institute and State University, VA, 2001.

[56] S. K. Borowski, D. R. McCurdy, and T. W. Packard, "Nuclear thermal Rocket/Vehicle Characteristics and Sensitivity Trades for NASA's Mars Design Reference Architecture (DRA) 5.0 Study," *Nuclear and Emerging Technologies for Space,* Atlanta, GA, 2009.

[57] G. P. Sutton, and O. Biblarz, "Nozzle Theory and Thermodynamic Relations," *Rocket Propulsion Elements,* 7th Edition, John Wiley & Sons, pp. 45 – 101, 2001.

[58] "Falcon Heavy The World's Most Powerful Rocket," *SpaceX,* Online, 2022.

[59] “NERVA – Detail Specification Part 1 Performance/Design and Qualification Requirements for Engine, NERVA, 75K, Full Flow,” *Aerojet Nuclear systems Company*, C002-CP090290A-F1, 1970.

[60] T. LATHAM, “Nuclear Light Bulb,” *United Technologies Research Center*, N92-11110.

[61] M. G. Houts, C. R. Joyner, J. Abrams, J. Witter, and P. Venneri, “Versatile Nuclear Thermal Propulsion,” *IAC 70*, International Astronautical Congress, Washington D. C., 2019.

[62] S. S. Voss, “Topaz II System Description,” *Los Alamos National Laboratory*, Los Alamos, NM, 1994.

[63] B. Campbell, *et al*., “Initial Experiment Designs Studying Gas Bubble Flows in Liquids for use in Centrifuge Nuclear Thermal Propulsion,” *Nuclear and Emerging Technologies for Space*, Cleveland, OH, 2022.

[64] P. D. Ayuthya, and J. Cassibry, “Three Dimensional Simulations of Bubble Dynamics in Centrifugal Nuclear Thermal Propulsion” *Nuclear and Emerging Technologies for Space*, Cleveland, OH, 2022.